Investigating PRMT6 Protein Interactions in Breast Cancer Cells

Janelle Nordin

Thesis submitted to the University of Ottawa in
partial fulfillment of the requirements for the
Master of Science degree in Cellular and Molecular Medicine

Department of Cellular and Molecular Medicine
Faculty of Medicine
University of Ottawa

Abstract

Breast cancer remains the most diagnosed cancer in women and a leading cause of death attributed to refractory tumours unresponsive to chemotherapeutics. Understanding breast cancer etiology and the molecular landscape contributing to chemoresistance is crucial for developing a novel treatment strategy in tumours to increase the chemotherapy response. PRMT6 is a type-I PRMT enzyme that catalyzes methylarginine post-translational modifications critical to the cell's physiological processes. PRMT6 has aberrant expression detected in breast cancer potentially contributing to poor prognosis. Our lab has previously observed a role for PRMT6 in mediating stress granule formation, which could represent a chemoresistance mechanism used by breast cancer cells. This study attempts to investigate the unknown PRMT6 molecular mechanism promoting bortezomib chemoresistance by identifying novel PRMT6 protein interactors or substrates that help govern these molecular functions. We engineered BirA-PRMT6 expressing BioID cells and found PRMT6 to interact with ADAR1 p110 in the nucleus of breast cancer cells. The ADAR1 p110 and PRMT6 interaction is not impacted by bortezomib treatment indicating a potential alternative form of regulation. Lastly, PRMT6 does not regulate the ADAR1 p150 isoform through N-terminal arginine methylation, however, ADAR1 p110 is not eliminated as a potential PRMT6 substrate involved in the regulation of the stress response.

Acknowledgements

First, I would like to thank my supervisor Dr. Jocelyn Côté for providing me with the opportunity to join his lab and pursue my MSc degree in the breast cancer research field. Thank you for your instrumental expertise and guidance that allowed me to develop into the scientist I am today! I would also like to thank my advisory committee members, Dr. Laura Trinkle-Mulcahy and Dr. Jean-François Couture who generously provided encouragement and insightful feedback to help further my research project into something I can be proud of.

To the past and present Côté lab members, your support, friendship, and our lab excursions will always be remembered fondly. Specifically, Geneviève Paris, Andréanne Didillon, and Julie Bourassa thank you for the technical support and mentorship that was imperative to my success as a Grad student. Andréanne, thank you for all the softball game invites. Grace Liu, thank you for our impromptu bench chats and shared appreciation for the homeland (AB). Julie, thank you for the endless laughs, extensive conversations, and attendance at our two-person office book club. I am lucky to have been surrounded by these brilliant labmates turned friends.

Lastly, thank you to my family, Isabelle, Willy, and Richard Nordin, for their unconditional love and support that I always felt, even from the other side of the country. Your encouragement through the highs and lows is what made pursuing my MSc possible. To the friends I made in Ottawa and the ones that facetimed, drove, or flew out to visit, thank you. Your continuous support and our memories will forever be cherished.

Table of Contents

List of Figures

List of Tables

List of Abbreviations

aa	Amino acid
ACACA	Acetyl-CoA carboxylase
ADAR1	Adenosine deaminase acting on RNA 1
ADMA	Asymmetric dimethylarginine
AKT	Protein Kinase B
ALS	Amyotrophic lateral sclerosis
ANOVA	Analysis of Variance
AP	Affinity Purification
BAG5	BAG family molecular chaperone regulator 5
BioID	Proximity-dependent biotin identification
BSA	Bovine serum albumin
Btz	Bortezomib
CARM1	Coactivator Associated Arginine Methyltransferase 1
CD44	P-glycoprotein 1
CDK4	Cyclin-dependent kinase 4
CIP2A	Cellular Inhibitor of PP2A
CPMA	Counts per minute in channel A
CRL4B	Cullin4B-Ring E3 ligase complex
DAPI	4′,6-diamidino-2-phenylindole
DDX3	DEAD-box RNA Helicase 3
DMEM	Dulbecco's Modified Eagle Medium
DMSO	Dimethylsulfoxide
DNA	Deoxyribonucleic acid
DTT	Dithiothreitol
DZF	Domain associated with zinc fingers
E2F-1	E2F transcription factor 1
eGFP	enhanced green fluorescent protein
eIF	Eukaryotic translation initiation factor
EMT	epithelial-to-mesenchymal transition
ER	Estrogen receptor
EWS	RNA binding protein EWS
FBS	Fetal bovine serum
FDR	False discovery rate
FUS	Fused in sarcoma protein
GAR	glycine-arginine-rich
GR	glucocorticoid receptor
GREB1	Growth regulating estrogen receptor binding 1
GSK3-3B	Glycogen synthase kinase-3 beta
GST	Glutathione-S-transferase
H2AR26	Histone 2A arginine 26
H2AR29	Histone 2A arginine 29
H3K27	Histone 3 lysine 27

H3K4	Histone 3 lysine 4
H3R17	Histone 3 arginine 17
H3R2	Histone 3 arginine 2
HC	Heavy chain
HER2	Human epidermal growth factor receptor-2
HIV	Human immunodeficiency virus
HRI	eIF2α kinase heme-regulated inhibitor
HRP	Horseradish peroxidase
HSP90	Heat shock protein 90
HTT	Huntingtin protein
IB	Immunoblot
ICC	Immunocytochemistry
IFN	Interferon
ILF2	Interleukin enhancer-binding factor 2
ILF3	Interleukin enhancer-binding factor 3
IP	Immunoprecipitation
IPTG	isopropyl-β-D-thiogalactopyranoside
IRF3	Interferon regulatory factor 3
KD	Knockdown
KO	Knockout
LC	Light Chain
LDS	Lithium dodecyl sulfate
LEF1	Lymphoid Enhancer Binding Factor 1
LLPS	Liquid-liquid phase separation
MCCC1	Methylcrotonyl-CoA carboxylase subunit 1
MCCC2	Methylcrotonyl-CoA carboxylase subunit 2
MLL1	Mixed lineage leukemia protein-1
MMA	Monomethylarginine
mRNA	Messenger ribonucleic acid
MS	Mass Spectrometry
NF-κB	Nuclear factor-κB
OD	Optical density
PARP1	Poly(ADP-ribose)polymerase 1
PBS	Phosphate buffered saline
PC	Pyruvate carboxylase
PCC	Propionyl-CoA Carboxylase
PCR	Polymerase chain reaction
PELP1	Proline-, glutamic acid-, and leucine-rich protein 1
PERK	Protein Kinase RNA-Like ER Kinase
PI3K	Phosphoinositide 3-kinase
PKR	Protein kinase R
Pol-β	DNA polymerase β
PP2A	Protein phosphatase 2A
PR	Progesterone receptors
PRMT	Protein arginine methyltransferase

PTEN	Phosphatase and TENsin homolog deleted on chromosome 10
PTM	Post-translational modification
$p21^{CDKN1A}$	Cyclin-dependent kinase inhibitor 1
RIPA	Radio-Immunoprecipitation Assay
RNA	Ribonucleic acid
RNP	Ribonucleoproteins
RUNX1	Runt-related transcription factor 1
SAH	S-Adenosyl-L-homocysteine
SAM	S-Adenosyl-l-methionine
SDS-PAGE	Sodium dodecyl-sulfate polyacrylamide gel electrophoresis
SD	Supplementary Data
SDMA	Symmetric dimethylarginine
SE	Standard error
SG	Stress Granules
SILAC	Stable isotope labeling by amino acids in cell culture
SMA	Spinal muscular atrophy
SMN	survival motor neuron protein
SNAIL	Zinc finger protein SNAI1
SOC	Super Optimal broth with Catabolite repression
TNBC	Triple-negative breast cancer
TNF	Tumor necrosis factor
TOP3B	DNA topoisomerase 3-beta-1
TSP-1	Thrombospondin 1
UHRF1	Ubiquitin-like containing PHD and RING finger domains, 1
UPR	Unfolded protein response
UTR	Untranslated region
WB	Western blot
WT	Wild type
YLPM1	YLP motif-containing protein
ZDBD	Z-DNA binding domain
ZFR	Zinc finger RNA binding protein
80S	Eukaryotic 80S ribosome
^{3}H	Tritium
R / Arg	Arginine
G / Gly	Glycine
K / Lys	Lysine
M / Met	Methionine

Chapter 1: Introduction

1.1 Arginine Methylation

Post-translational modifications (PTMs) are indispensable protein chemical modifications for cellular regulation and are mediated by enzymatic activity. Protein arginine methyltransferases (PRMTs) are enzymes that catalyze the stable arginine methylation PTM on target proteins (Blanc & Richard, 2017). PRMTs can also act as epigenetic regulators by methylation of histones and non-histone proteins to alter transcription and influence the functional diversity of proteins and their physiological roles. Epigenetic regulation is known as the modification of DNA or histones without altering the DNA sequences. PRMTs role in epigenetic regulation and protein PTMs are recognized in cellular processes including signal transduction, pre-mRNA splicing, transcriptional control, DNA repair, cell fate decision and protein translocation.

Arginine methylation alters the protein's biophysical properties leading to changes in protein stability, localization, and interactions, ultimately, influencing these cellular processes (Bedford & Clarke, 2009; Guccione & Richard, 2019). PRMTs catalyze the addition of one or two methyl groups on arginine's guanidino nitrogen atom. The methyl donor S-adenosylmethionine (AdoMet or SAM) provides the methyl group to an acceptor forming S-adenosylhomocysteine (AdoHcy or SAH) and methylarginine by-products (Bedford & Richard, 2005; Guccione & Richard, 2019). There are nine mammalian PRMTs classified as type I (PRMT1, PRMT2, PRMT3, PRMT4/CARM1, PRMT6, PRMT8), type II (PRMT5, PRMT9), and type III (PRMT7). All PRMTs enzymatic activity generates a monomethylarginine (MMA) intermediate, however, types I and II are further categorized by

the additional formation of an asymmetric dimethylarginine (ADMA) or symmetric dimethylarginine (SDMA), respectively (Blanc & Richard, 2017) (Figure 1).

The substrate's modified arginine residue retains its positive charge and gains structural bulkiness and hydrophobicity while losing hydrogen bonding capacity (Bedford & Richard, 2005; Guccione & Richard, 2019). Arginine methylation is the most frequently methylated residue of human proteins compared to the lysine, histidine, cysteine, glutamine, glutamate, and aspartate residues (Brown et al., 2023). These arginine methylation modifications are often found at protein-protein and protein-nucleic acid interactions indicating their functional consequence in specificity for biological interactions and protein stability (Lorton & Shechter, 2019).

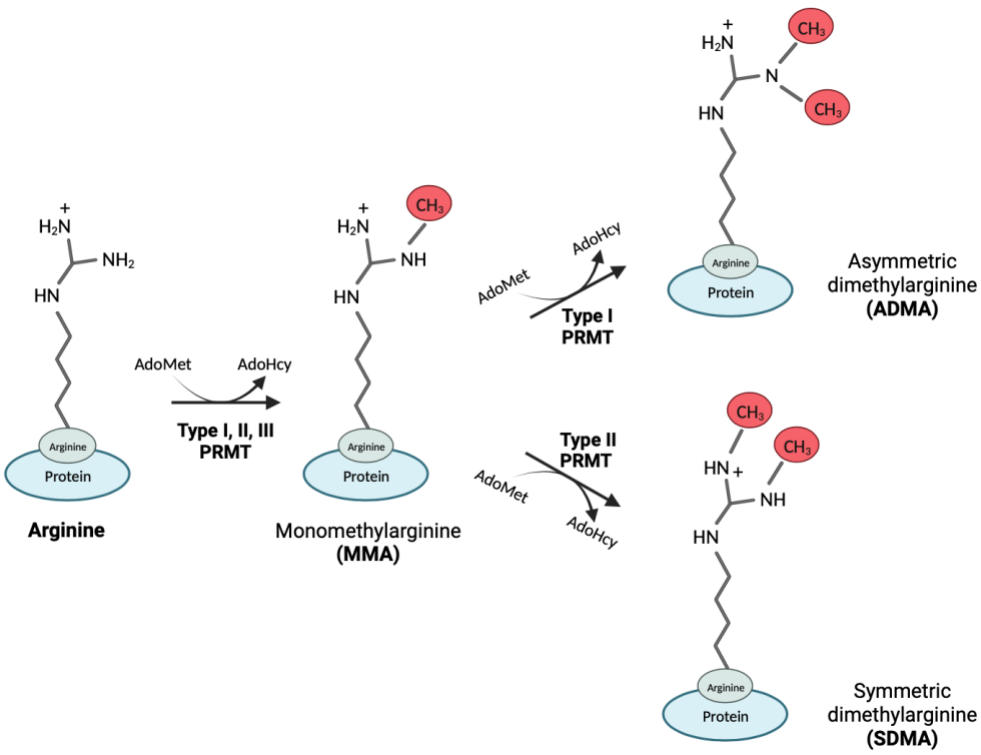

Figure 1: Arginine methylation reactions catalyzed by PRMTs.

All nine of the mammalian PRMTs catalyze an MMA intermediate before type I PRMTs catalyze an ADMA product and type II PRMTs catalyze an SDMA product. Classification of the PRMT enzymes are as follows; PRMTs 1, 2, 3, 4, 6, and 8 are type I, PRMT 5, 9 are type II and PRMT 7 is a type III. Created with BioRender.com.

1.2 Dysregulation of Arginine Methylation

The critical contributions of PRMTs in fundamental cellular pathways make them a likely candidate to be implicated in disease progression and development. Dysregulation of PRMT expression levels and enzymatic activity can promote anomalous molecular processes regulated by arginine methylation and have a considerable effect on human diseases (Bedford & Richard, 2005). For example, PRMTs have frequently been found to be upregulated and associated with a myriad of cancers. PRMTs (PRMT1, PRMT6 and CARM1) function as a coactivator for nuclear receptors that influence hormone-dependent cancers like prostate and breast cancer when

dysregulated (Y. Yang & Bedford, 2013). Many tumorigenesis characteristics associated with PRMT overexpression are cell-type dependent. PRMT1 and PRMT6 overexpression both promote the growth of bladder and lung cancers. Dysregulated PRMT1, 2, 4, 5, 6, and 7 have all been found associated with breast cancer cells (H. Wei et al., 2014). The PRMT1 isoform, PRMT1v2, has increased relative expression in both breast cancer cell lines and tumours resulting in enhanced invasion in aggressive and non-aggressive cell lines (Baldwin et al., 2012). Similar results of enhanced invasiveness were found with overexpression of PRMT7 in breast cancer cells. PRMT7 promotes expression of the breast cancer metastasis mediator, matrix metalloproteinase (MMP9), to promote this cellular invasion (Baldwin et al., 2014). The dysregulated enzymatic activity of PRMT and therefore dysregulation of arginine methylated substrates has been linked to promoting tumorigenesis. One way this occurs is when PRMTs negatively regulate tumour-suppressor gene expression and therefore function as an oncogene (H. Wei et al., 2014). This was evident with PRMT6 methylation of the tumour suppressor genes p21 and p16, resulting in the inhibition of growth suppressive function by p21 and impeding the blockade of the cell cycle by p16 (Poulard et al., 2016). Epithelial-mesenchymal transition (EMT), a hallmark of metastasis that promotes cancer cell migration and invasion, is another tumorigenic property facilitated by PRMT activity. PRMT5 is a corepressor of the EMT regulator, SNAIL, leading to a loss of E-cadherin, a characteristic of EMT (Bedford & Clarke, 2009). Another example of EMT regulation was observed with PRMT7 suppressing E-cadherin transcriptional activity by altered histone methylation of H4R3me2s in breast cancer cells (Yao et al., 2014). PRMT up- or downregulation can have extensive consequences on PRMT regulation and lead to the promotion of tumorigenic properties.

Investigating PRMT dysregulation with different models is important for understanding the mechanisms contributing to disease pathology and developing new therapeutic targets. Exploring PRMT knockdowns (KD) with transgenic models and selective PRMT inhibitors has linked them to numerous other diseases such as neurodegeneration and muscular diseases. In ALS neurodegenerative disease, mutated FUS is methylated by PRMT1 and accumulates in the cytoplasm forming inclusions. PRMT1 depletion resulted in nuclear localizing mutant FUS and decreased inclusions (Tradewell et al., 2012). In Alzheimer's disease, PRMT5 was found to mediate neuronal death through the E2F-1/NF-κB/GSK3-3B apoptotic pathways (Quan et al., 2015). Another neurodegenerative disease promoted by a PRMT mechanism is spinal muscular atrophy (SMA), described as the loss of SMN1 gene function (Hubers et al., 2011; Tadesse et al., 2008). SMN protein is characterized to have a Tudor domain identified as a methyl binding module that when mutated cannot bind a known CARM1 substrate, HuD (Bedford & Clarke, 2009; Hubers et al., 2011; Tadesse et al., 2008). In SMA models, defects in SMN/HuD binding impede efficient HuD recruitment to neuronal RNA granules and dysregulation of HuD axonal mRNA targets (Hubers et al., 2011). The vast role of arginine methylation in disease is due to the expansive role of PRMT in physiological processes, therefore, many molecular mechanisms linked to pathogenesis remain unidentified.

1.3 Protein Arginine Methyltransferase 6 (PRMT6)

1.3.1 Biochemical and Structural Features

PRMT6 is the second smallest member of the PRMT family with a 42 kDa molecular weight and 375 amino acids in length (Frankel et al., 2002; H. Wei et al., 2014). The PRMT6 family classification is partially based on its methyltransferase domain, which is found in the conserved catalytic core region and conserved PRMT family double E loop and THW motif to

help with substrate binding by interacting with the substrate arginine residue (Figure 2) (Frankel et al., 2002; Gupta et al., 2021). The N-terminus contains the AdoMet binding pocket, also known as the Rossman fold (Gupta et al., 2021) PRMT6, like the other PRMTs, also contains a β-barrel and dimerization arm helices (Figure 2) (Z. Chen et al., 2022). Structural analysis utilizing X-ray crystallography revealed a PRMT6 homodimer that brings two active sites close together, forming a flat ring dimer structure with a central cavity for substrates to bind and stabilize the enzyme-AdoMet complex. This contrasts the concave surface cavity of other Type I PRMT dimers implying potential unique substrate selectivity (Gupta et al., 2021; Lakowski & Frankel, 2008). PRMT6 has been observed to automethylate at Arg35 for protein stability which is required for its catalytic activity (Cao et al., 2023; Frankel et al., 2002; Singhroy et al., 2013). In summary, dimerization and automethylation are two essential features of PRMT6 for both its proteolytic stability and enzymatic activity.

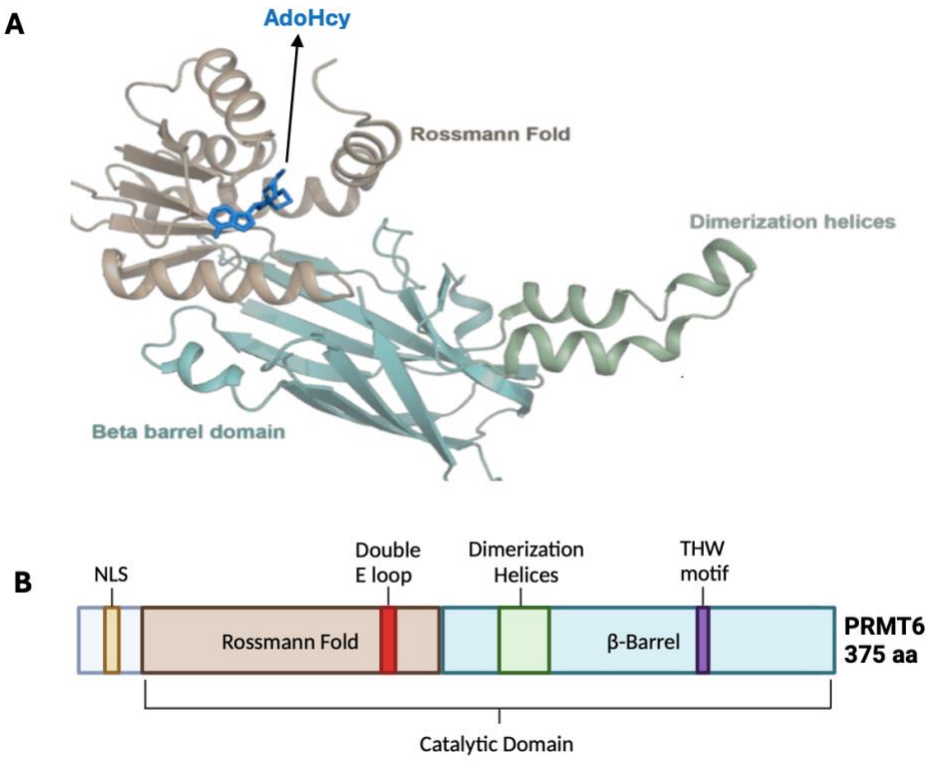

Figure 2. PRMT6 Crystal and Domain Structure.

(a) The AdoMet binding pocket is in the N-terminus also known as the Rossmann Fold. The PRMT6 crystal structure is in complex with AdoHcy (dark blue). The C-terminus consists of the β-barrel domain (light blue) where the dimerization helices are also located (light green). **(b)** The PRMT6 protein domain structure displaying the nuclear localization signal (yellow), Rossmann fold (brown), double E loop motif (red), dimerization helices (green), THW motif (purple) and β-barrel domain (blue) embedded within the catalytic domain. The PRMT6 crystal structure figure is adapted from (Gupta et al., 2021) and the PRMT6 domain structure is adapted from (Herrmann et al., 2009; H.-H. Wei et al., 2021; Wu et al., 2016) and created with BioRender.com.

1.3.2 Protein and Substrate Binding

PRMT6 is a Type I PRMT that preferentially catalyzes an ADMA reaction in the glycine-arginine-rich (GAR) domain of proteins but is also capable of methylating arginine outside this sequence (Lakowski & Frankel, 2008). More recently it was found that PRMT6 can precisely recognize a single RG motif denoted by a single glycine immediately following the arginine targeted for methylation (Hamey et al., 2021). Additionally, PRMT6 substrates have been found

to contain more basic, bulky amino acid residues around the target arginine with fewer glycine residues compared to PRMT 1 and 5 substrates that also preferentially methylate GAR domains (Hamey et al., 2021; Thandapani et al., 2013). Although PRMT6 has broad amino acid sequence specificity for its substrates, the sequence context differs for other PRMT substrates providing PRMT6 with a unique substrate specificity (Hamey et al., 2021). Observations have been made for PRMT6 having both relaxed substrate specificity, due to PRMT6 methylating substrates of other PRMTs, and methylating unique substrates like H3R2me2a (Frankel et al., 2002; Hyllus et al., 2007). PRMT1, CARM1 and PRMT6 were found to all methylate p16, a cell cycle inhibitor showing shared substrate specificity.

Similar to other PRMTs, PRMT6's N-terminal region (1-86 amino acids) is essential in protein-protein interactions with PRMT substrate specificity potentially being modified by the sequence variability in the N-terminus; although this region is conserved between PRMT6 and PRMT1 (Sardo et al., 2013). It was also found that the N-terminal domain of PRMT6 is sufficient for specific protein interactions, like IRF3 (Zhang et al., 2019). Crystal structure analysis of PRMT6 bound to different substrates may further reveal structural features correlated with substrate binding preferences (Hamey et al., 2021). The importance of the N-terminal region has been implied both in its role concerning protein and substrate interactions and PRMT6's regulation of methyltransferase activity (Sardo et al., 2013; Winter et al., 2018).

Substrate binding occurs by an ordered sequential mechanism where the binding of the AdoMet cofactor precedes target substrate binding. The methylated substrate product is then the first to dissociate from PRMT6 followed by AdoHcy (Lakowski & Frankel, 2008). In contrast to this previous report, a rapid equilibrium random mechanism for AdoMet and substrate binding order was found (Obianyo & Thompson, 2012). AdoMet and the substrate both bind and release

in a random order, regenerating a free enzyme. During this enzymatic reaction described, there is potential to produce dead-end complexes if either an AdoHcy or ADMA substrate binds before both the original cofactor and substrate are released, resulting in unproductive enzyme/substrate complexes (Obianyo & Thompson, 2012). The rapid equilibrium random mechanism was further scrutinized with additional support of the ordered sequential mechanism found in other PRMTs (Frankel, 2012).

1.3.3 Regulation of PRMT6

As previously mentioned, one method of PRMT6 regulation occurs through both its dimerization and automethylation capabilities (Gupta et al., 2021; Lakowski & Frankel, 2008). PRMT activity has also been reported to be regulated by PTMs, although, there is a noticeable research gap regarding the regulation mechanism by PTMs on PRMT6. A potential regulatory mechanism regarding PTM of PRMT6 activity is present in the N-terminal tail where extensive modification is detected. Specifically, a monomethylation hotspot was found in the first 45 amino acid residues of the N-terminus of PRMT6, while phosphorylation PTM sites were found in and outside the N-terminal region (Winter et al., 2018). N-terminal tails of some PRMTs have been discovered to regulate methyltransferase activity influenced by PTMs present in the tail (Sayegh et al., 2007; Winter et al., 2018).

Regulation of PRMT6 RNA levels by microRNA (miRNA) was also uncovered in endometrial cancer cells. PRMT6 expression is downregulated by miR-372-3p's downstream targeting (N. Jiang et al., 2020). Another regulator of PRMT6 activity is through cofactors; PELP1 (transcription coregulator) and RUNX1 (transcription factor) bind PRMT6 in separate complexes and promote PRMT6 methylation of H3R2me2a (Herglotz et al., 2013; Mann et al., 2014). Given the widespread downstream effects of PRMT6 regulation, there is a necessity for

further research into novel regulators of PRMT6, such as miRNAs and cofactors. This will help bridge the knowledge gap on PRMT6 regulation compared to other more extensively researched PRMTs.

A recent study by Cao and colleagues discovered PRMT6 to be a novel substrate of PRMT1 through a heteromeric interaction; with PRMT1 acting as a negative regulator of PRMT6. PRMT1 methylates Arg106, suppressing the enzymatic activity of PRMT6, interpreted by decreased methylation levels of the PRMT6 substrate, histone H3 (H3R2me2a) (Cao et al., 2023). This insight into PRMT1 regulation of PRMT6 highlights the potential for PRMT crosstalk relationships as well as relates to redundancy found between PRMTs. Although limited, PRMT1 and PRMT6 share some substrate overlap (H4R3, NPl3, TOP3B), possibly contributed by their similarities in sequence and size (Cheng et al., 2020; H. Wei et al., 2014). CARM1 and PRMT6 are the only PRMTs that generate the H3R17me2a mark for epigenetic regulation. Global levels of this histone mark are not impacted by a CARM1 Knockout (KO), but reduced levels are seen with a double CARM1 and PRMT6 KO in mouse embryos. This shared methylation mark on histone 3 highlights a degree of redundancy in epigenetic regulation between these two PRMTs (Cheng et al., 2020). However, PRMT redundancy is limited in literature, emphasizing the importance of structural differences impacting the dynamic conformation during catalysis (Frankel et al., 2002; Gupta et al., 2021).

Northern blot examination uncovered two different PRMT6 transcript lengths attributed to varied 5’- or 3’-untranslated regions (UTR); potentially a result of absent alternative splicing in one of the PRMT6 transcripts (Frankel et al., 2002). The UTR is important in regulating both mRNA processes such as its localization, stability, and translation but also mediates protein features and protein-protein interactions regardless of amino acid sequence (Mayr, 2019). It is

then plausible that alteration to the UTR of the PRMT6 mRNA through alternative splicing (Frankel et al., 2002) impacts the self-regulation of PRMT6 mRNA.

The regulation of PRMT6 and its activity is ultimately dependent on an abundance of distinctive regulatory factors like automethylation, dimerization, PTMs, cofactors and mRNA modifications. Numerous regulatory factors of PRMT6 require further investigation to uncover the specific mechanisms involved.

1.3.4 Epigenetic Regulation

Arginine methylation is a crucial PTM contributing to epigenetic regulation through histone and non-histone proteins. Non-histone proteins like the nuclear estrogen receptor (ER) become coactivated by PRMT6 methyltransferase activity and stimulate transcription of the ER cofactor, GREB1 resulting in another form of epigenetic regulation (Z. Chen et al., 2022). Non-epigenetic regulation is also evident in PRMT6's role in signal transduction through PTEN methylation and subsequent PI3K-AKT cascade activation to promote cellular growth and survival (Feng et al., 2019). Epigenetic regulation by histones occurs through the modification of histone tails in the nucleosome, composing the structural support of DNA (Z. Chen et al., 2022). Histone tails are abundant in arginine residues providing a suitable target for ADMA (Di Lorenzo & Bedford, 2011). PRMT6 can act as an epigenetic regulator of gene expression through the methylation of histones (Z. Chen et al., 2022). PRMT6 is known for its role as a transcriptional repressor and the main enzyme to generate H3R2me2a as a repressive mark on histone H3 in inactive gene promoters (Gupta et al., 2021). The H3R2me2a repressive mark generated by PRMT6 facilitates chromosome condensation during mitosis through downstream recruitment of Aurora B. The H3 tail encompassing H3R2me2a preferentially binds Aurora B to phosphorylate Ser10 of H3 to modulate chromatin structure (S. Kim et al., 2020).

H3R2me2a global levels counteract the H3K4me3 activation mark in the promoter, but interestingly, H3K4me3 inhibits PRMT6 activity on the H3 histones (Di Lorenzo & Bedford, 2011; Dowhan et al., 2012). The transcriptional repression implemented by PRMT6 at H3R2me2a also expands to other sites of PRMT6 methylation such as histone 3 at Arg 17, and Arg42 (H3R17me2a, H3R42me2a), histone H2A at Arg26, and Arg29 (H2AR26me2a, H2AR29me2a), and H4 at Arg3 (H4R3me2a) (Gupta et al., 2021).

PRMT6 can also act as a transcriptional activator by generating an H3R2me2a modification on a gene's enhancer region. The presence of this modification on an associated active gene tends to exclude modification in the promoter; indicating that the genomic location of PRMT6 catalytic activity has a role in either transcriptional activation or repression (Gupta et al., 2021). Enhancer region H3R2me2a modifications influence adjacent histone modifications H3K4me1 and H3K27ac to promote transcription activation (Bouchard et al., 2018). A study by Yoshimatsu and colleagues looked at expression profiles after siPRMT6 transfection found PRMT6 to be a transcriptional regulator of RNA processing, DNA replication and cell cycle in lung and bladder cancer cell lines. Utilizing siPRMT6 resulted in altered gene expression in the expression profile resulting in growth suppression. PRMT6 overexpression in cancer cells consequently promotes DNA replication and cell proliferation, hallmarks of cancer (Yoshimatsu et al., 2011).

PRMT6's H3R2me2a modification negatively regulates DNA methylation by inhibiting UHRF1 chromatin association at histone H3 resulting in DNA demethylation (Veland et al., 2017). PRMT6 and UHRF1 upregulation and resulting elevated H3R2me2a also correlate with global DNA hypomethylation, an aberrant DNA methylation pattern in breast, lung and

colorectal cancer cells (Veland et al., 2017). Global DNA hypomethylation is implicated in oncogenic events such as genomic instability (Baylin & Jones, 2016).

1.2.5 Nuclear and Cytoplasmic Localization

Subcellular compartmentalization can result as a form of protein regulation by influencing protein function in cellular pathways dependent on its localization in the cell. For instance, distinct interactomes were found for PRMT1 isoforms dependent on the isoform subcellular localization. PRMT1v1 enriched mainly nuclear protein interactors and PRMT1v2 enriched cytoplasmic interactors affiliated with each isoform's corresponding localization and unique protein functions (Baldwin et al., 2015). This is comparable to the predominantly nuclear PRMT6 that functions as a transactivator of nuclear receptors and interacts with specific nuclear substrates, like histones, attributed to PRMT6's subcellular localization (Di Lorenzo & Bedford, 2011; Gupta et al., 2021).

As previously described, PRMT6 prefers basic residues around the target arginine, a characteristic found in the amino acid sequence of nuclear localization signals of proteins (Hamey et al., 2021). The PRMT6 substrates, HIV Tat and CDKN1A both have methylated arginine present in the nuclear localization signal ultimately regulating their localization (Hamey et al., 2021). PRMT6 methylates Tat at R52/53 to inhibit nucleolar retention (Fulcher et al., 2016). Similarly, the translocation of $p21^{CDKN1A}$ from the nucleus to the cytoplasm is regulated by PRMT6 arginine methylation at Arg156 by promoting $p21^{CDKN1A}$ phosphorylation (Nakakido et al., 2015). The hormone-binding portion of the estrogen receptor fused to PRMT6 in transgenic mice was found to translocate to the nucleus upon tamoxifen, a breast cancer drug treatment. The increase in the PRMT6-mediated H3R2me2a methylation mark was observed as a

consequence of the ER*-PRMT6 nuclear translocation, implying the self-regulating role of PRMT6 localization (Di Lorenzo et al., 2014).

1.3.6 Cell Cycle Regulation

PRMT6 contributes to cell cycle regulation via direct protein-protein interactions involving different pathways. First, transcription factors recruit PRMT6 to cell cycle-related genes due to PRMT6's inability to bind DNA alone. LEF1 facilitates PRMT6 binding to the central cell cycle regulator (Cyclin D1) (Schneider et al., 2021). LEF1 or PRMT6 KD reduces Cyclin D1 expression, increasing the G1 phase cell cycle population (Schneider et al., 2021).

Cell cycle regulators, and tumour suppressors, p21 and p16 are direct, repressive targets of PRMT6. Tumour suppressors are often repressed in human cancer leading to dysregulation of cell cycle progression observed with PRMT6 methylation of p21 at R156 inhibiting its growth-suppressive role (Poulard et al., 2016; Stein et al., 2012). Similarly, cell proliferation is induced following p16 methylation by PRMT6 resulting in decreased p16/CDK4 association (Poulard et al., 2016; X. Wang et al., 2012). These events describe specific tumour suppressors inhibited by PRMT6, removing cell cycle blockades, and ultimately contributing to tumour etiology.

1.3.7 DNA Repair

PRMT6 is involved in the DNA repair process by methylating DNA polymerase β's (Pol β) at Arg83 and Arg152. PRMT6 directly enhances Pol β's DNA binding and processivity and promotes cellular resistance in response to a DNA alkylating agent MMS that induces DNA strand breaks (El-Andaloussi et al., 2006). Although Pol β is a substrate of both PRMT1 and PRMT6, Pol β activity is only enhanced by PRMT6 to promote DNA damage repair (Brobbey et al., 2022; El-Andaloussi et al., 2006). In contrast, PRMT1-mediated methylation of Pol β functions as a termination signal to halt activity after repair. Therefore, Pol β is not a redundant

PRMT substrate and instead requires methylation by multiple PRMTs to execute diverse Pol β roles. Aberrant PRMT6 function may lead to altered DNA repair, genomic instability and higher disease risk including cancer (Brobbey et al., 2022).

1.3.8 PRMT6 Dysregulation

Dysregulation of PRMT6-protein interactions and histones can occur through PRMT6 up- or down-regulation causing deleterious effects. These effects can manifest as breast, prostate, colon, endometrial, ovarian and lung cancers (Gupta et al., 2021) and other disease pathologies, such as neurodegeneration of lower motor neurons (Scaramuzzino et al., 2015).

Overexpression of PRMT6 in spinobulbar muscular atrophy cells showed a toxic gain-of-function effect and subsequent neurodegeneration through PRMT6 methylation and activation of the mutant polyglutamine expanded androgen receptor. The mutant androgen receptor activity leads to selective lower motor neuron loss (Scaramuzzino et al., 2015). Like spinobulbar muscular atrophy, polyglutamine expansion in the huntingtin (HTT) protein contributes to Huntington's disease. PRMT6-mediated methylation of HTT is required for efficient axonal transport of vesicles and neuron viability (Migazzi et al., 2021). Loss of PRMT6 methylation impedes axonal trafficking by HTT, or augments similar characteristics observed in mutant polyglutamine expansion HTT. Interestingly, trafficking is rescued in diseased cells following PRMT6 overexpression (Migazzi et al., 2021).

Disease pathologies instigated by dysregulated PRMT6 can emerge as either PRMT6 downregulation or upregulation, as demonstrated in the following findings. Downregulated PRMT6 leads to increased HIV-1 production and viral infectiousness through increased transactivation of the PRMT6 substrate, Tat (Boulanger et al., 2005). PRMT6 upregulation is

implicated in cardiac hypertrophy contributing to cardiac disease through the H3R2me2a modification (Raveendran et al., 2020).

Cancer is a leading cause of death in the world with varying disease etiology. Identifying consistent molecular features such as the role of PRMTs in cancer can improve understanding of cancer pathology and potential future targeted treatments. One of these consistent features detected was reports of PRMT6 overexpression found in bladder, lung, breast (Poulard et al., 2016), colorectal, bladder, gastric, cervical, prostate and endometrial (Z. Chen et al., 2022) cancer cells. A study analyzing bladder, lung, and breast clinical cancer tissues exhibited PRMT6 overexpression compared to normal cells (Yoshimatsu et al., 2011). To investigate the role of the elevated PRMT6 expression, the authors used siRNA against PRMT6 to demonstrate suppressed cancer cell growth and revealed genes involved in the regulation of RNA processing and DNA replication from a pathway analysis for gene ontology methods. Various cancers may benefit from PRMT6 therapeutic targeting (Yoshimatsu et al., 2011). PRMT6 KD in prostate cells with reported PRMT6 upregulation revealed decreased cell viability, migration, and invasion of prostate cancer cells (Almeida-Rios et al., 2016). It has also been reported that gastric cancers with PRMT6 overexpression have a strong correlation to global H3R2me2a levels and tumorigenicity (Okuno et al., 2019).

PRMT6 downregulation is another type of dysregulation that impacts the cell's physiological processes observed in osteosarcoma, melanoma, hepatocarcinoma, ovarian cancer and invasive breast ductal carcinoma (Z. Chen et al., 2022). PRMT6-deficient osteosarcoma U2OS cells accumulate at the G2 checkpoint due to the upregulation of the direct PRMT6 transcriptionally repressed targets, p21 and p27 (Kleinschmidt et al., 2012). PRMT6 is downregulated in hepatocarcinoma cell lines and drives cancer stemness, promotes tumour

initiation and metastasis and decreases treatment potential (Chan et al., 2018). PRMT6 arginine methylation has also been described to functionally regulate the tumour-suppressor, PTEN by R159 methylation. Disruption of PTEN methylation by PRMT6 results in overactivation of the PI3K-AKT cascade leading to decreased apoptosis and increased proliferation, a characteristic of numerous cancers (Feng et al., 2019). PRMT6 regulation of the PI3K-AKT cascade was experimentally demonstrated when PRMT6 silencing in prostate cancer increased p21, p27, and CD44 and was associated with downregulation of the PI3K-AKT cascade (Almeida-Rios et al., 2016). Dysregulation of PRMT6 contributes to disease pathology and tumorigenesis in a myriad of cancer types. Understanding molecular features of PRMT6 in a broad disease context will better equip further investigation focused on PRMT6 involvement in breast cancer.

1.4 PRMT6 and Breast Cancer

Globally, breast cancer is the most prevalent cancer diagnosed in women with population-based incidence rates continuing to slowly increase (Roheel et al., 2023; Siegel et al., 2023). The American Cancer Society reports breast cancer to account for 31% of female cancers and is attributed as the leading cause of cancer death among women aged 20-49 years in the United States (Siegel et al., 2023). It is estimated that in 2023, there were 29,400 Canadian women diagnosed with breast cancer and about 18% of those women did not survive the breast cancer diagnosis (Canadian Cancer Society, 2023). Breast cancer can be differentiated by etiology, clinical screening and invasiveness; characteristics that contribute to the variation in risk factors and disease progression (Roheel et al., 2023).

A study found that 58.6% of breast tumour samples expressed high PRMT6 levels with a positive correlation with tumour stage (Phalke et al., 2012). PRMT6 depletion caused cell cycle arrest in MCF7 and MDA-MB-231 breast cancer cells (Phalke et al., 2012). Widely used for

replicability of human breast cancer, MCF7 cells are the most studied human breast cancer cell and MDA-MB-231 is the most studied triple-negative breast cancer cell (Lee et al., 2015; Wagner, 2022). Following cell cycle arrest induced by PRMT6 depletion, tumour growth was inhibited *in vitro* and *in vivo*. This loss of PRMT6 impedes its direct transcriptional repressor function on the p21 promoter resulting in upregulated p21 and induced cell cycle arrest through a p53-independent mechanism (Phalke et al., 2012). Similarly, another study found an increase in p21 expression after PRMT6 KD in MCF7 cells, attributed to the absence of PRMT6 transcriptional repressor function on the p21 promoter (Kleinschmidt et al., 2012). Contradictory to the previous studies, MCF7 cells overexpressing PRMT6 suppressed breast cancer cell proliferation, migration, and invasion. This decrease in tumorigenesis resulted from p21 and TSP-1 (Thrombospondin 1) induction through PRMT6 histone modification. PRMT6 upregulated TSP-1 and p21 expression promoting TSP-1 anti-migration effect and p21 cell growth suppression (N. H. Kim et al., 2013). Regardless of potential unidentified factors leading to these contradictory findings, PRMT6 remains of interest in the context of cancer proliferation.

Invasive breast ductal carcinoma was observed to have aberrantly downregulated PRMT6 mRNA levels compared to normal breast tissue. PRMT6-regulated gene signatures correlate to clinical outcomes observed with a PRMT6 KD in MCF7 cells affecting the transcription of 159 genes. This suggests PRMT6 dependent genes play a role in breast cancer disease progression (Dowhan et al., 2012). Dowhan and colleagues also revealed that PRMT6 regulates proteins involved in alternatively spliced transcripts in breast cancer demonstrated with a PRMT6 KD affecting alternative splicing of 449 genes. PRMT6 dysfunction and therefore aberrant alternative splicing of genes in cell death and cell cycle progression pathways may then contribute to breast cancer tumourigenesis (Dowhan et al., 2012).

Xenograph models utilizing NOD-SCID mice were injected with PRMT6 -knockdown or -overexpressing MDA-MB-231 cells and exhibited enlarged subcutaneous tumour growth, migration, and invasive potential (T. Yang et al., 2023). PRMT6 was reported to promote breast tumorigenesis through oncogenes demonstrated with reduced mRNA levels for tumour suppressor genes (BARD1, ETAA1, AXIN1, ARID1B, EED, TP53BP1, CASP8, and BCORL1) and increased mRNA levels for oncogenes (PRKCI, PIK3CB. ALT3, ETV1, FYN, IDH1, EGFR, and SETD1A) in PRMT6 overexpressing MDA-MB-231 cells. The opposite effect was seen with PRMT6 KD breast tumours, highlighting PRMT6 governance of key tumour regulatory genes (T. Yang et al., 2023). The same study discovered tumorigenic progression maintained by the interrupted tumour circadian clock. Specifically, the PRMT6/PARP1/CRL4B complex reduced the amplitude of circadian rhythms and circadian oscillations through transcriptional activity regulation. The prominence of PRMT6 as an oncogene was highlighted in its interference with circadian rhythm oscillation via the transcriptional-repression PRMT6/PARP1/CRL4B complex (T. Yang et al., 2023).

The discrepancy in PRMT6 dysregulation of differing breast cancer tumours was previously reported (Dowhan et al., 2012; N. H. Kim et al., 2013; Phalke et al., 2012; Yoshimatsu et al., 2011) and emphasizes breast cancer's disease heterogeneity and molecular variability. This heterogeneity was further observed in MCF7 breast cancer cell lines that were found to generate new variants or phenotypes in culture. Characteristics similarly found in breast cancer tumours (Leung et al., 2014). Further investigation into the molecular mechanisms contributing to PRMT6 dysregulation and similar breast cancer tumorigenesis variability is required. The disparity in reports for tumorigenic properties dependent on PRMT6 activity and

up- or downregulation can be partially attributed to specific cancer and cancer cell types (Gupta et al., 2021).

PRMT6's role in breast cancer cell migration, proliferation and invasiveness potential (Phalke et al., 2012; T. Yang et al., 2023) further reiterates PRMT6's involvement in breast cancer etiology and, therefore, the importance of researching PRMT6 molecular target therapy for potential future treatment. The evident association between PRMT6 and poor clinical outcomes (Dowhan et al., 2012) characterizes PRMT6 as a potential cancer biomarker.

1.4.1 MCF7 and MDA-MB-231 Breast Cancer Cell Lines

Breast cancer can be classified by molecular features affecting potential treatment approaches (Roheel et al., 2023). The majority of breast cancers have all three receptors present known as the estrogen receptors (ER), progesterone receptors (PR) and human epidermal growth factor receptor-2 (HER2). A smaller breast cancer subset will only have the ER/PR+ HER2- or ER/PR- HER2+ present (Leung et al., 2014). The receptors bind estrogens that are required for human breast epithelial cell growth and differentiation by regulating cellular responses through estrogen-responsive genes. Therefore, estrogen in excess can promote breast cancer development through altered cellular pathways or creating estrogen metabolite inducing oxidative stress (J.-Q. Chen & Russo, 2009). Therapies exploiting these molecular features include inhibition of estrogen, blocking estrogen-receptor interactions and impeding carcinogenic overexpression of HER2.

The commonly used MCF7 culture model is human breast cancer cells from metastatic adenocarcinoma cells and is recognized for possessing all three receptors (ER, PR and HER2). These estrogen-sensitive cells are heterogeneous with different class characterizations for

varying nuclear receptor expression. These cells also possess a non-aggressive and poorly invasive phenotype (Comşa et al., 2015).

Triple-negative breast cancer (TNBC) consists of approximately 15% of all diagnosed breast cancers and lacks the expression of all three receptors (ER/PR- or HER2-). The lack of molecular therapeutic targets in TNBC makes hormonal and receptor therapies ineffective, contributing to relapse and poor patient outcomes. With minimal treatment options, chemotherapy is the main course of treatment for TNBC (J.-Q. Chen & Russo, 2009). MDA-MB-231 is utilized as a TNBC cell culture model of invasive ductal carcinoma displaying invasive and metastatic properties in xenograft models (Chavez et al., 2010; Welsh, 2013). MDA-MB-231 cells were used to identify and investigate specific genes and pathways regulating their metastatic ability, unlike the non-metastatic MCF7 cells (Chavez et al., 2010). MCF7 and MDA-MB-231 breast cancer cells are widely used for replicability of estrogen-dependent or triple-negative breast cancers, respectively. The contradicting characteristics between breast cancer cell lines like MDA-MB-231 and MCF7 cells are imperative to research that differentiates the molecular mechanisms contributing to specific carcinogenic traits.

1.4.2 PRMT6 in MCF7 and MDA-MB-231 cells

Veland and colleagues reported PRMT6 expression in multiple human cancer cell types and PRMT6 upregulation to correlate with DNA hypomethylation. No correlation was seen between PRMT6 expression and DNA methylation in breast cancer cells. Instead, MCF7 cells with depleted PRMT6 restored DNA methylation (Veland et al., 2017). PRMT6 upregulation was typically detected in the tumorigenic breast cell lines, like MCF7, compared to the non-tumorigenic 76NF2V and MCF 10A. In comparison, some breast cancer cell lines did not follow this trend, as detected in the lower PRMT6 expressing MDA-MB-231 cell line. Both tumorigenic

MCF7 and MDA-MB-231 cell lines have differing PRMT6 expression, indicating a multifaceted and unspecified relationship between invasive potential, breast cancer cell subtype and PRMT6 expression (Veland et al., 2017).

1.4.3 PRMT6 and Nuclear Receptors

Regarding estrogen-sensitive MCF7 cells, PRMT6 is required for their proliferation stimulated by estrogen (Harrison et al., 2010). PRMT6 also enhanced ligand-dependent transcriptional activity of the ER, PR, and glucocorticoid receptor (GR). Further analysis found that PRMT6 functions as a coactivator for steroid-hormone receptors of nuclear receptors (Harrison et al., 2010). ER activity was repressed by a selective PRMT6 inhibitor, Licochalcone A, that impeded PRMT6-dependent H3R2me2 modification (Gong et al., 2021). Utilizing an PRMT6 inhibitor demonstrates the necessity of PRMT6's enzymatic activity required for receptor coactivation.

Oncogenic activity seen in gene expression signatures of PRMT6 is possibly mediated through ER signalling (Dowhan et al., 2012). In MCF7 cells PRMT6 mediates ER signalling by binding and activating the ER in the nucleus, independent of estrogen and PRMT6 methyltransferase activity. ER activation is further speculated to occur due to the ER release from the HSP90 chaperone complex following PRMT6 – ER binding (Y. Sun et al., 2014). In summary, PRMT6 has an important role in the coactivation of nuclear receptors in estrogen-sensitive breast cancer. PRMT6 binding nuclear receptors leads to a variation of functional outcomes which emphasizes PRMT6 as an interesting target in nuclear receptor-positive cells such as MCF7 cells.

1.4.4 PRMT6 Drug Targeting

Targeting PRMT methyltransferase activity can vary with different compound drug mechanisms. Inhibition of AdoHcy hydrolase results in the accumulation of intracellular AdoHcy due to feedback inhibition halting further methyltransferase reactions. Similarly, analogs for AdoMet also can be utilized to inhibit cellular methylation reactions (Bedford & Richard, 2005). Different inhibitors against AdoHcy hydrolase and AdoMet analogues are utilized to test therapeutic hypotheses by remedying aberrant expression and cellular roles imparted by dysregulated methyltransferases, like PRMT6. For instance, induction of cellular differentiation, activation of gene expression through increased expression of transcription factors, or repression of genes was observed following the implementation of the inhibitor (P. K. Chiang, 1998). However, both these methods target all enzymes, such as arginine and lysine methyltransferase, that use AdoMet and AdoHcy by-products and act with limited specificity (Bedford & Richard, 2005). Limited specificity can have unwarranted impacts on cellular methylation of proteins, small molecules, phospholipids, DNA and RNA (P. K. Chiang, 1998). The complex effects of these broad inhibitors encourage the pursuit of a more specific inhibitor for a viable therapeutic option.

Other inhibitors are more selective and may only target type I PRMTs like the inhibitor MS023. The MS023 inhibitor was revealed by x-ray co-crystal structure to bind the PRMT6 substrate arginine-binding site (Qian et al., 2018). Further, a PRMT6 inhibitor EPZ020411 is selective >100-fold over other PRMTs by also occupying the substrate arginine-binding site (H. Hu et al., 2016). Specificity for PRMT6 by EPZ020411 is attributed to a cyclobutoxy group on the inhibitor that is replaced by a smaller functional group with the MS023 inhibitor design (Samuel et al., 2021). MS023 is a broad inhibitor of type I PRMTs in contrast to the more potent

PRMT6 specific inhibition by EPZ020411, however, both inhibitors have a non-competitive mechanism to SAM and the peptide substrate determined by enzymatic activity assays (Ferreira de Freitas et al., 2016; H. Hu et al., 2016). MS117 is a potent, irreversible, cell-active, PRMT6 inhibitor that covalently binds and modifies PRMT6 for increased selectivity compared to noncovalent inhibitors (Shen et al., 2020). The progression to more specific and less toxic inhibitors is evident with the previously mentioned covalently binding MS117 inhibitor. The advantages of covalent inhibitors include improved efficiency, lower dose, less frequent dosing, and reduced drug resistance, all contributing to minimal off-target toxicity (Sutanto et al., 2020).

The competitive SAM binding would bind the same area annotated on the PRMT6 crystal structure to bind SAH (AdoHcy) or SAM (Figure 2), selective PRMT6 inhibitor, licochalcone A, was effective in MCF7 breast cancer cell toxicity by upregulating p53 expression, blocking the cell cycle and therefore cell proliferation and subsequent apoptosis. Importantly, licochalcone A was not toxic in MCF-10A human breast epithelial cells (Gong et al., 2021). Similar anti-cancer effects were seen with EPZ020411 decreasing glioblastoma cell proliferation via H3R2me2 methylation and subsequent CDC20 transcription (J. Wang et al., 2023). PRMT6 inhibitors show promising results in both cell and mouse models, but few PRMT inhibitors are being investigated in clinical trials except for PRMT1 and PRMT5 inhibitors (Zhu et al., 2024). With the rising popularity of utilizing inhibitors in cancer therapeutics, it is imperative to explore the efficacy of PRMT6 inhibitors for potential cancer treatment strategies alone or combined with other therapeutics.

1.4.5 Chemotherapy Resistance

Resistance to chemotherapeutic agents remains a constant barrier in treating patients with breast cancer. Various mechanistic features contribute to intrinsic resistance (present before chemotherapy) or extrinsic resistance (developed during treatment) (Coley, 2009).

Bortezomib, clinically known as the FDA-approved chemotherapeutic drug Velcade™, is a selective proteasome inhibitor that binds the 26S proteasome to prevent pro-apoptotic protein degradation (Adams & Kauffman, 2004). Although bortezomib can be used as an effective myeloma and hematological cancer treatment, some solid breast tumours can be refractory to bortezomib treatment (Fournier et al., 2010). The bortezomib-resistant MCF7 breast cancer cells induce autophagy and the unfolded protein response (UPR) as a resistance mechanism to promote cell survival (Milani et al., 2009). This is distinct from the bortezomib-mediated apoptosis of MDA-MB-231 cells.

PRMT6 methylation and transcriptional repression of p21 mediates reduced chemosensitivity leading to potential chemoresistance characteristics in cancer cells. Nuclear localization of p21 leads to its role in cell cycle arrest of cancer cells. PRMT6 induces p21 dysfunction by methylating p21 at Arg156, leading to p21 phosphorylation at Thr145 to inhibit nuclear translocation. The subsequent p21 cytoplasmic subcellular localization increases resistance to cytotoxic agents (Nakakido et al., 2015). PRMT6's coactivation of NF-κB and regulation of NF-κB target genes increases after stress induced by TNF-α stimulation. Coactivation promotes the NF-κB anti-apoptotic signalling pathway potentially imparting chemoresistance (Di Lorenzo et al., 2014).

Treatment failure is mainly attributed to chemotherapy resistance. The development of novel, effective chemotherapeutic agents remains an obstacle in combating resistance (Coley,

2009). Instead, targeted drug strategies for specific molecular mechanisms promoting resistance, like PRMT6, provide a more optimistic approach.

1.4.6 Stress Granules in the Stress Response

Stress Granules (SGs) are membraneless, cytoplasmic structures made of aggregating ribonucleoprotein (RNP). These RNP also include stalled translating mRNA and pre-initiation complexes (Campos-Melo et al., 2021). Although the molecular mechanisms encompassing assembly and disassembly of SGs are not fully understood it remains a distinctive characteristic of SGs. Assembly occurs due to liquid-liquid phase separation (LLPS) promoting the compartmentalization of biomolecules into an organelle in the absence of a membrane (Guzikowski et al., 2019). A concentrated condensed phase is surrounded by a larger, more diluted phase. This phenomenon occurs when the interaction energy of condensing RNP is more thermodynamically favoured compared to the entropic energy required for a homogenous macromolecule mixture (Guzikowski et al., 2019). LLPS dynamics are driven by multivalent proteins, intrinsically-disordered protein regions (Hofmann et al., 2021), and weak electrostatic, hydrophobic, and homo- and heterotypic protein interactions (Campos-Melo et al., 2021).

Cellular stress and exposure to adverse environmental conditions can elicit SG formation as a cell survival tactic by altering gene expression through the accumulation of RNP to impede translation (Guzikowski et al., 2019). The cellular reprogramming that occurs for SG formation results in repression of general translation to conserve cellular energy for the translation of critical survival and gene repair (Guzikowski et al., 2019). SGs preferentially accumulate non-translating mRNAs, but recently it was found that translating mRNA useful to cell survival pathways also localized to SGs cell and can shuttle in and out of SGs (Mateju et al., 2020). Tactfully cells induce SG formation as a stress response to subsequently reinitiate cellular

homeostasis while reducing proliferation. The composition of SG is also found to be dependent on the stress and cell type (Guzikowski et al., 2019). Some proteins exhibit changes in phase separation and SG association was determined to be regulated by arginine methylation. FUS (fused in Sarcoma protein) when arginine methylated displayed reduced LLPS and SG association of FUS (Hofweber et al., 2018). FUS mutations result in unmethylated FUS that promotes SG association and potentially contributes to FUS aggregation in motor neurons, a pathological hallmark of ALS (Hofweber et al., 2018). The dynamic composition and regulation of SG formation mechanisms emphasize the strategies utilized in the stress response to promote cell survival.

1.4.7 Stress Granules in Bortezomib Treated Breast Cancer

Adverse environmental stimuli such as heat shock, oxidative stress, viral infection, osmotic stress, UV irradiation, hypoxia, and nutrient starvation can induce SG formation (Guzikowski et al., 2019; Hofmann et al., 2021). Chemical inhibitors, like the previously mentioned drug bortezomib, have also been shown to induce SG formation after treatment. SG formation triggered by bortezomib involves the canonical eIF2α-dependent pathway by inducing eIF2α phosphorylation at Ser51 by HRI to promote refractory cancer tumours (Fournier et al., 2010; T. Hu et al., 2022). Phosphorylation of eIF2α by other kinases like PKR and PERK is dependent on the type of stressor type (F. Wang et al., 2020). A second process of SG assembly can transpire by a non-canonical eIF2α-independent pathway initiated by inhibition of the eIF4F complex (Fournier et al., 2013). One form of this eIF4F complex inhibition triggered by mitochondrial stress was observed with eIF4E and eIF4G1 translation initiation factor dissociation leading to SG formation through the eIF2a independent pathway (F. Wang et al., 2020). Interestingly, the eIF4E-eIF4G1 association plays a role in both pathways; when induced

by bortezomib the canonical eIF2α-dependent pathway accumulates stalled eIF4E-eIF4G1 factors eventually leading to SG assembly (Fournier et al., 2013) (Figure 3). Although the canonical and non-canonical pathways both involve eIF4E and eIF4G1, different translation initiation factor mechanisms comprise each pathway that leads to translation arrest and SG assembly.

The tumour microenvironment has dynamic stress conditions like hypoxia and nutrient starvation that trigger SG formation in cancer cells (Anderson et al., 2015). Core components that constitute SGs regulate oncogenesis through cellular signalling pathways involved in cancer cell proliferation, invasion and metastasis (Li et al., 2023). The stress induced by chemotherapy promotes the formation of SG in the breast tumour microenvironment (M. Hu & Polyak, 2008). Stress induced by the tumour microenvironment or chemotherapeutics leads to context-dependent SG formation influenced by the stress response pathway (Guzikowski et al., 2019). Following initial SG formation, further SG regulation occurs to promote cellular adaptation. This regulation in tumour cells includes anti-apoptotic and oncogenic mechanisms governed partly by SGs (Anderson et al., 2015; M. Hu & Polyak, 2008). Similarly, MCF7 breast cancer cells potentially utilize SG formation to foster its resistance against bortezomib. Inhibition of SG formation in MCF7 cells increased bortezomib efficacy, indicating an association between bortezomib resistance and SG formation (Christen et al., 2019). SGs promoting bortezomib resistance suggest a novel avenue for therapeutics that can be used in combination therapy along with FDA-approved chemotherapy treatments for wider use. Investigating the molecular mechanisms behind SG formation and therefore bortezomib resistance will create new avenues for improved drug targeting.

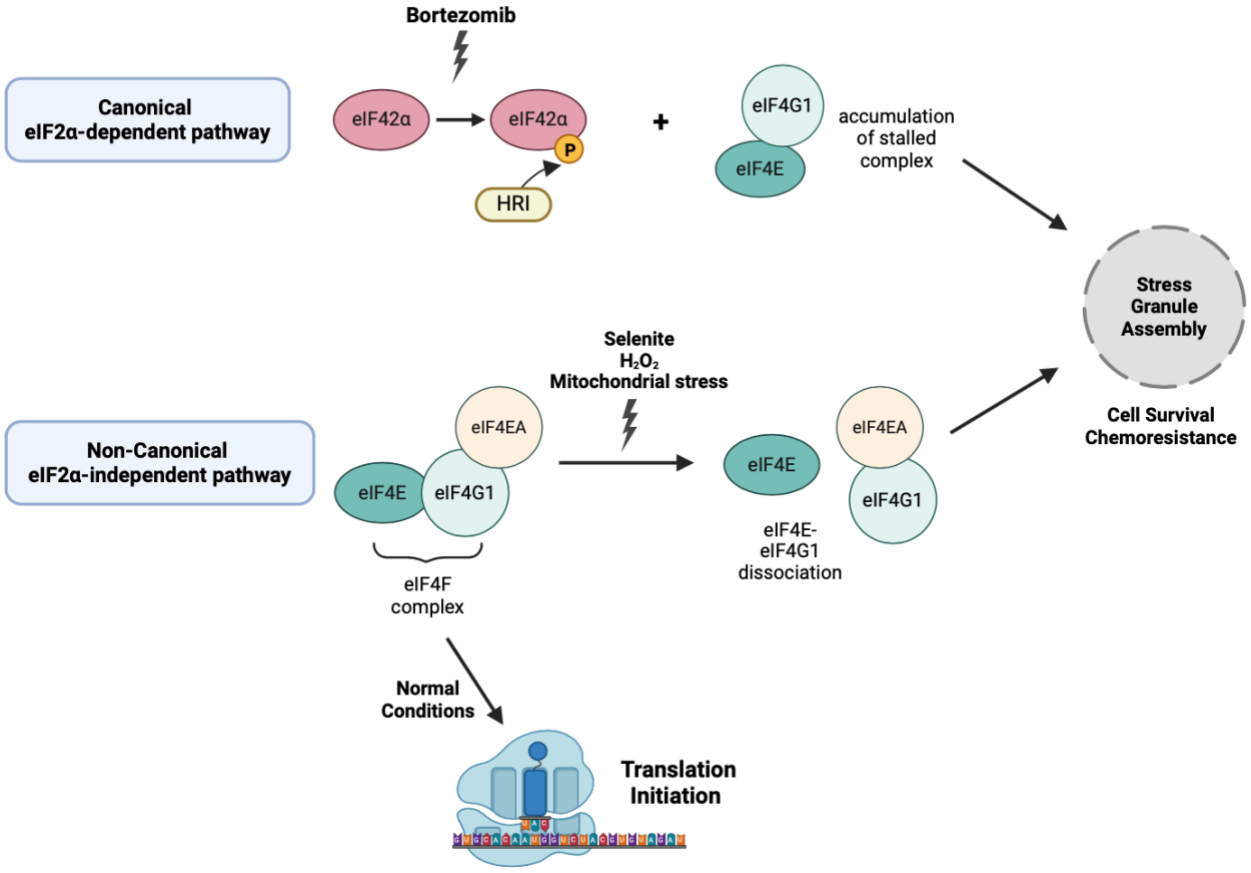

Figure 3: The eIF2α -dependent and independent pathways of stress granules assembly.

Bortezomib-induced SG formation is an eIF2α-dependent process that results in eIF2α phosphorylation by HRI and eIF4E and eIF4G1 stalled complex accumulation. Other stressors (i.e. Selenite, H2O2, and mitochondrial stress) induce an eIF2α-independent pathway for SG assembly resulting in eIF4E and eIF4G1 dissociation and translational arrest. SG assembly supports chemoresistance by promoting cell survival. The figure is adapted from published graphical abstracts (Fournier et al., 2013; F. Wang et al., 2020). Created with BioRender.com.

1.4.8 PRMT6 and Stress Granule-Induced Chemoresistance

Arginine methylation is an important PTM regulating protein-protein or protein-RNA interactions that influences SG assembly and disassembly (Hofmann et al., 2021; Lorton & Shechter, 2019). The recruitment or retention of arginine methylated proteins to SGs requires methylation in the protein's GAR domain for their proper localization (De Leeuw et al., 2007; Y.

Yang & Bedford, 2013). A methylation-deficient version of the PRMT6 substrate TOP3B exhibited reduced SG localization compared to the wild type (WT) control (Huang et al., 2018).

Previously, our lab investigated the role of PRMT6 in bortezomib resistance through its involvement in SG formation. Bortezomib treatment induced PRMT6 overexpression and SG formation, an effect that was lost through KD of PRMT6 in HeLa cells (A. J. Morettin, 2015). PRMT6 depletion inhibits SG formation and cellular survival after bortezomib treatment in MCF7 and HeLa cells. Bortezomib-induced SG formation could then be partially rescued in PRMT6 depleted HeLa cells after the re-introduction of PRMT6 (A. J. Morettin, 2015). The bortezomib-sensitive MDA-MB-231 cells, in contrast, do not form SG after bortezomib treatment and remain unaltered by PRMT6 depletion (A. J. Morettin, 2015). Different cancer or breast cancer cell lines vary in their ability to form SGs, or the type of stressor that initiates their formation. The discrepancy in this stress response indicates the varying but sophisticated regulation of SG formation (T. Hu et al., 2022).

The mechanism by which PRMT6 promotes SG-induced chemoresistance is through the downregulation of eIF4E. PRMT6 depletion inhibited the eIF4E-eIF4G1 complex formation, and SG formation and decreased cell survival in bortezomib-treated cells (A. J. Morettin, 2015). This is consistent with findings by Fournier and colleagues that demonstrated eIF4E depletion impaired bortezomib-induced SGs, and SG formation is required for bortezomib chemoresistance (Fournier et al., 2013).

1.5 ADAR1 Enzyme

Adenosine deaminase acting on RNA (ADAR1) is an enzyme prevalent in the RNA editing process to generate RNA diversity. ADAR1 recognizes double-stranded RNA and destabilizes it through site-specific deamination of adenosine (Kung et al., 2021). Specifically,

the PTM occurs when ADAR1 catalyzes the deamination of adenosine to inosine. A- to I- editing ultimately inhibits the ability of uracil pairing to the previous adenosine site to disrupt double-stranded RNA structures (Kung et al., 2021; Sagredo et al., 2018).

ADAR1 is expressed as either the predominantly nuclear p110 isoform (110 kDa) or the predominantly cytoplasmic p150 isoform (150 kDa). ADAR1 p150 is capable of nuclear-cytoplasmic shuttling, credited to the presence of a nuclear export signal in its Zα domain that is not present in ADAR1 p110's truncated N-terminus (Figure 4). Localization of either isoform may alter RNA target or protein binding selectivity (T. Sun et al., 2021). Another isoform distinction is the p110 isoform being constitutively expressed in contrast to the type I interferon (IFN) inducible ADAR1 p150 isoform. Decoupling expression of the two isoforms revealed that ADAR1 p150 edits a broader range of target sites compared to p110 (T. Sun et al., 2021).

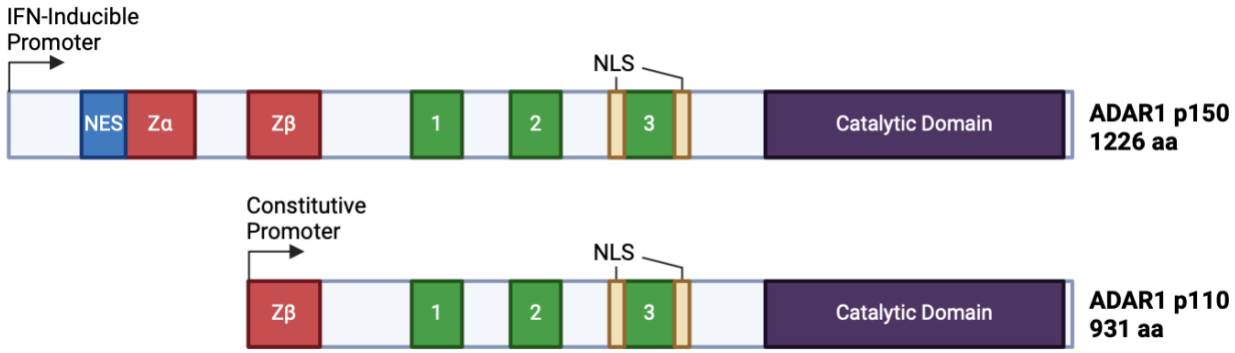

Figure 4. ADAR1 Protein Domains of Isoforms p150 and p110.

Protein Domains of ADAR1 isoforms. ADAR1 p150 has IFN-inducible promoter. ADAR1 p110 has constitutive promoter starting in the Zβ domain. Red domains are Z-DNA-binding domains, blue is nuclear export signal (NES), yellow is nuclear localization signal (NLS), green is dsRNA-binding domains, and purple is the catalytic domain. This figure is adapted from published figure (Ashley et al., 2024). Created with BioRender.com

1.5.1 ADAR1 and Breast Cancer

ADAR1's increased expression and therefore increased RNA editing is prevalent in breast cancer, responsible for tumour development and contributes to poor prognosis (Kung et al., 2021; Paz-Yaacov et al., 2015). ADAR1 introduces transcriptomic diversity, proteomic diversity, and RNA mutations through its targets in breast cancer (Fumagalli et al., 2015; Paz-Yaacov et al., 2015; Peng et al., 2018). The increased editing was found in 3'UTRs and exonic regions in targets of cancer-relevant pathways further specifying ADAR1's function in breast cancer (Sagredo et al., 2018).

1.5.2 ADAR1 and Stress Granules

ADAR1 p150's N-terminal Z-DNA binding domain (ZDBD) is sufficient for its localization to SGs induced by oxidative stress and IFNs. Additionally, ADAR1 p150 also requires Z-RNA or Z-DNA bound to ZDBD to localize to SGs. The absence of the ZDBD in ADAR1 p110 prevents its ability to localize to SGs (D. C. Chiang et al., 2021; Ng et al., 2013).

ADAR1's inhibitory role on SG formation was demonstrated with ADAR1 KD cells exhibiting increased IFN-induced SG formation. ADAR1 inhibits SG formation through translation inhibition and repressing PKR activation which is important for stress-dependent eIF2α phosphorylation (Corbet et al., 2021; John & Samuel, 2014). Further investigation uncovered a separate mechanism for ADAR1 inhibition of SG formation by modulating mRNPs and dsRNA-binding activity that is independent of deaminase activity (Corbet et al., 2021).

The type I IFN inducible ADAR1 p150 isoform also acts as a negative regulator by suppressing type I IFN production and signalling, demonstrating ADAR1's ability to suppress the stress response through multiple strategies (John & Samuel, 2014).

ADAR1 p110 suppresses apoptosis after its export from the nucleus in stressed cells. Export occurs after stress-activated phosphorylation by MKK6–p38–MSK MAP. ADAR1 p110 acts to protect anti-apoptotic gene transcripts by antagonizing Staufen1 binding and mediated mRNA decay (Sakurai et al., 2017).

1.5.3 ADAR1 and PRMT6

Mouse brain and embryo were assessed for ADAR1 ADMA sites and found to have methylation on Arg -30, -42, -55, -79, and -88 but lacking GAR domains (Guo et al., 2014); while ADMA is the PTM that could be catalyzed by PRMT6, it typically prefers methylating in a GAR domain (Di Lorenzo & Bedford, 2011). Although the GAR domain is preferred, other arginine methylation motifs including ones with SR- and DR-rich peptides were found to be robustly arginine methylated by PRMT6 (H.-H. Wei et al., 2021). ADAR1 is not a confirmed PRMT6 interactor or substrate, but ADAR1's GAR domains are an intriguing indication of a potential PRMT6 substrate.

1.6 Investigating Novel PRMT6 Interactors

Understanding PRMT6's binding partners will help elucidate the complex cellular pathways and protein interactions that PRMT6 is involved in. Identification of PRMT6 interactors or substrates in a physiologically relevant context remains a challenge. Previously, there have been studies for screenings of PRMT6's potential interaction partners utilizing *both in vitro* and *in vivo* methods (Frankel et al., 2002; Sardo et al., 2013). PRMT6 kinetic studies identified high catalytic activity and substrate dissociation rates (Frankel & Brown, 2019), making it difficult to accurately detect all biological relevant interactions using typical protein-protein detection methodology. Large-scale MCF7 cell proteomic work by the Côté laboratory characterized a greater proportion of novel PRMT6 substrates utilizing inhibitors with SAM-like

structures to compete for the SAM binding site of PRMT6. Utilizing a small molecular inhibitor prevented PRMT6 substrate methylation and lower dissociation rates, followed by an affinity purification and mass spectrometry approach (AP/MS) for novel substrate identification (A. Morettin et al., 2020). Substrates are only a portion of total PRMT6 interactors, considering non-methylated protein-protein interactions can be transient as well. Utilization of improved methods to investigate PRMT6 transient substrate and non-substrate protein interactors and potential regulators is still required in a physiologically relevant breast cancer cell context.

1.6.1 Proximity-dependent Biotinylation Labelling

The functional protein network is a necessity to thoroughly understand breast cancer disease pathology related to PRMT6. Previous techniques do not fully reveal how PRMT6 protein-protein interactions operate in complex disease processes. BioID (proximity-dependent biotin identification) aids detection of transient or weak interactions for mapping live cell protein networks. Unlike conventional methods for protein interaction screening, BioID utilizes relevant biological settings that include the proper PTM machinery, binding partners, molecular chaperones, and insoluble proteins that once remained elusive using previous techniques (Roux et al., 2012). BioID evades these limitations providing a more complete interactome dataset retrieval.

BirA (35 kDa) is an *Escherichia coli* biotin protein ligase, designed by Roux et al., 2012, that can be fused to the protein of interest being researched (PRMT6). The biotin ligase fusion protein when introduced into mammalian cells will selectively biotinylate proximate or interacting proteins with PRMT6 that is dependent on availability of free biotin supplemented in the cell culture media during a defined time frame. Biotinylated proteins can be isolated with AP methods and further identified and analyzed by MS or immunoblot methods (Figure 5) (Roux et

al., 2012). This technique can be utilized to monitor PRMT6 protein interactions in live MCF7 and MDA-MB-231 breast cancer cells while potentially revealing specific cellular disease contexts related to varied bortezomib treatment responses. Identifying novel PRMT6 candidate interactors may also reveal potential cellular functions of PRMT6 previously unknown.

A systematic survey of PRMT interactomes has been previously completed with BioID AP/MS methods in HEK293T cells thus determining the PRMTs interactome and substrates based on analyzing enriched arginine methylation motifs (H.-H. Wei et al., 2021). Another study in BirA-PRMT6 transfected lymphoblast cells completed BioID AP/MS experiments and found ADAR1 as an enriched SILAC-analysed protein, provided in supplemental data. Following this result, no further validation was pursued for ADAR1 as a potential PRMT6 interactor (Schneider et al., 2021). Although the BioID method has been used for PRMT6 interactome investigation, evidence is absent for PRMT6-ADAR1 interactions in MCF7 or MDA-MB-231 cells with further validation by other methods such as immunoprecipitation.

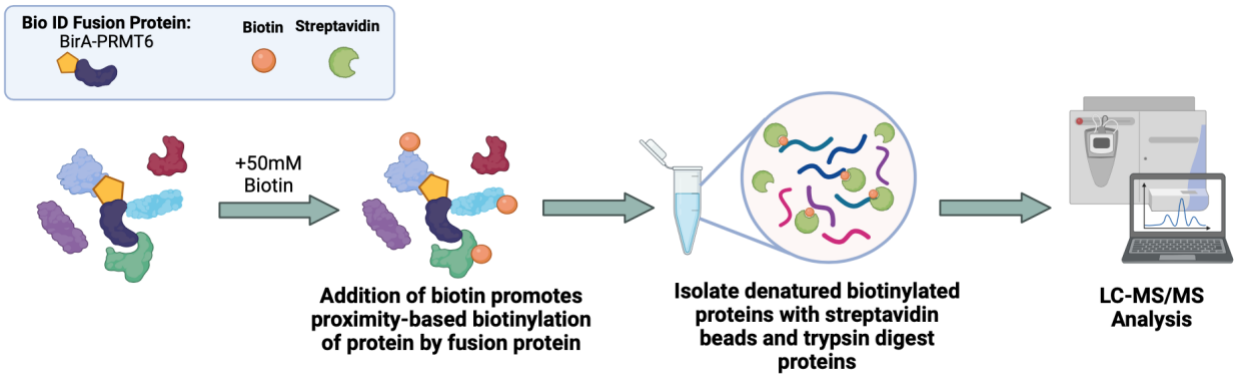

Figure 5: Proximity-dependent biotinylation labelling method (BioID).

The PRMT6-BirA fusion protein ectopically expressed in cells enables the biotinylation of proteins in proximity to the fusion protein with the biotin ligase. This method is utilized for physiologically relevant, protein-protein interaction identification that benefits both stable or weak and transient protein interactions without the limitation of the protein's continued

proximity or binding affinity to each other. Biotinylated proteins can be isolated with streptavidin beads for further MS analysis for protein identification. Created with BioRender.com.

1.7 Rationale, Hypothesis, Objectives and Significance

1.7.1 Rationale

Currently, breast cancer is the leading cause of death among young female adults which can be partly attributed to the variation in breast cancer etiology and refractory tumours (Siegel et al., 2023). Understanding the molecular landscape of breast cancer pathology is key for a molecular targeting treatment strategy in tumours to increase the chemotherapy response (N. Wang et al., 2023). Our lab has observed a role for PRMT6 in SG formation, which could represent a chemoresistant mechanism used by the MCF7 breast cancer cells. Depleting PRMT6 prevents SG formation and decreases cell viability in the presence of bortezomib in MCF7 cells but not MDA-MB-231 cells (A. J. Morettin, 2015). This indicates potential mechanistic changes with PRMT6 that are cell-type dependent concerning the SG formation. Revealing the mechanistic changes will begin with further investigation of PRMT6-protein interactions relating to the stress response.

1.7.2 Hypothesis

The protein arginine methyltransferase 6 (PRMT6) interacts with proteins or other substrates that contribute to stress granule formation and/or breast cancer tumour formation and resistance to chemotherapies.

1.7.3 Objectives

1. Identify candidate proteins that interact with PRMT6 in breast cancer cells.

Aim 1.1: Identify potential interactors and substrates of PRMT6 using SILAC quantitative mass spectrometry combined with BioID.

Aim 1.2: Validate interactions between PRMT6 and potential interacting candidate proteins.

2. Determine if interactors are PRMT6 substrates regulated through methyltransferase activity.

Aim 2.1: Identify if validated interacting proteins are PRMT6 arginine methylated substrates *in vitro*.

1.7.4 Significance

PRMT6 can promote breast tumour development through metastasis, invasion, and drug resistance mechanisms. Identifying specific molecular functions of PRMT6 in breast cancer will help us understand its specific disease function in crucial cellular pathways. One aspect of this research is exploring novel interactors and potential substrates of PRMT6. Elucidating the underlying molecular mechanism associated with PRMT6 and how it contributes to breast cancer prognosis and resistance through SG formation can provide support to improve existing and novel anti-tumour therapeutic targets for breast cancer.

Chapter 2: Materials and Methods

2.1 Mammalian Cell Culture

HEK293T, MDA-MB-231, MCF7 and HeLa cell lines were purchased from the American Type Culture Collection. The cells were cultured in Dulbecco's Modified Eagles Medium (DMEM) (319-015-CL; Wiset) with 10% fetal bovine serum (FBS) (080150; Wisent) and 1% penicillin-streptomycin (SV30010; Cytiva). The MCF7 cell line was supplemented with 3.75ug/mL Insulin-Transferrin-Selenium-A (51300044; Thermo-Fisher). Cells were grown in 10cm or 6-well polystyrene dishes at 37^{o}C and 5% CO_2. Cells were regularly monitored for mycoplasma using a mycoplasma detection kit (G238; abm).

2.2 Cloning and PCR

PRMT6 was sub-cloned into the pLVX-TetOne doxycycline-inducible vector with a puromycin resistance marker (631849 Clontech) containing a Myc-tagged BirA on the N-terminus. The PRMT6 insert was amplified from the pEGFP-PRMT6 plasmid using forward ataagaatgcggccgcatgtcgcagcccaagaaa and reverse gccgcggatcctcagtcctccatggcaaag primers with PCR. The pLVX-TetOne-BirA vector was digested using BamHI (R0136S; New England BioLabs) and NotI-HF (R3189S; New England BioLabs) restriction enzymes and CIP to keep digested plasmid in open conformation for PRMT6 insertion. The digested pLVX-TetOne-BirA and PRMT6 insert were ligated to make the final recombinant plasmid product. The recombinant product was transformed before DNA purification. The primers for sequencing pLVX-Myc-BirA-PRMT6 are forward gcttatgtaaaccagggcgc, forward agcaggacggaatcatcaag, and reverse tgacggccctcctgtcttag primers to confirm the construct's DNA sequence and verify the gene insert with Sanger sequencing by Génome Québec (Figure 7).

2.3 Transformation

DH5α cells were transformed with pLVX-TetOne-BirA-PRMT6 to propagate the product. DH5α competent cells were first incubated with the pLVX-TetOne-BirA-PRMT6 DNA product using heat shock at 42ºC and incubated in a shaking incubator at 37ºC in SOC for 1 h. After incubation, cells were transferred to 100µg/mL ampicillin LB plate overnight. Transformed colonies were amplified in LB containing 100µg/mL of ampicillin to complete DNA purification with kits for miniprep (K210010; Promega) or maxiprep (K210007; Promega).

2.4 Generation of Stable Cell Lines with Tet-One Inducible Expression

Stably expressing MCF7, MDA-MB-231 cell lines were established by lentiviral transduction. HEK293T were transfected with packaging plasmids pMD2.G (12259 Addgene), psPAX2 (12260 Addgene) and 10µg of the expression plasmid plvx-TetOne-BirA or plvx-TetOne-BirA-PRMT6. After 72 h incubation, lentivirus was collected and filtered through a Millex-HV 0.45µm syringe filter (SLHV033RS; Millipore). Target cells were transduced with lentivirus media diluted 2:1 with normal cell culture media with 8µg/ml polybrene. Selection with 2µg/ml puromycin was used to maintain stable cell pools 48 h post-transduction. BirA or BirA-PRMT6 construct was induced with 0.5µg/mL doxycycline (10592-13-9; Fisher) for 48 h.

2.5 Protein Preparation, SDS-PAGE, and Immunoblotting

MDA-MB-231 and MCF7 cells were washed twice with cold 1X PBS and subsequently harvested and lysed by scrapping in freshly prepared cold RIPA lysis buffer (50mM Tris-HCl pH 7.5, 150mM NaCl, 1% NP-40, 0.5% deoxycholate, protease inhibitor cocktail (04693159001; Roche)) and lysate then incubated on ice for 20 min with intermittent vortexing. Lysates were centrifuged at 21,300x g for 15 min at 4ºC. The supernatant's protein concentrations were determined by Bradford Assay (5000112; Bio-Rad DC Protein Assay). The total protein amount

was normalized for each sample, 5X laemmli reducing buffer was added (25% glycerol, 125mM Tris-HCl pH 6.8, 4mM SDS, 700mM β-mercaptoethanol, 0.1% bromophenol blue) and samples were boiled at 95°C for 10 min. Proteins were resolved on a 10% polyacrylamide gel by SDS-PAGE using 1X SDS running buffer (0.1% SDS, 0.2M Glycine, 25mM Tris-Base) at 180V for about 60 min. The separated proteins in the gel are transferred with 1x transfer buffer (0.01% SDS, 0.2M Glycine, 25mM Tris-Base) onto a nitrocellulose membrane (Bio-Rad; #1620115). Blocking of the membrane is completed with 5% non-fat milk powder in 1X PBS containing 0.05% Tween-20 (PBS-T), for 1 h at room temperature. Membranes were incubated with primary antibody diluted in antibody solution (10mM Tris pH 7.5, 150mM NaCl, 0.25% Gelatin, 0.05% Tween-20, 0.05% sodium azide) for at least 90 min before 3 x 5 min washes with PBS-T and incubated 1 h with the secondary antibody followed by 3 x 5 min washes. Protein detection with chemiluminescent luminata Crescendo Western HRP Substrate (WBLUR0500; Millipore) when required before being imaged using the ChemiDoc MP Touch Gel Imaging System (12003154; Bio-Rad). Antibody details are listed in Table 1.

To complete cellular fractionation a mild detergent buffer (20mM Tris pH 7.5, 10mM KCl, 3mM $MgCl_2$, 0.1% NP-40, 10% glycerol and protease inhibitor cocktail (04693159001; Roche)) was used to break open cells and pellet nuclei and other fragments after lysates were centrifuged at 1350x g for 10 min at 4°C. Supernatant is retained for cytoplasmic extract and RIPA buffer (50mM Tris-HCl pH 7.5, 150mM NaCl, 1% NP-40, 0.5% deoxycholate, protease inhibitor cocktail (04693159001; Roche)) added to supernatant for final clearing step after centrifugation step 2800x g for 10 min at 4°C. Nuclear Extract pellet is resuspended in S1 buffer (0.25M sucrose, 10mM $MgCl^2$) and layered over S2 buffer (0.88M sucrose, 0.5mM $MgCl^2$) and centrifuged 2800x g for 10 min at 4°C. The pellet containing purified nuclei is resuspended in

RIPA buffer (50mM Tris-HCl pH 7.5, 150mM NaCl, 1% NP-40, 0.5% deoxycholate, protease inhibitor cocktail (04693159001; Roche)) and sonicated (6 x 10 sec pulses, 10 sec rests between). Final clearing step with centrifugation at 2800x g for 10 min at 4°C.

2.6 Immunoprecipitation

Specific protein preparation and SDS-PAGE details are as earlier described. Cells were lysed in 1% Triton lysis buffer (10mM Tris-HCl pH 7.5, 150mM NaCl, 1% Triton X-100, protease inhibitor cocktail (04693159001; Roche)) or RIPA lysis buffer (50mM Tris-HCl pH 7.5, 150mM NaCl, 1% NP-40, 0.5% deoxycholate, and protease inhibitor cocktail (04693159001; Roche)). Inputs of 1-5% were saved from protein extract. Lysates were then pre-cleared with A/G agarose bead slurry (sc-2003; Santa Cruz) in a final volume of 1mL for 30 min at 4°C before incubation with 7µg/mL of the PRMT6 antibody (A300-928A; Bethyl Laboratories) or IgG rabbit antibody (sc2027; Santa Cruz) control for 2 h at 4°C. Immuno-protein complexes were isolated using agarose A/G bead slurry (sc-2003; Santa Cruz) incubated for 1 h. Beads were washed 4X with lysis buffer before samples were prepared for SDS-PAGE and western blotting (WB) described previously.

2.7 SILAC-based BioID and Mass Spectrometry (LC-MS/MS) Protein Identification

MDA-MB-231 and MCF7 cells stably expressing either the biotin ligase alone (BirA) or fusion protein BirA-PRMT6 were differentially labelled with light media containing essential amino acids, Arg0Lys0 (R0K0) or the heavy media containing isotopic Arg10Lys8 (R10K8) (Cambridge isotope Laboratories) supplemented with dialyzed fetal bovine serum, and penicillin/streptomycin. Cells are grown for 5-10 cell doublings (about 14 days of culture) in SILAC media for amino acid incorporation into cellular proteins. BirA or BirA-PRMT6 construct expression was induced with doxycycline. Doxycycline at 0.5ug/mL and excess biotin

at 50μM (B4639; Sigma) were added to the cell media 48 h and 24 h, respectively before each 10cm plate of cells was harvested at 85% confluency. Cells were harvested by scrapping in high salt RIPA buffer (50 mM Tris pH 7.5, 500 mM NaCl, 1% NP-40, 0.5% deoxycholate, protease inhibitor cocktail (04693159001; Roche)) before snap-freezing and short-term storage at -80ºC. Rapidly thawed cell lysate at 37ºC underwent sonication to disrupt cellular membranes and normalize the total protein extract amount per sample before decreasing the salt concentration to 250mM and pre-cleared 10 min with Protein A/G Agarose beads (sc-2003; Santa Cruz). Affinity purification was completed with streptavidin-sepharose beads (17511301; Cytiva) 4ºC, 4 h incubation was used to optimize biotinylated protein capture. After incubation, beads from both BirA and BirA-PRMT6 conditions were combined for each cell line during washes, followed by protein elution from beads with buffer 2% SDS, 30 mM biotin. Eluted protein samples with 4x LDS were loaded and resolved on a 10% NuPage™ Bis-Tris Gel (NP0301BOX; Thermo-Fisher) by electrophoresis. The gel was stained with SimplyBlue™ SafeStain (LC6060; Thermo-Fisher) Coomassie to visualize protein bands in each lane. Half of the lane was cut into 5 2x1 mm gel sections therefore providing only half the total protein to be submitted for analysis. Samples were submitted to the Ottawa Hospital Institute Proteomics Core Facility (OHRI) to be trypsin digested (Promega) following the protocol by Shevchenko (Nat Protocols 2006; 1(6):2856-60) and LC-MS/MS, HCD 45% was performed using a Dionex Ultimate 3000 RLSC nano HPLC (Thermo Scientific) and Orbitrap Fusion Lumos mass spectrometer (Thermo Scientific) with a FDR of <2%. Proteomics analysis to infer protein identities was completed with MASCOT software version 2.8.2 (Matrix Science, UK) and data was searched using 1 missed cleavage. The raw data files provided by OHRI were analyzed by MaxQuant software V2.4.9 and searched against the Human UniProt Database (proteome ID UP000005640).

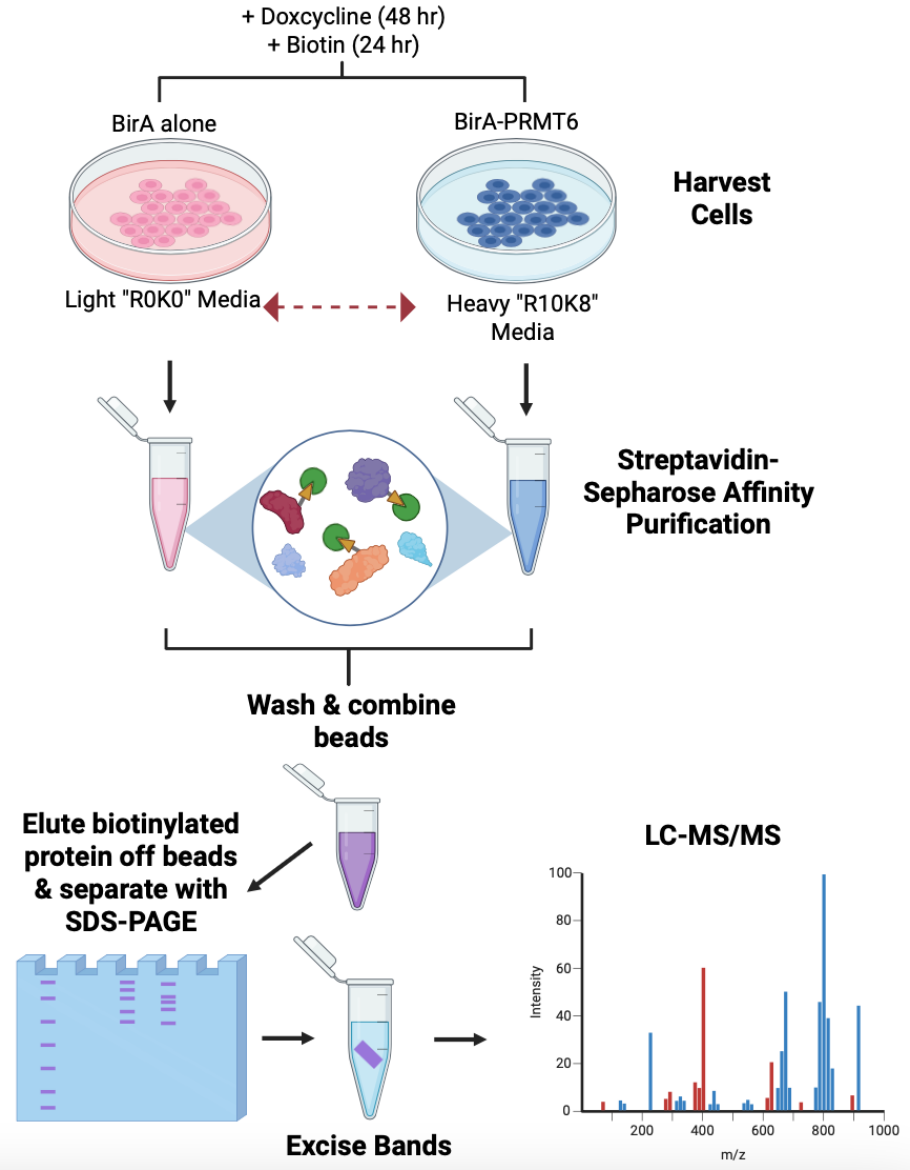

Figure 6: Protocol for SILAC-based BioID and AP/MS analysis and protein identification.

Doxycycline at 0.5ug/mL and excess biotin at 50µM were added to MDA-MB-231 and MCF7 cells stably expressing either the biotin ligase alone (BirA) or fusion protein BirA-PRMT6. Cells were differentially labelled with Arg0Lys0 (R0K0) or Arg10Lys8 (R10K8) isotopic media. We flipped the SILAC labelling in the second experiment replicate so that BirA control cells were labelled with heavy (R10K8) media and BirA-PRMT6 cells with light (R0K0) media. Whole cell extracts were prepared for biotinylated protein capture with streptavidin-sepharose beads followed by elution of isolated biotinylated protein before separation with SDS-PAGE. Gel bands containing proteins were sent for LC-MS/MS analysis for identification. Created with BioRender.com.

2.8 BioID Assay

The proximity biotinylation labelling assay was completed as described in "SILAC based BioID and Mass Spectrometry (LC-MS/MS) Protein Identification" without the isotopic media labelling of cells. Cell lysates were prepared with equal total protein amounts before biotinylated protein capture and affinity purification with streptavidin-sepharose beads (17511301; Cytiva) 4^{o}C, 4 h incubation. After biotinylated proteins are isolated with an affinity matrix, the protein is eluted from the bead matrix to undergo sample preparation, SDS-PAGE and immunoblotting analysis as previously described.

2.9 Immunocytochemistry

Coverslips added to 6 well or 10cm plates were seeded with MDA-231-MB or MCF7 cells with the addition of doxycycline at 0.5ug/ml 48 h and 24 h labelling with 50µM biotin prior to immunocytochemistry (ICC) in preparation 48 h later. Cells were washed twice with 1X PBS and fixed with warmed 4% paraformaldehyde for 10 min at 37^{o}C. Cells were permeabilized with 1% Triton-X in 1X PBS and blocked with 0.1% Tween-20, and 1% BSA in 1X PBS. Streptavidin-Alexafluor488 conjugate (S11223; Thermo-Fisher) in blocking buffer was used for a 1 h incubation in the dark. PRMT6 primary antibody (365018; Santa Cruz) or ADAR1 antibody (81284; Cell Signaling) is used for 1 h, the secondary antibody Alexa Fluor 594 (A11005; life technologies) or Alexa Fluor 488 (A21206; Invitrogen) was used after for 1 h. Two washing steps with 1X PBS were completed between each immunoblotting step. Cells were counter-stained with DAPI 0.2ug/mL for 10 min in the dark before cells are mounted with Vectashield Vibrance Antifade Mounting Media (H-1700; Vector Laboratories) onto glass slides. The Zeiss AxioImager Z1 microscope and AxioCamERc5s camera using the Axiovision 4.8.2 SP3 software was operated for fluorescence microscopy and images.

2.10 GST Protein Purification

pGEX-4T2 sGST-PRMT6 was transformed from *Escherichia coli* BL-21 as described above. The GST-PRMT6 expressing BL-21 cells were grown in 1L of LB and induced by 1mM isopropyl-β-D-thiogalactopyranoside (IPTG) until an optical density (OD) of 0.6 was reached at 600nM. Pelleted cells were lysed in 1X PBS and protease inhibitor cocktail (04693159001; Roche) by sonication 5 x 15 sec. GST-PRMT6 was affinity purified using glutathione-agarose beads (G4510; Sigma Aldrich) overnight. Beads were washed with 1xPBS-1% Triton X-100 and GST-PRMT6 eluted from beads with 32.5 mM glutathione (G6529; Sigma) in 1X PBS, pH 7.5. The elution product was further purified by dialysis overnight at 4^{o}C in 1X PBS and then concentrated with Amicon Ultra 15 – Ultracel 10K column (UFC901024; Millipore). Protein concentration was quantified using a Bradford Assay for future use.

2.11 *In Vitro* Methylation Assay

The methylation reaction included 5µg of GST-PRMT6 enzyme incubated at 37^{o}C for 3 h with 5µg of one of the substrate proteins, GST-ADAR1 1-176aa, GST-DDX3, GST (A. J. Morettin, 2015), Histones (H9250; Sigma), or without substrate present. GST-ADAR1 (1-176aa partial protein sequence) recombinant purified protein from *E.coli* host (MBS951221_e0; MyBioSource) was used for the ADAR1 substrate. The reaction was also in the presence of 0.55µCi S- adenosyl-L-[methyl-^{3}H] methionine (^{3}H-SAM) (Perkin Elmer) in reaction buffer including 50mM Tris-HCl pH 7.4. Reactions were quenched with 5X laemmli reducing buffer addition (25% glycerol, 125mM Tris-HCl pH 6.8, 4mM SDS, 700mM β-mercaptoethanol, 0.1% bromophenol blue) and diluted with PBS to load into a dot-blot well (Schleicher & Schuell). Methylated products were bound to a nitrocellulose membrane using a vacuum. ^{3}H-labeled proteins were measured with a radioisotope counter (Tri-Carb 4910TR Beta Liquid Scintillation

Analyzer) with 10 min reads and 2mL of scintillation liquid added to each sample. Raw scintillation counting data indicating methylation is read as the radiological unit, CPMA (Counts per minute in channel A) where channel A registers ^{3}H ionizing radiation signal.

2.12 Statistical Analysis

Statistical analysis of the western blot protein quantification and methylation assay was done using GraphPad PRISM software V10.0.3. Quantified data represents the calculated average of the experiments ± the standard error of the mean. Statistical significance was calculated by performing an unpaired parametric t-test for experiments with at least three independent replicates. Statistical significance is denoted as $*P < 0.05$; $**P < 0.01$; $***P < 0.001$.

Table 1: Antibodies

Target of Interest	Working Dilution	Manufacturer and Product #
PRMT6	1:2000	Bethyl Laboratories #A300-929A
PRMT6 (Immunofluorescence)	1:300	Santa Cruz (H-2): sc-365018
PRMT6 (Immunoprecipitation)		Bethyl Laboratories #A300-928A
c-Myc	1:2000	Santa Cruz 9E10: sc-40
α-Tubulin	1:2000 or 1:5000	Sigma-Aldrich #T6199
Streptavidin-HRP Conjugate	1:5000	Thermo-Fisher Scientific #N100
Streptavidin Alexa Fluor™ 488 conjugate (IF)	1:800	Thermo-Fisher Scientific #S1123
ADAR1 (WB ad IF)	1:2000	Cell Signaling Technology #81284 (E6X9R) XP
DDX3		Bethyl Laboratories #A300-474A
Secondary mouse anti-rabbit	1:10,000	Jackson ImmunoResearch Laboratories Inc #211-032-171
Secondary goat anti-mouse	1:10,000	Jackson ImmunoResearch Laboratories Inc #115-035-174
Phospho-eIF2α (Ser51)	1:1000 – 1:750	Cell Signaling Technology #119A11
eIF2α (D7D3) XP	1:5000	Cell Signaling Technology # 5324S

*Antibodies are primary antibodies and are used for western blot immunodetection unless stated otherwise.

Chapter 3: Results

3.1 BioID BirA-PRMT6 Mammalian Breast Cancer Cell Model

Before completing the first objective of this project, inducible stable BioID MCF7 and MDA-MB-231 breast cancer cell lines were established by first cloning PRMT6, the protein of interest, into a pLVX-Tet-One vector expressing the biotin ligase, BirA. The biotin ligase permits proximity-dependent biotinylation labelling for PRMT6. The doxycycline-inducible pLVX-Tet-One vector system constitutively expresses Tet-On 3G transactivator protein from the PhPGK promoter. The TREG3G promoter (pTRE3GS) transcribes the gene of interest, Myc-BirA-PRMT6 or Myc-BirA alone, only when bound by Tet-On 3G protein in the presence of doxycycline (Figure 7a). Cells containing the pLVX-Tet-One-BirA-PRMT6 or pLVX-Tet-One-BirA are selected with puromycin to establish the doxycycline-inducible BirA-PRMT6 and BirA MCF7 and MDA-MB-231 expressing cells.

The BirA alone construct is utilized as a control for unspecific biotinylation by the biotin ligase due to background interactions or proteins with increased affinity to the ligase itself. BirA control during AP is used to identify if the protein of interest is non-specifically binding to the streptavidin-sepharose beads or BirA construct independent of BirA-PRMT6 biotinylation.

A western blot (WB) analysis was conducted to confirm doxycycline-induced BirA-PRMT6 and BirA expressing MCF7 or MDA-MB-231 cells. Both cell lines expressed their protein of interest with doxycycline addition either 24 h or 48 h after induction and before cell lysate collection. The DMSO, no doxycycline control group confirmed expression required doxycycline addition without detectable leaked expression (Figure 7b).

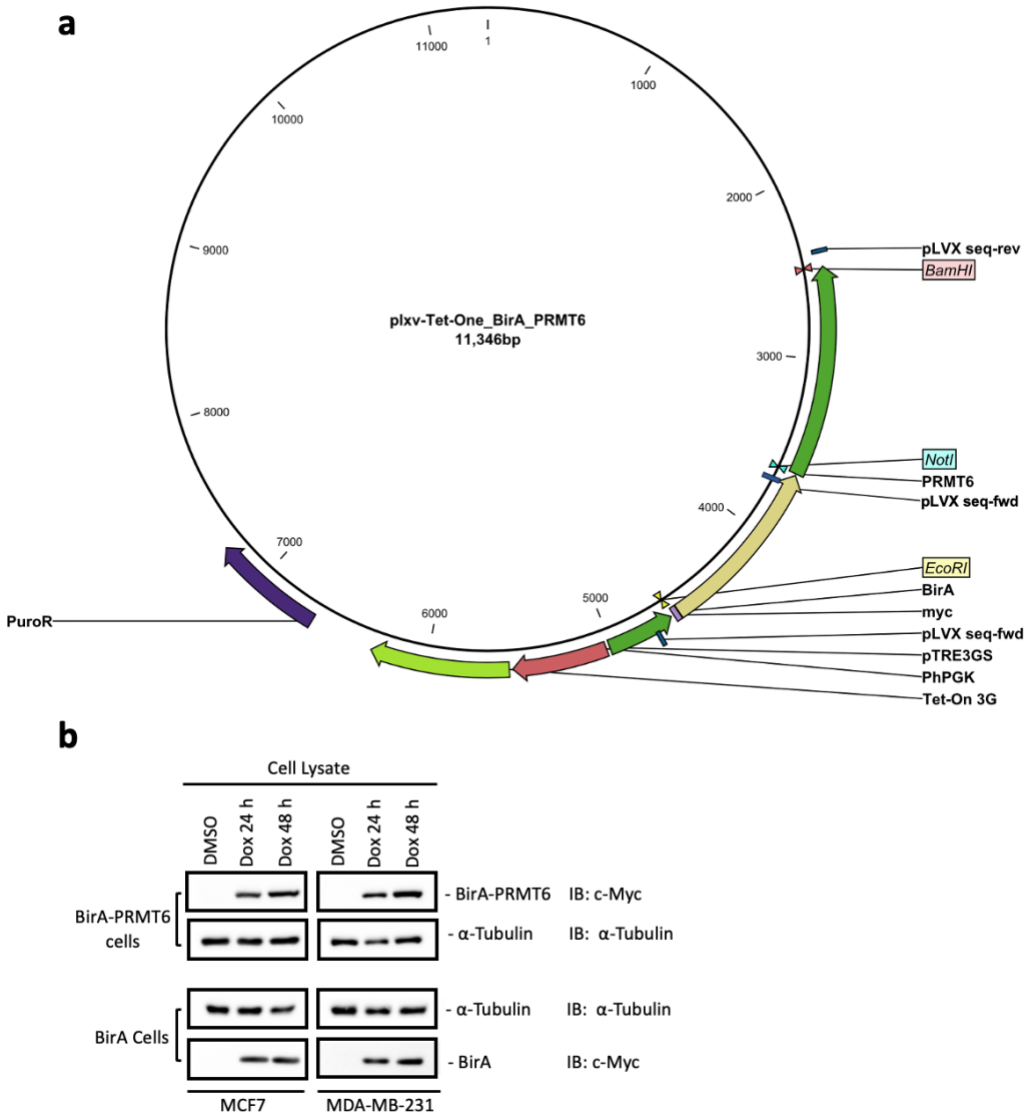

Figure 7: BioID BirA-PRMT6 fusion protein mammalian cell model.

(a) Schematic representation of the PRMT6 protein fused with biotin ligase (BirA) cloned into a pLVX-Tet-One puro vector. DNA plasmid construct is 11.35kb in size. Important vector map features are annotated including the restriction sites and pLVX forward/reverse primer locations used for subcloning and sequence validation, respectively. **(b)** Western blot analysis of MCF7 and MDA-MB-231 lysate using PRMT6 and c-Myc immunoblotting (IB) shows BirA-PRMT6 or BirA protein levels, respectively. The α-tubulin IB was used as a loading control. Cells were treated for 48 h DMSO (vehicle control) or 24 h and 48 h with 0.5 µg/mL doxycycline.

3.2 Functional analysis of BioID constructs for BirA-PRMT6 and BirA expressing cells.

Our goal was to isolate PRMT6 stable, transient, or weak protein interactors and proximal proteins using the BioID/AP method. To identify candidate PRMT6 protein interactors with BioID AP/MS experiments, first, BirA-PRMT6 and BirA expressing MCF7 and MDA-MB-231 cells were first established as functional BioID cells. The BioID BirA-PRMT6 and BirA construct activity was confirmed by strong biotinylated protein labelling observed with fluorescent microscopy. BirA-PRMT6 expressing cells showed predominantly nuclear localization of biotinylated proteins. Less specific localization was observed in BirA expressing cells that displayed biotinylated protein diffused throughout the cytosol and nucleus (Figure 8a). BirA cells exhibited more promiscuous biotinylation of proteins compared to BirA-PRMT6 cells with biotinylation localized to the nucleus, coinciding with PRMT6 known localization (Figure 8a).

ICC and fluorescent microscopy displayed BirA-PRMT6 localization in transfected MCF7 and MDA-MB-231 cells similar to endogenous PRMT6 in WT cells. BirA-PRMT6 and PRMT6 localization was predominantly nuclear in all cell types. Although, MDA-MB-231 cells displayed predominantly nuclear PRMT6, more cytoplasmic PRMT6 localization was observed compared to the other cell lines (Figure 13).

The functional activity of BirA-tagged proteins was further verified with HRP-conjugated streptavidin WB analysis. Biotinylated proteins were readily visualized as a smear-like banding of varying intensities in BirA and BirA-PRMT6 whole-cell lysate. Protein WB banding was seen to a lesser extent in BirA-PRMT6 lysate (Figure 8c).

Before BioID AP/MS experiments were completed, transfected cells were assessed for the presence of the doxycycline induced BirA-PRMT6 and BirA exogenous proteins by WB

analysis. The MDA-MB-231 and MCF7 cells stably expressed an inducible 77 kDa ligase-bait fusion protein, BirA-PRMT6 while control cells expressed a 35 kDa BirA (Figure 8b).

These SILAC-labelled doxycycline-induced cells underwent AP to capture biotinylated proteins. The highly efficient streptavidin-sepharose bead pull-down of biotinylated proteins is observed with the depletion of biotinylated proteins after AP compared to before AP (Figure 8c).

Next, the beads with isolated biotinylated protein from BirA and BirA-PRMT6 samples were combined during washes to decrease sample variability during the LC-MS/MS experiment. Combined eluted protein samples are resolved by electrophoresis and visualized following Coomassie staining to validate the presence of combined eluted protein before MS analysis (Figure 8d).

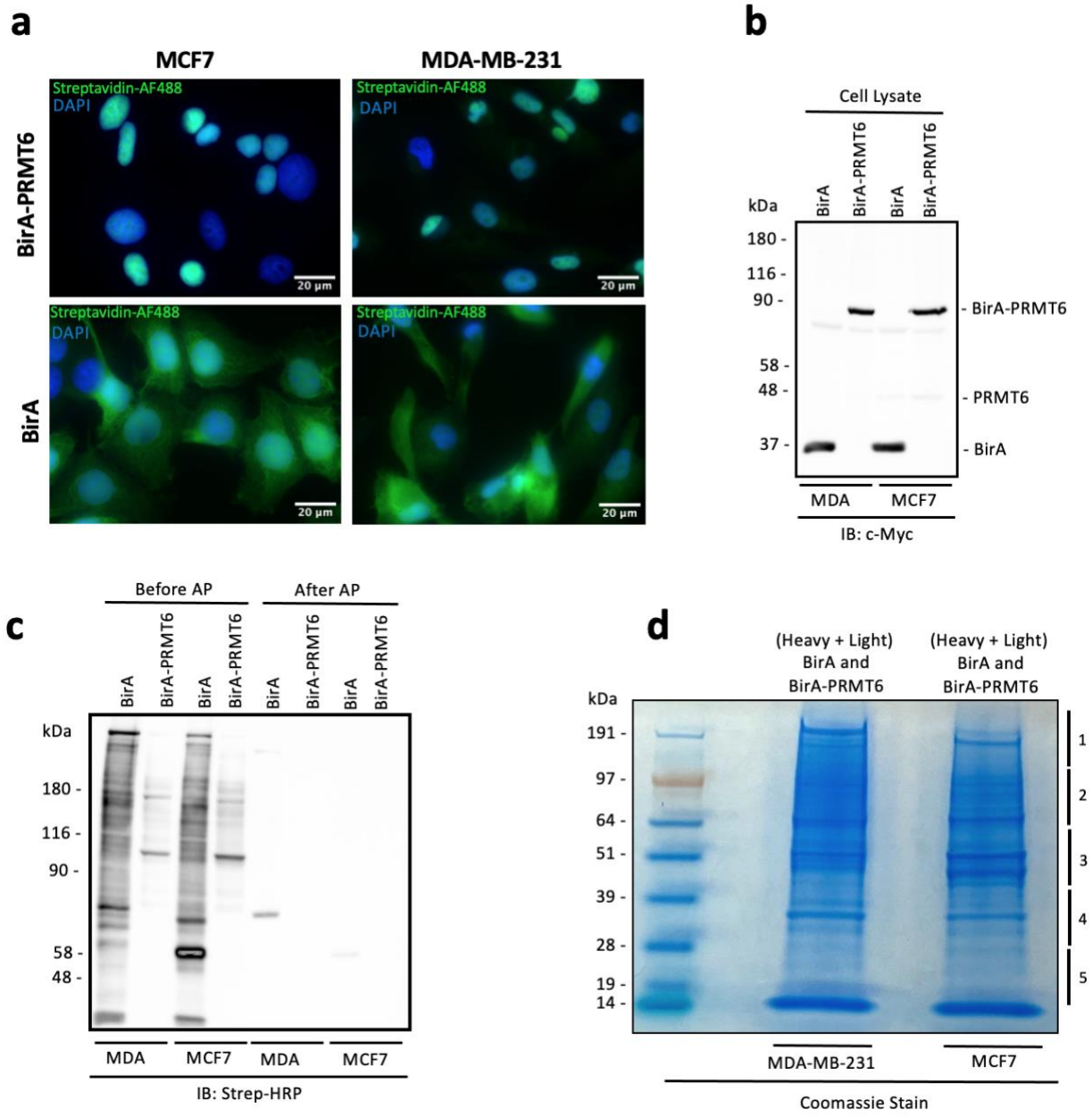

Figure 8: Controls and validation of active BioID cells for BioID AP/MS experiment.

(a) Immunocytochemistry (ICC) of MDA-MB-231 and MCF7s grown in SILAC media after 0.5 µg/mL doxycycline for a 48 h induction of BirA-PRMT6 and BirA, and 50 µM biotin. MCF7 and MDA-MB-231 cells were blotted with streptavidin-AlexaFluor 488 (green; biotinylated proteins) and DAPI (blue; DNA stain). Magnification 63X, scale bars correspond to 20 µm. Images are representative of each cell line and construct. **(b)** WB analysis of apparent 77 kDa ligase-bait fusion protein, BirA-PRMT6 and 35 kDa BirA-induced expression detected with an anti-c-Myc antibody **(c)** WB analysis of whole-cell lysate with streptavidin-HRP conjugate before and after AP. **(d)** Coomassie stained AP product prior to tryptic digestion and MS analysis.

3.3 Combined SILAC BioID AP/MS approaches identify BirA-PRMT6 protein interactors.

LC-MS/MS is advantageous for its sensitive and selective quantification by preserving ion ratios and increasing ion resolution promoting abundant protein identification. Experiment 1 resulted in 1146 and 1304 total proteins identified in MCF7 and MDA-MB-231 samples, respectively. Experiment 2 resulted in 1173 and 1120 total proteins identified in MCF7 and MDA-MB-231 samples, respectively. A smaller portion of the identified proteins (5-35) were identified as unique to BirA-PRMT6 in each experiment sample (SD Table 1).

The log2 ratio (BirA-PRMT6:BirA) vs. relative abundance was plotted for all quantified proteins (Figure 9a,c,e,g). Mitochondrial carboxylases, indicated by grey dots plotted on the graphs, are endogenously biotinylated proteins considered as background contaminants in BioID experiments. Therefore, the carboxylase background H/L ratio is used in the normalization of the identified biotinylated protein (Trinkle-Mulcahy, 2019). By method standard, the threshold was set as >2-fold above the ratio. Proteins that were enriched >2-fold above the ratio of mitochondrial carboxylase contaminants are signified by a red dot in the plotted graphs (Fig 7,8). To better visualize the highly enriched proteins, the log2 ratio (BirA-PRMT6:BirA) vs. relative abundance for only the top proteins detected in both experiments 1 and 2 were plotted on a graph (Figure 9b,d,f,h). The blue plotted dots include top proteins with ratios around the mitochondrial carboxylase proteins H/L ratio but not necessarily enriched above the >2-fold threshold (Figure 9b,d,f,h). These proteins are potentially specific but low abundance protein interactors resulting in a lower heavy and light isotope ratio. Some of these proteins labelled are still notable compared to non-specific, BirA biotinylated proteins or bead matrix binding proteins.

In the MS experiment 1, BirA-PRMT6 expressing MDA-MB-231 cells exhibited one interactor, ESYT1, enriched >2-fold threshold. BirA-PRMT6 expressing MCF7 and MDA-MB-

231 cells had no other interactors that were enriched >2-fold, but known breast cancer cell PRMT6 interactors, ILF2 and ILF3 (Schneider et al., 2021), were still highly enriched in experiment 1 (Figure 9a,b,e,f). Interestingly, ADAR1 was identified as the second most enriched protein after ILF3 in MCF7 cells (Figure 9a,b).

In the MS experiment 2, BirA-PRMT6 expressing MCF7 and MDA-MB-231 cells both identified ILF2 and ILF3 enriched >2-fold above background. BirA-PRMT6 MCF7 cells also identified ADAR enriched >2-fold above the background and MDA-MB-231 identified ADAR as the third most enriched non-carboxylase protein but <2-fold above the ratio (Figure 9c,d,g,h).

The top enriched protein hits identified were plotted on a graph in both experiments 1 and 2. The mitochondrial carboxylases were also included to visualize the enrichment above background. ILF2, ILF3, ADAR1, ZFR and TPR were identified in MCF7 cell replicates (Figure 10a). ILF2, ILF3, and YLPM1 were identified in MDA-MB-231 cell replicates (Figure 10b). Among the top enriched protein hits, ADAR (ADAR1 protein) is a novel PRMT6 interactor that was consistently identified in MCF7 cells and had a H/L ratio similar to ILF2 and ILF3 in MCF7 cells (experiments 1 and 2) (Figure 10a).

The ADAR1 peptide sequences identified by the MS analysis matched the sequence present in both the ADAR1 p110 and p150 isoforms for both cell lines and replicates (SD Figure 10). Therefore, the specific ADAR1 isoform detected in the MS analysis cannot be distinguished.

ADAR1 was chosen for further analysis due to consistent enriched protein identification from MS results in MCF7 replicates and ADAR1's involvement in the prevention of SG through dsRNA modification (Corbet et al., 2021) and SG localization (Ng et al., 2013). The potential PRMT6 and ADAR1 novel interaction requires supplementary validation to support the MS

analysis since a proximity assay with an MS analysis cannot solely confirm the bona fide interactor.

a

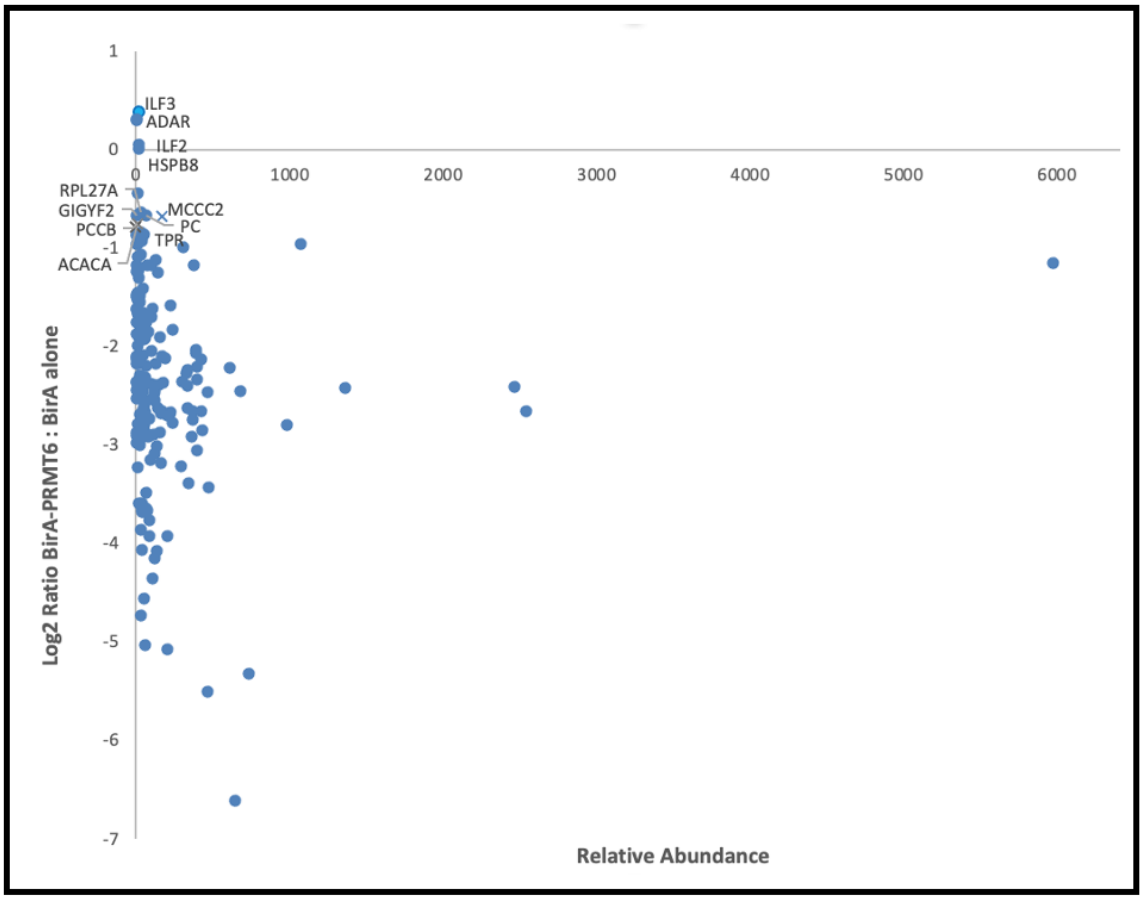
ILF3
ADAR
ILF2
HSPB8
RPL27A
GIGYF2
MCCC2
PC
PCCB
TPR
ACACA
Log2 Ratio BirA-PRMT6 : BirA alone
Relative Abundance
1
0
-1
-2
-3
-4
-5
-6
-7
0
1000
2000
3000
4000
5000
6000

b

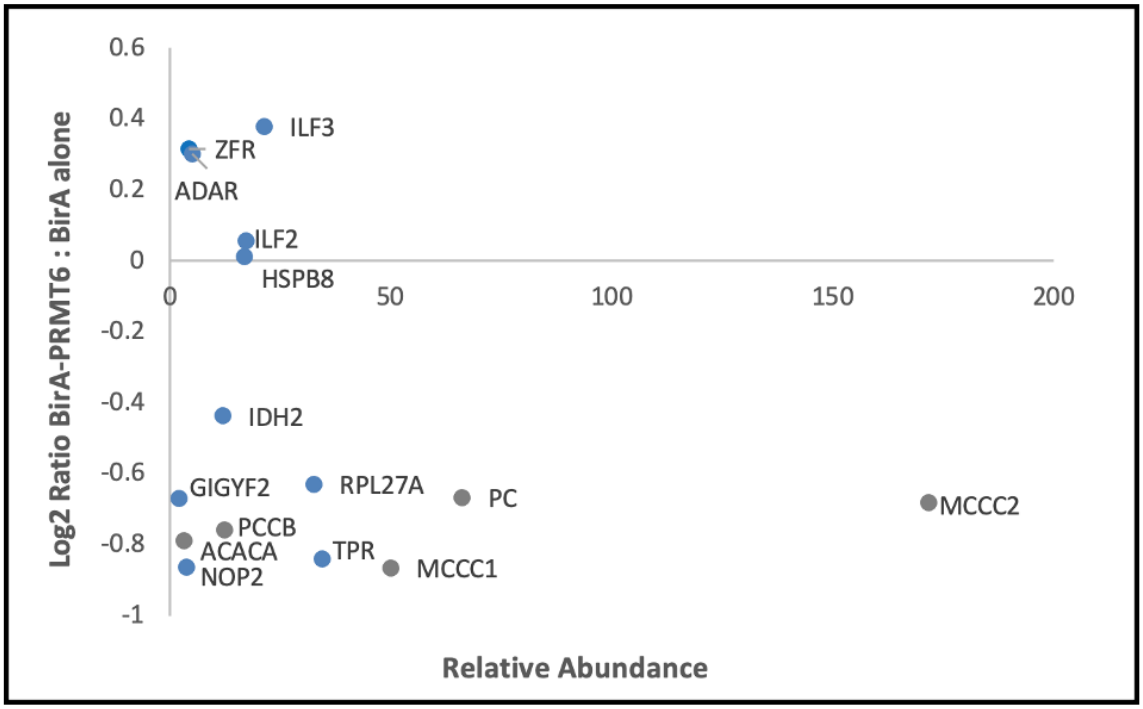
ILF3
ZFR
ADAR
ILF2
HSPB8
IDH2
GIGYF2
RPL27A
PC
MCCC2
PCCB
ACACA
TPR
MCCC1
NOP2
Log2 Ratio BirA-PRMT6 : BirA alone
Relative Abundance
0.6
0.4
0.2
0
-0.2
-0.4
-0.6
-0.8
-1
0
50
100
150
200

c

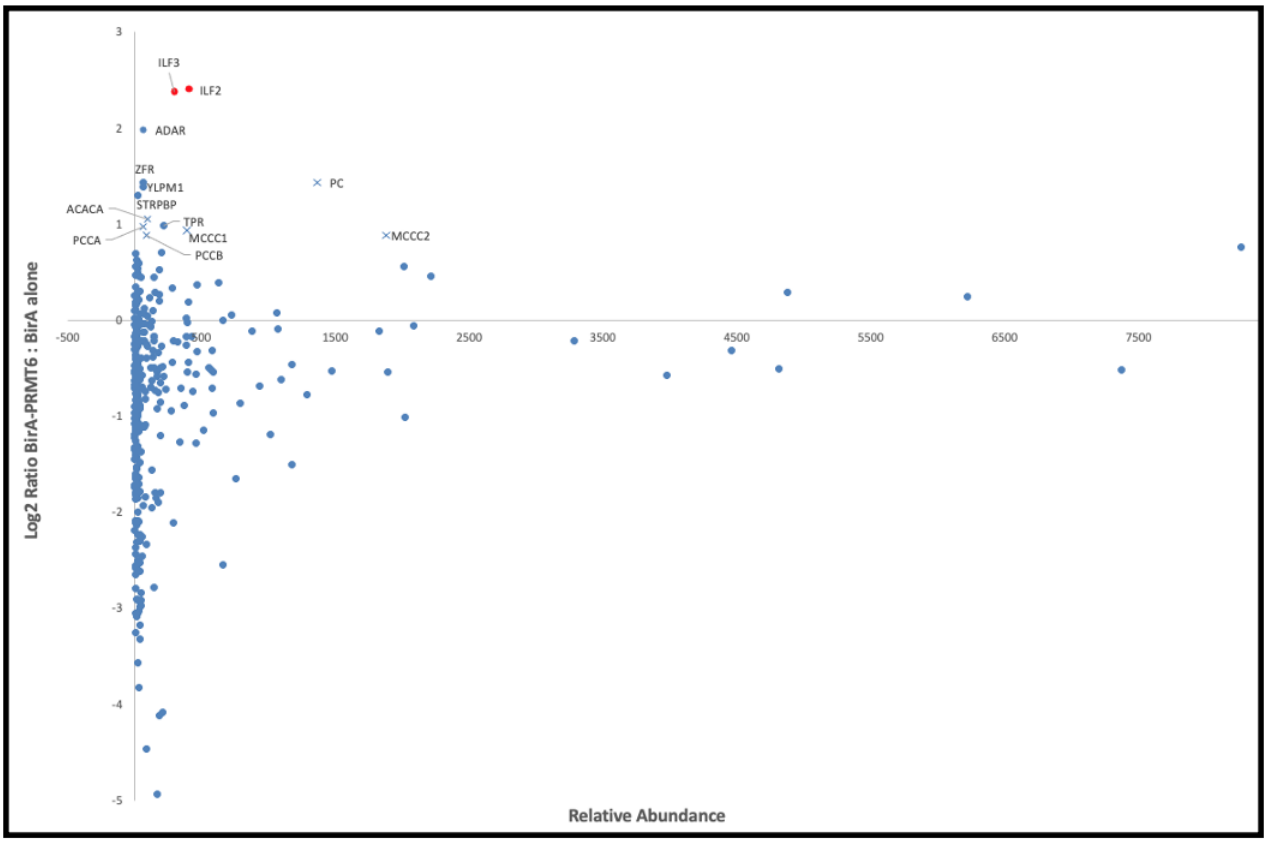
ILF3
ILF2
ADAR
ZFR
YLPM1
STRPBP
ACACA
PCCA
TPR
MCCC1
PCCB
PC
MCCC2
Log2 Ratio BirA-PRMT6 : BirA alone
Relative Abundance

d

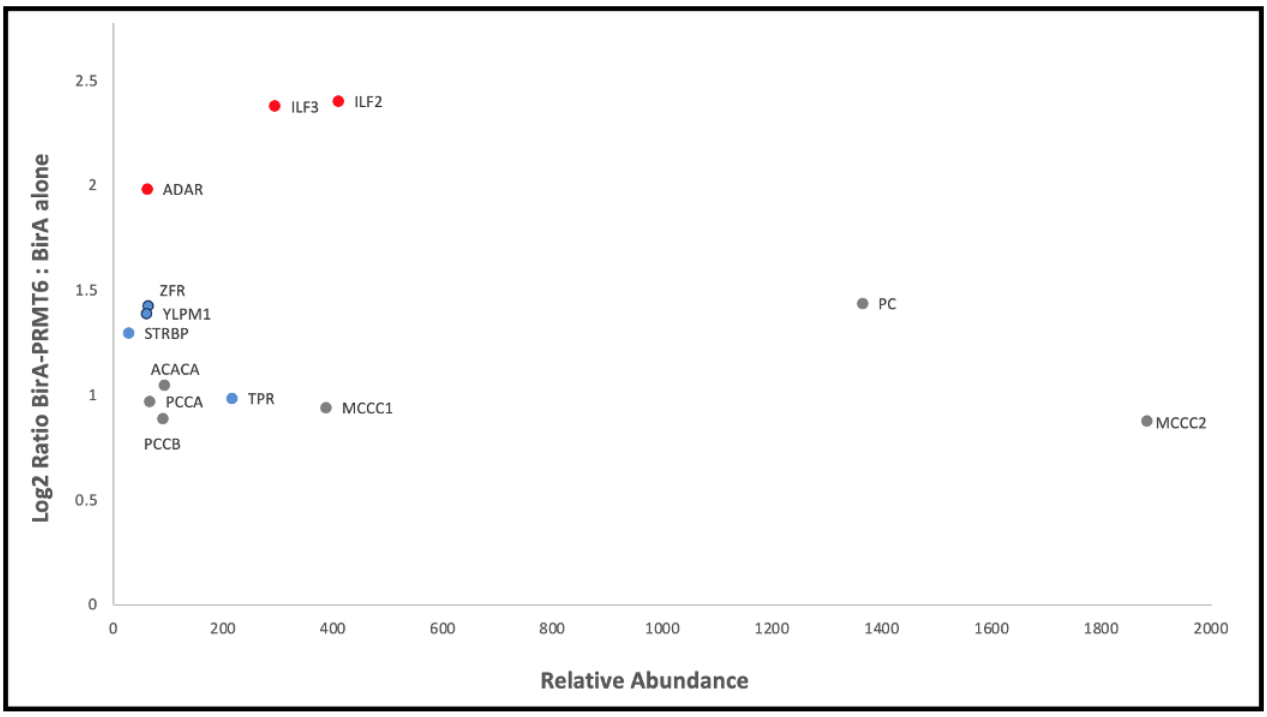
ILF3
ILF2
ADAR
ZFR
YLPM1
STRBP
ACACA
PCCA
TPR
MCCC1
PCCB
PC
MCCC2
Log2 Ratio BirA-PRMT6 : BirA alone
Relative Abundance

e

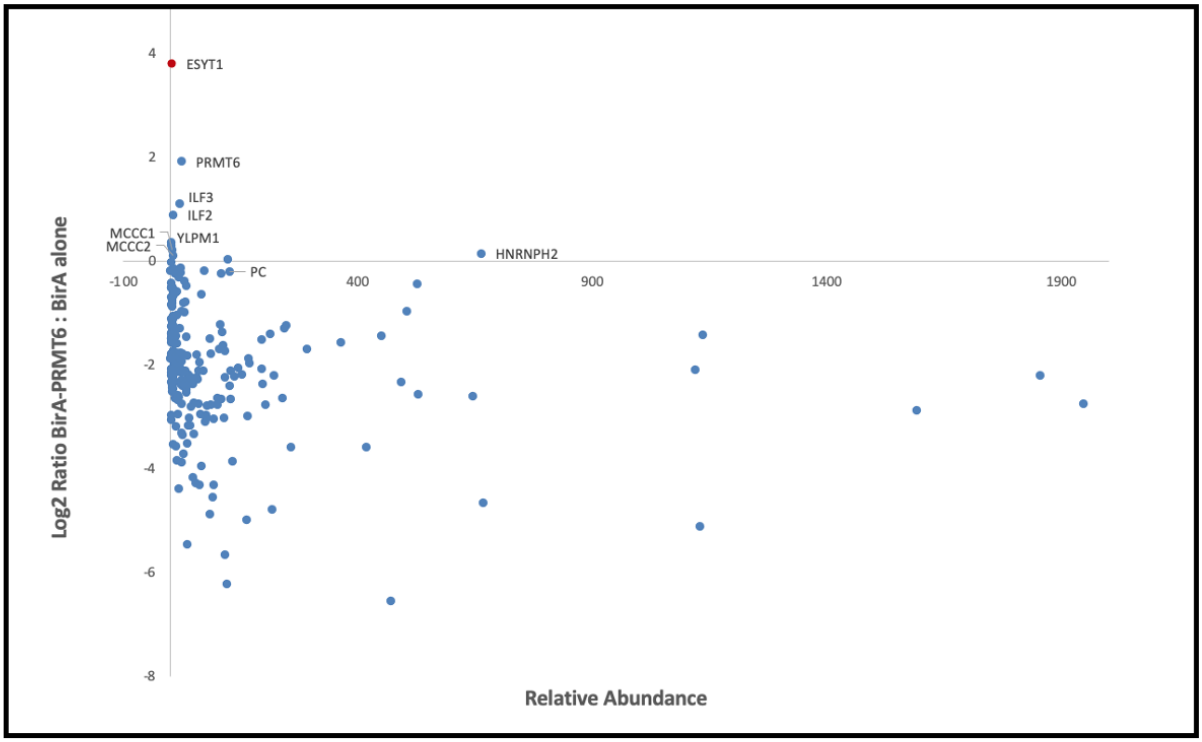
ESYT1
PRMT6
ILF3
ILF2
MCCC1
MCCC2
YLPM1
PC
HNRNPH2
4
2
0
-2
-4
-6
-8
-100
400
900
1400
1900
Log2 Ratio BirA-PRMT6 : BirA alone
Relative Abundance

f

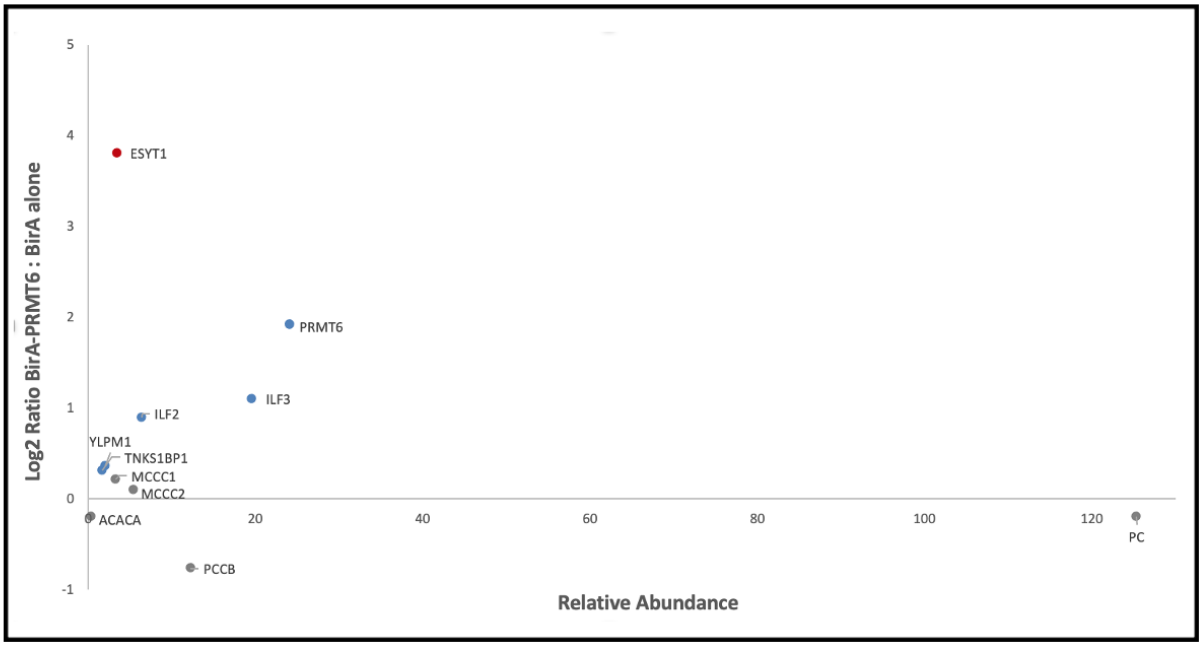
ESYT1
PRMT6
ILF3
ILF2
YLPM1
TNKS1BP1
MCCC1
MCCC2
ACACA
PCCB
PC
5
4
3
2
1
0
-1
20
40
60
80
100
120
Log2 Ratio BirA-PRMT6 : BirA alone
Relative Abundance

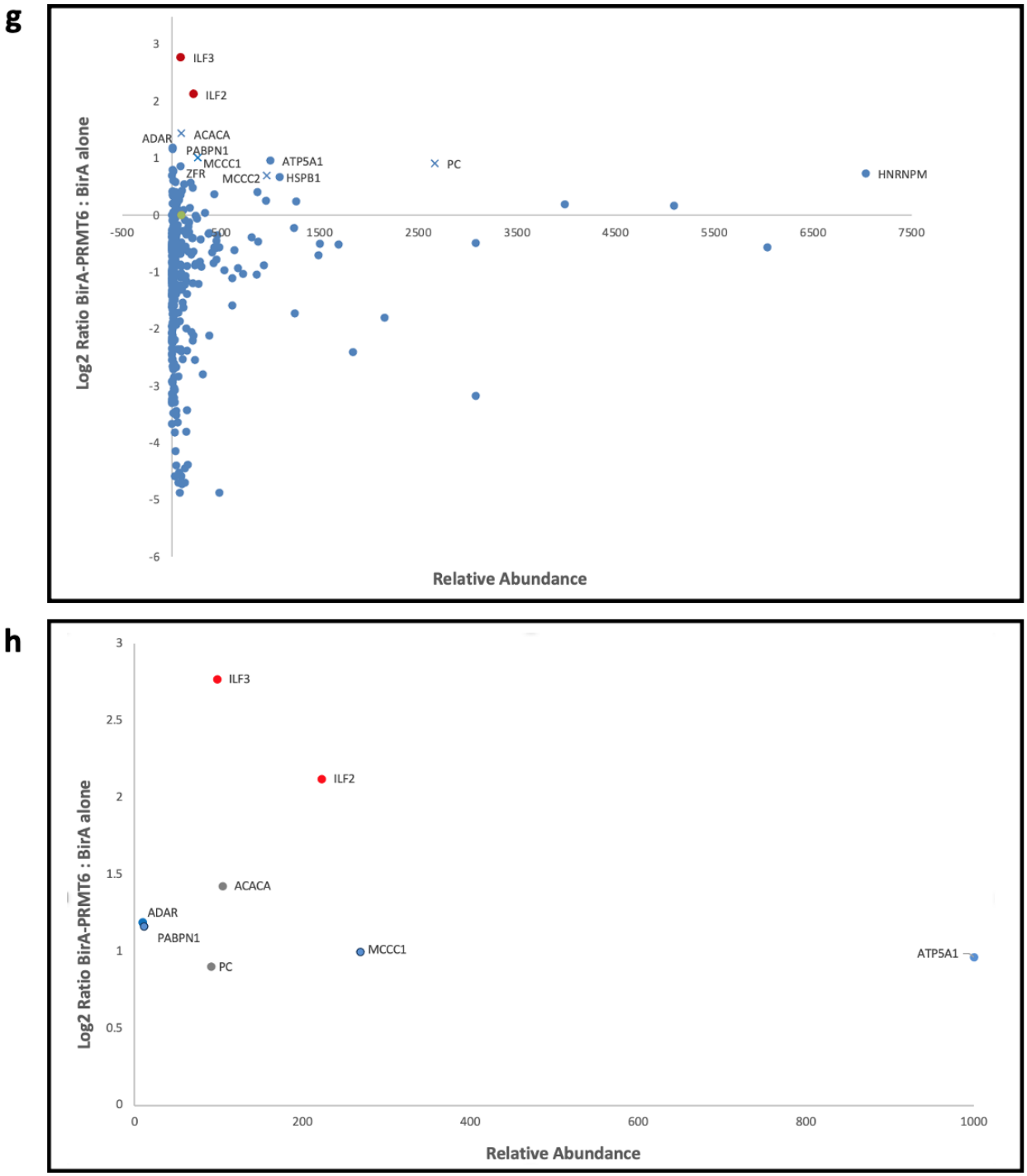

Figure 9: Log2 BirA-PRMT6:BirA ratio vs relative abundance for experiments 1 and 2.

Proteins that were enriched >2-fold above the ratio of mitochondrial carboxylase contaminants are indicated by a red dot. **(a, c)** MCF7, experiments 1 and 2, respectively; normalized distribution of MS data. **(b, d)** MCF7, experiments 1 and 2, respectively; top proteins highly enriched or protein hits with H/L ratio similar to mitochondrial carboxylase contaminants

displayed at a different scale. **(e, g)** MDA-MB-231, experiments 1 and 2, respectively; normalized distribution of MS data. **(f, h)** MDA-MB-231 experiment 1 and 2, respectively; top proteins highly enriched or protein hits with H/L Ratio similar to mitochondrial carboxylase contaminants displayed at a different scale. Proteins that were enriched >2-fold above the ratio of mitochondrial carboxylase contaminants are signified by a red dot. Grey dots or "x" signify mitochondrial carboxylases.

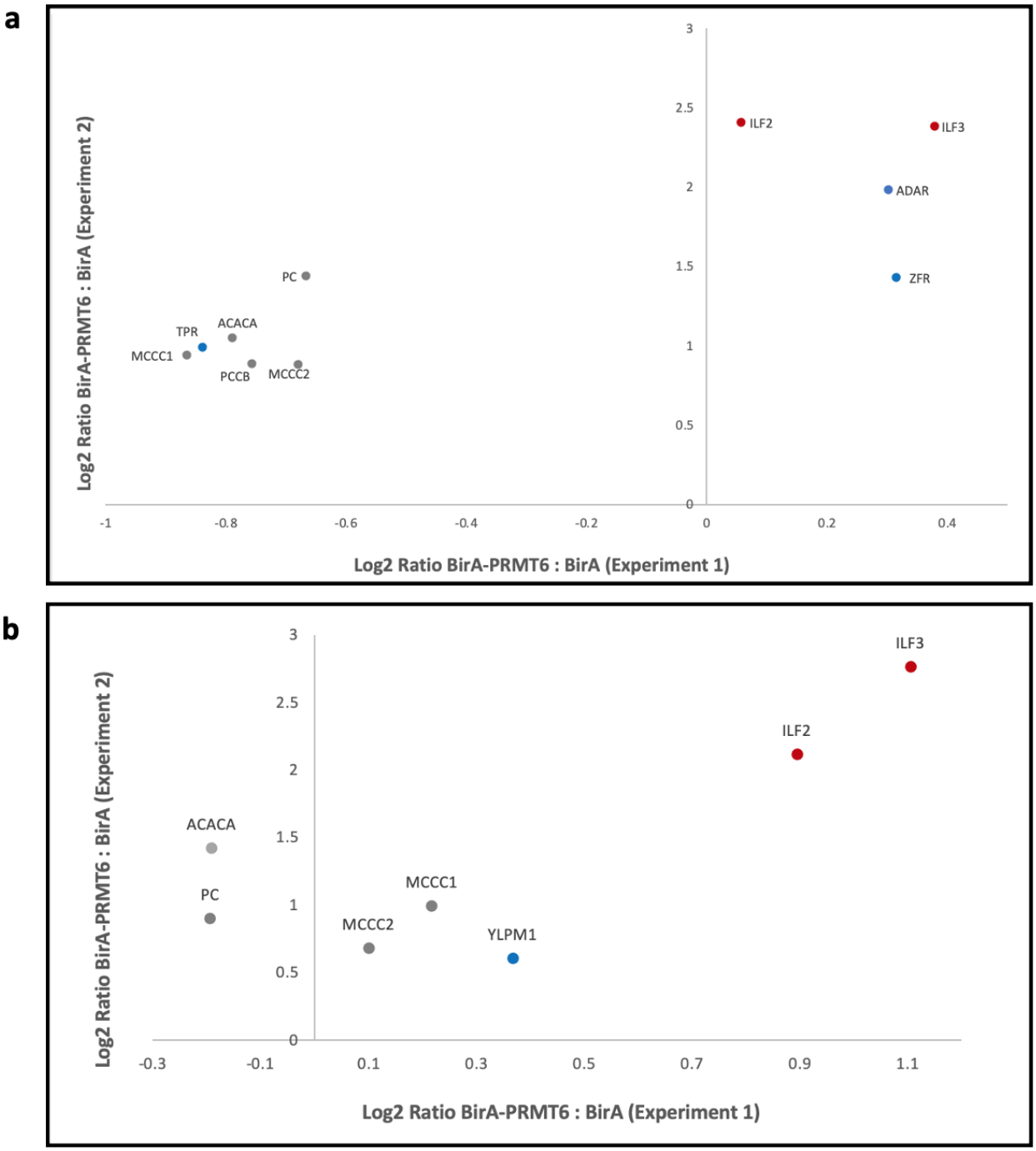

Figure 10: Log2 Ratio BirA-PRMT6:BirA for both experiments 1 and 2.

(a) MCF7 distribution of the identified BirA-PRMT6 biotinylated proteins enriched in both experiments. **(b)** MDA-MB-231 distribution of the identified BirA-PRMT6 biotinylated proteins enriched in both experiments. A red dot in the plotted graphs signified proteins that were enriched >2-fold above the ratio of mitochondrial carboxylase contaminants. Grey dots signify mitochondrial carboxylases.

3.4 ADAR1 is a novel PRMT6 interaction partner candidate.

From the candidate PRMT6 interacting proteins, ADAR1 was a top enriched protein from the MS analysis comparable to the ratios of previously described PRMT6 interactors, ILF2 and ILF3. Next, our goal is to confirm this PRMT6-ADAR1 potential interaction by other methods to support the MS analysis findings. It was also of interest to distinguish MDA-MB-231 and MCF7 cell line differences between PRMT6-ADAR1 interactions due to the cell line's different mechanistic involvement in SG formation and the variability found in our MS analysis.

Utilizing the inducible BirA-PRMT6 and BirA alone stable cells in a BioID/AP experiment allowed PRMT6 proximity-dependent biotinylated proteins to be identified from the streptavidin-sepharose affinity bead matrix. From the streptavidin-sepharose pulldown, ADAR1 (p110 and p150) was detected and validated by WB (Figure 11a,b). BirA-PRMT6 expressing cells displayed a statistically significant 2.6-fold and 2.1-fold increase of biotinylated ADAR1 p110 compared to the control BirA lysate in MCF7 and MDA-MB-231 cell lysate, respectively (Figure 11a,b). ADAR1 p150 requires IFN induction for protein expression. With the absence of IFN induction, ADAR1 p150 could not be assessed for biotinylation in BirA-PRMT6 transfected cells. The fusion protein itself is biotinylated (Roux et al., 2012) allowing BirA-PRMT6 to be utilized as a positive control for functional biotinylation by the fusion protein (Figure 11a,b).

The biotinylated proteins were successfully depleted after AP, demonstrating the depletion of biotinylation labelled proteins from the lysate (Figure 11c). The presence of the BirA or BirA-PRMT6 expression in transfected cells was also validated by WB (Figure 11d). BioID/AP with WB analysis supports the MS data (Figure 9) and confirms ADAR1 p110 as either a PRMT6 indirect or direct interacting partner.

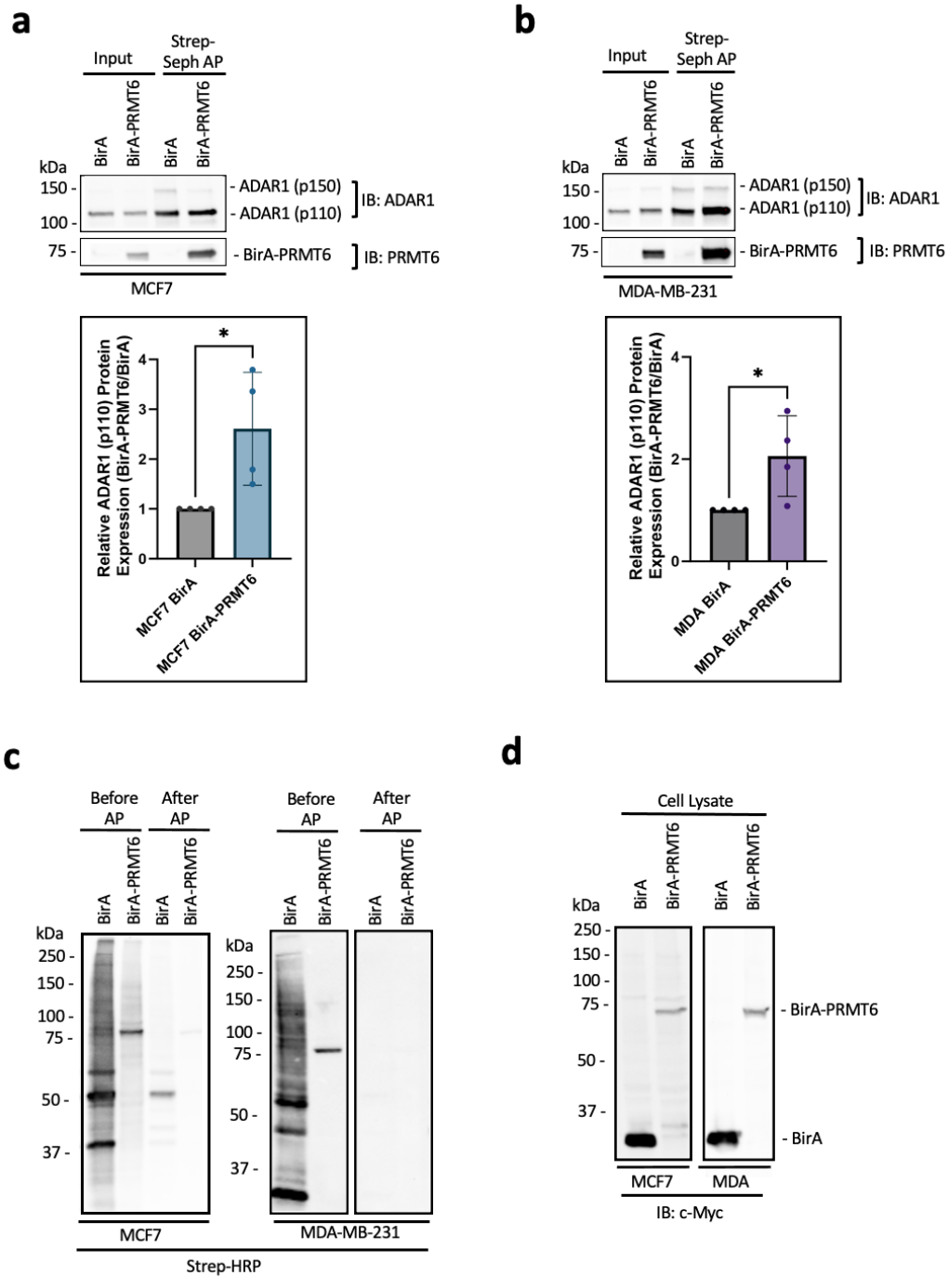

Figure 11: Confirmation of candidate PRMT6 interaction partner ADAR1 p110 using BioID.

Media of BirA-PRMT6 and BirA MCF7 and MDA cells was supplemented with 0.5 µg/mL doxycycline for 48 h for induction of BirA-PRMT6 and BirA before addition of 50 µM of biotin for labelling **(a,b)** Streptavidin-sepharose AP of biotinylated ADAR1 in MDA-MB-231 and MCF7 cells, respectively. Input is 3%. **(a)** The mean quantification of relative ADAR1 p110

protein expression in MCF7 cells was a 2.6-fold increase in BirA-PRMT6 cells relative to BirA cells. * indicates statistical significance at $p<0.05$ ($p=0.03$, $N=4$) **(b)** The mean quantification of relative ADAR1 p110 protein expression in MDA-MB-231 cells was a 2.1-fold increase in BirA-PRMT6 cells relative to BirA cells. * indicates statistical significance at $p<0.05$ ($p=0.036$, $N=4$ **(c)** Western blot analysis of whole cell lysate with streptavidin-HRP conjugate before AP and biotinylated protein depletion after AP. **(d)** Western blot analysis of Myc tagged protein in BirA-PRMT6 and BirA expressing cells. Quantified data represents $N=4 \pm$ the standard error of the mean and significance determined by parametric unpaired t-test.

3.5 BirA-PRMT6 Biotinylated ADAR1 p110 is nuclear.

Based on PRMT6's predominantly nuclear localization (Blanc & Richard, 2017) we wanted to explore the subcellular localization of the PRMT6 and ADAR1 p110 interaction. First, BioID combined with cellular fractionation was performed to isolate the cytoplasmic and nuclear cellular components. Fractionation was followed by WB analysis to reveal the majority of AP biotinylated ADAR1 p110 being in the nuclear fraction for both MCF7 and MDA-MB-231 cells (Figure 12a,b). WB quantification of relative protein expression displayed BirA-PRMT6 biotinylated ADAR1 p110 to be increased 2-fold and 2.3-fold compared to BirA control in MCF7 and MDA-MB-231 cells, respectively (Figure 12a,b).

Western blot analysis with streptavidin conjugated-HRP revealed increased total biotinylated protein by BirA-PRMT6 in the nuclear fraction compared to the cytoplasmic fraction. Efficient AP depletion of biotinylated protein was also observed (Figure 12c). BirA-PRMT6 and BirA protein were predominantly found in the cytoplasmic fraction. The α-tubulin protein in the cytoplasmic fraction and EWS protein in the nuclear fraction confirm efficient cellular fractionation (Figure 12d). The lack of BirA detection in the nuclear fraction is potentially due to part of the gel not being transferred or protein close to being run off gel (Figure 12d).

WT and transfected MCF7 and MDA-MB-231 cells were assessed with ICC for ADAR1, BirA-PRMT6, and PRMT6 localization. ADAR1, BirA-PRMT6 and PRMT6 localization was visualized with fluorescent microscopy as predominantly nuclear. Transfected MDA-MB-231 cells displayed additional cytoplasmic localization of the predominantly nuclear proteins compared to transfected MCF7 cells and WT MCF7 and MDA-MB-231 cells (Figure 13).

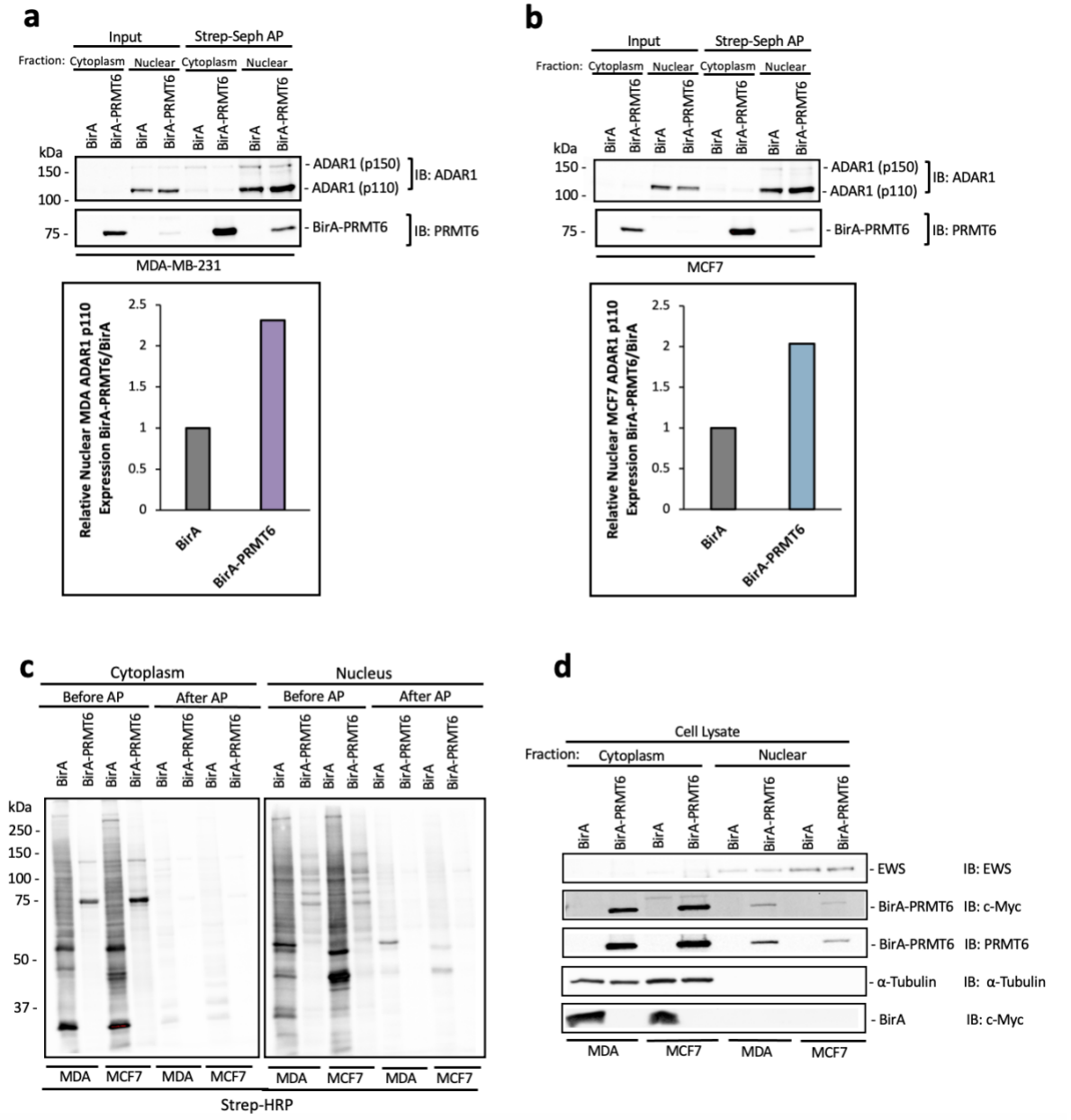

Figure 12: Cellular fractionation with BioID reveals PRMT6 and ADAR1 interaction is nuclear.

Media was supplemented with 0.5 µg/mL doxycycline for a 48 h induction of BirA-PRMT6 and BirA expression, followed by 50 µM biotin and streptavidin-sepharose beads AP **(a,b)** Cell fractionation WB analysis of MDA-MB-231 and MCF7 cells. Quantification of relative ADAR1 p110 protein expression by WB shown in panel. Input is 3%. **(c)** Western blot analysis of whole cell lysate with streptavidin-HRP conjugate **(d)** Western blot analysis of BirA-PRMT6 and BirA induced cells with anti-c-Myc antibody. Fractionation of cytoplasm and nucleus confirmed with cytoplasmic marker α-Tubulin and nucleus marker EWS, respectively.

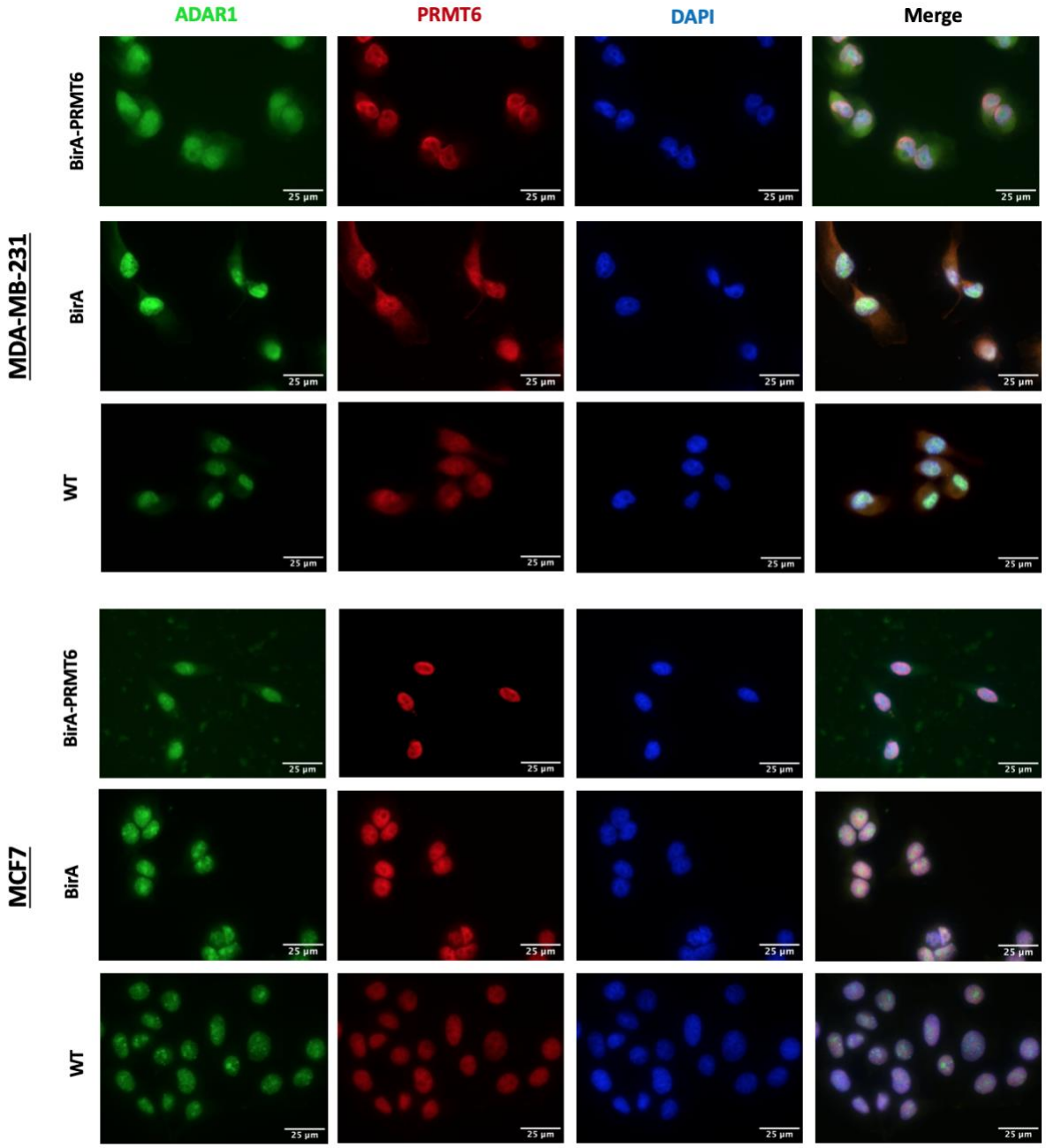

Figure 13: PRMT6, BirA-PRMT6 and ADAR1 localization is predominantly nuclear.

Cell media was supplemented with 0.5 µg/mL doxycycline for a 48 h induction of BirA-PRMT6 and BirA expression. ICC of WT and transfected MDA-MB-231 and MCF7 cells blotted for ADAR1 and PRMT6 and observed with fluorescent microscopy. DAPI was used to stain and visualize DNA. Magnification 63X, scale bars correspond to 25 µm. Images are representative of each cell line and construct.

3.6 ADAR1 p110 is a direct endogenous PRMT6 interactor in MCF7 cells.

Our BioID experiment identified ADAR1 p110 as a potential interactor of BirA-PRMT6 that is either a stable, transient, weak, or proximal interaction. Next, co-immunoprecipitation (co-IP) was performed *in vivo* with WT MCF7 and MDA-MB-231 cells to test if ADAR1 p110 is a direct interactor of endogenous PRMT6. Both MCF7 and MDA-MB-231 cells demonstrated successful PRMT6 immunoprecipitation by detection of PRMT6 protein with co-IP. ADAR1 p110 co-IP protein was enriched above the IgG control levels in MCF7 (Figure 14a) cells but not in MDA-MB-231 cells (Figure 14b). This may be attributed to inherent differences in protein expression as observed with higher PRMT6 protein levels in MCF7 cells compared to MDA-MB-231 cells (Figure 14c). This was reflected in the IP input of MDA-MB-231 cells (Figure 14b). Lower protein expression of PRMT6 may impose difficulty in WB identification of direct protein interactors with lower protein quantifications.

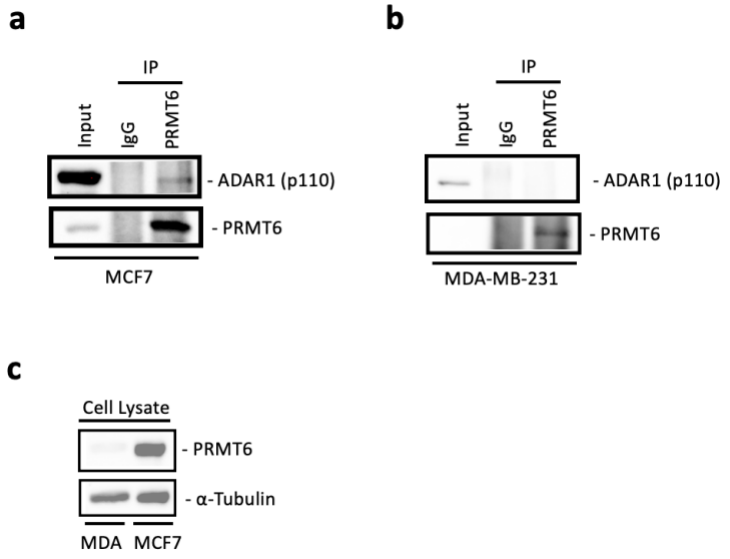

Figure 14: Validation of endogenous PRMT6-ADAR1 (p110) interaction in MCF7 cells.

Co-IP of PRMT6 in WT MCF7 **(a)** and MDA-MB-231 cells **(b)** 1% input. WB analysis of endogenous PRMT6 IP and ADAR1 p110 co-IP detected with anti-ADAR1 and anti-PRMT6 antibodies in MCF7 cells, respectively. **(c)** Western blot analysis of endogenous PRMT6 expression in cell lysate of WT MDA and MCF7 cells.

3.7 The PRMT6 and ADAR1 p110 interaction is not altered by chemotherapeutic treatment.

Next, we investigated if PRMT6 and ADAR1 p110's interaction is impacted by stress induction through bortezomib-induced SG formation. Stress may impact the protein-protein interaction due to ADAR1 p110's export from the nucleus upon stress (Sakurai et al., 2017) and ADAR1 SG localization (D. C. Chiang et al., 2021; Ng et al., 2013). Relocalization of ADAR1 may decrease the ADAR1 p110 available to interact with PRMT6 in the nucleus. In contrast, bortezomib-induced stress may also have a specific influence on ADAR1 and PRMT6 protein cellular stress functions resulting in increased interaction. Determining if the PRMT6 and ADAR1 p110 interaction is altered upon chemotherapeutic treatment with bortezomib may

reveal a mechanism through which PRMT6 may be contributing to MCF7 bortezomib resistance in the context of breast cancer.

Immunoprecipitation of PRMT6 was completed after a 4 h bortezomib treatment. ADAR1 p110 co-IP with PRMT6 in both bortezomib treatment and DMSO control conditions (Figure 15a). WB analysis displayed no significant difference in ADAR1 p110 interaction with PRMT6 during bortezomib treatment compared to DMSO control (Figure 15b). These results confirm that the physical PRMT6 and ADAR1 p110 interaction is not significantly altered with bortezomib-induced stress in MCF7 cells. MDA-MB-231 cells were excluded from this experiment due to their lower PRMT6 expression (Figure 14c) and ADAR1 p110 expression seen in the MDA-MB-231 input (Figure 14b) as well as the difficulties observed in ADAR1 p110 co-IP detection (Figure 14b).

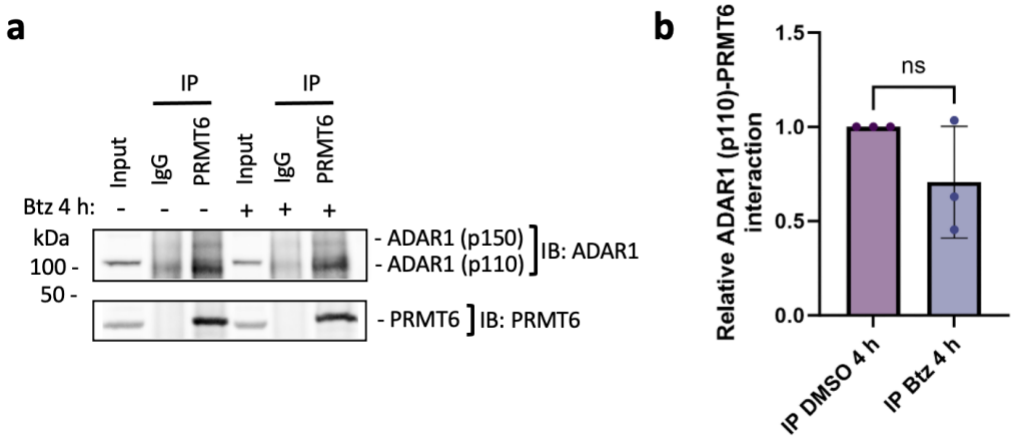

Figure 15: The PRMT6 and ADAR1 p110 interaction does not change upon bortezomib treatment.

(a) WB analysis of PRMT6 IP and ADAR1 co-IP in MCF7 WT cells treated with 10μM of bortezomib (Btz) or DMSO for 4 h. 5% input. **(b)** The mean quantification is normalized co-IP ADAR1 p110 protein and PRMT6 bait protein to input. Control ADAR1 p110-PRMT6 interaction protein levels are relative to Btz conditions. Statistical analysis was nonsignificant (ns) ($p>0.05$, $N=3$) determined by parametric unpaired t-test.

3.8 ADAR1 (1-176aa) is not regulated through PRMT6 methyltransferase activity.

We previously validated ADAR1 p110 as a novel, direct PRMT6 interactor but there remains to be determined if ADAR1 is a PRMT6 substrate. An *in vitro* methylation assay was performed to determine if a partial sequence of ADAR1 (1-176aa) was capable of being arginine methylated. Due to the limited access to other recombinant ADAR1 protein sequences commercially available and the difficult nature of purifying the larger-sized full-length ADAR1 protein, we required an alternative option. For this reason, the ADAR1 protein (1-176aa) was used. Although this sequence is in the truncated N-terminus of the ADAR1 p110 isoform, it will be useful to observe if there is potential PRMT6 methylation of the GAR motifs in this sequence related to the ADAR1 p150 isoform.

An *in vitro* methylation assay was completed with a dot-blot, where the ^{3}H methylated products bound to a membrane could be analyzed by a radioisotope counter. Methylation was then quantified as the radiation unit, CPMA. The assay was performed to detect ADAR1 (1-176aa) methylation by PRMT6 using the tagged purified GST-PRMT6 protein as the enzyme. First, the background methylation is determined by both the GST-PRMT6 alone to account for PRMT6 automethylation and GST-PRMT6 with a GST tag to account for additional GST methylation. The methylation assay with GST-PRMT6 and GST was significantly increased compared to GST-PRMT6 alone indicating the presence of GST methylation additional to PRMT6 automethylation. PRMT6 substrates will display significant methylation above the indicated GST-PRMT6 automethylation and GST methylation background. DDX3 (402-662aa) is the specific region of the DDX3 protein found to be arginine methylated by PRMT6 (A. J. Morettin, 2015). Known PRMT6 substrates, GST-DDX3 (402-662aa) and histones are used as a

positive control and methylation was found to be significantly increased in these controls compared to background methylation. With GST-ADAR1 (1-176aa), the methylation was not significantly increased compared to background methylation indicating GST-PRMT6 was unable to methylate GST-ADAR1 (1-176aa). Instead, GST-PRMT6 with GST-ADAR1 (1-176aa) displayed a significant decrease in methylation compared to the background thus indicating potential hindrance to PRMT6 automethylation (Figure 16a).

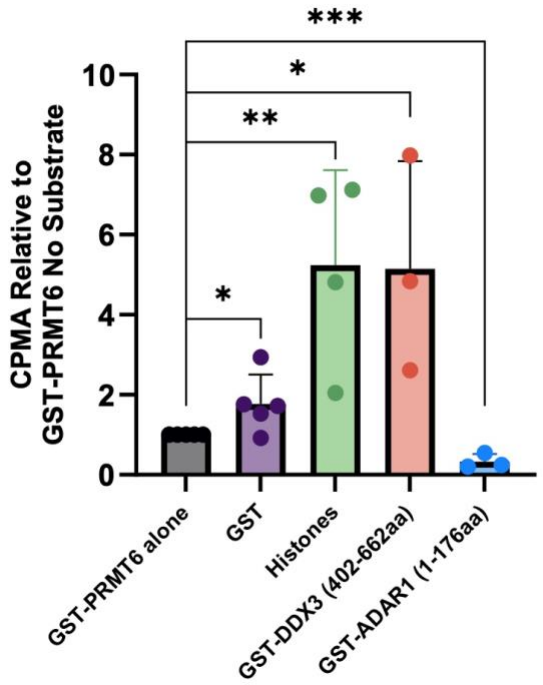

Figure 16: ADAR1 (1-176aa) is not a PRMT6 substrate.

(a) CPMA of *in vitro* methylation reaction with GST-PRMT6 purified protein alone (n=5), or with purified protein substrate GST (p=0.045, n=5), histones (p=0.0048, n=4), GST-DDX3 (402-662aa) (p=0.011, n=3), or GST-ADAR1 (1-176aa) (p=0.0002, n=3), in the presence of ^{3}H-SAM. Statistical significance of the unpaired parametric t-test is denoted as *P < 0.05; **P < 0.01; ***P < 0.001. Error bar represents SE. Methylation was measured by an ionizing radiation unit, CPMA.

Chapter 4: Discussion

Breast cancer is the second leading cause of death for Canadian women. The lifetime probability of developing breast cancer remains high with an estimated one in eight women receiving a diagnosis. Although the five-year net survival is close to 100% for stage I diagnoses, the survival rate decreases substantially to around 23% with later-stage diagnoses (Canadian Cancer Society, 2023). The poor prognosis of breast cancer is attributed to refractory tumours of local recurrence or distant metastasis. Refractory tumours are susceptible to chemotherapy drug resistance resulting in the inability to treat tumours successfully (M.-P. Jiang et al., 2022). Investigating the molecular mechanisms conferring resistance in breast cancer will uncover novel therapeutic targets that could take advantage of an acquired sensitivity to chemotherapy to improve patient outcomes.

Aberrant regulation of PRMT6 is implicated in breast cancer etiology and chemoresistance. PRMT6 promotes resistance to the chemotherapy drug, bortezomib, by mediating SG formation and is upregulated in MCF7 breast cancer cells. Depleting PRMT6 impedes SG formation resulting in decreased cell survival following bortezomib treatment (A. J. Morettin, 2015). SG mediation by PRMT6 represents a chemoresistant mechanism in breast cancer. PRMT6 has been demonstrated previously to mediate resistance through SG formation, but the mechanism by which PRMT6 mediates SG formation remains elusive. We reasoned this unknown mechanism likely involves novel PRMT6 protein interactions. With this established rationale our current study hypothesized that PRMT6 interacts with proteins or other substrates contributing to SG formation.

4.1 BioID BirA-PRMT6 Mammalian Breast Cancer Cell Model.

Our goal was to confirm our transfected breast cancer cells as inducible BirA-PRMT6 and BirA expressing cells. The addition of doxycycline to cell media will induce specific protein expression cloned into the Tet-One expression system that is integrated into the cell's genome. Doxycycline enables strict regulation over the timing of gene expression for minimal side effects and better analysis of gene regulation. This is beneficial over constitutive expression that can lead to side effects such as delayed growth, development and potential cellular death (Kallunki et al., 2019). BirA-PRMT6 and BirA protein expression had high induction 24 h and 48 h after the addition of doxycycline at low concentrations without detectable cytotoxicity. The lack of BirA-PRMT6 and BirA protein expression in the absence of doxycycline ensured the expression system was not leaky for the genes of interest. Our results determine that the BirA-PRMT6 and BirA plasmid vectors incorporating a Tet-One inducible expression system were stably integrated into the cellular genome.

4.2 Functional analysis of BioID constructs for BirA-PRMT6 and BirA expressing cells.

BioID is advantageous for its portrayal of physiologically relevant candidate proximal and interacting proteins of the fusion protein due to live cell biotinylation labelling. Verification of BioID functionality is demonstrated in BioID screens by Roux and colleagues who specified BioID as a novel approach to identifying proximal and interacting proteins (Roux et al., 2012, 2018). Verification of our BioID breast cancer cell model first requires evidence for inducible BioID cell expression. Visualized by WB analysis, the BirA-PRMT6 (77 kDa) and BirA (35 kDa) proteins were expressed after induction with bands appearing at the expected molecular weight. BioID cells were then determined to be functionally active by assessing BirA enzymatic activity through the biotinylation of endogenous proteins observed through WB analysis.

Differences in total biotinylated protein in cell lines were observed. Higher levels of biotinylated protein in the BirA control cells can be attributed to promiscuous labelling of non-specific proteins compared to BirA-PRMT6 displaying more specific, lower levels of protein biotinylation consistent with the smaller pool of interactors anticipated from the BirA-PRMT6 protein construct.

A strong biotinylation signal was also detected by ICC exhibiting a functional BirA ligase in both cell lines. BirA-PRMT6 cells displayed a distinct, primarily nuclear biotinylation pattern in contrast to the BirA cells with unspecific protein biotinylation diffused throughout the nucleus and cytoplasm. The fluorescence localization indicates BirA-PRMT6 likely interacts or is proximal to proteins that are localized to the nucleus and the proteins identified by using this method should be representative of PRMT6's endogenous state.

BioID is advantageous for the identification of proximal and stable, weak, or transient interactions with the fusion protein that transpire in a temporal and spatial biological context. Biotin labelling has temporal inducibility that is initiated with the addition of excess biotin to cell media with increasing quantities of biotinylated proteins corresponding to the duration of biotin exposure (Roux et al., 2012). Compared to alternative biotin ligases like ultraID, TurboID and miniTurbo, BirA can be larger, require more biotin, and has a conventional longer labelling period (Kubitz et al., 2022). Although smaller biotin ligases can be advantageous our application of proximity-dependent biotinylation requires a labelling period not relevant to a particular cellular event and instead requires a longer labelling period. The typical cell cycle duration is about 24 hours for a proliferating cell in culture (Cooper, 2000) and provides an applicable and efficient biotinylation labelling time frame to monitor physiologically relevant interactions (Roux et al., 2012; Varnaitė & MacNeill, 2016). This larger time frame reflects the localization

changes expected of PRMT6 interactors associated with cell cycle progression and therefore leads to a representative pool of interactors. Identifying potential PRMT6 interacting partners at all cell cycle phases aids in predicting the functions of PRMT6 through its interacting proteins and subsequent complexes or signalling pathways. Without the need for high temporal resolution of protein interactions, BirA can circumvent protein instability, persistent biotinylation without excess biotin addition and larger labelling radius found while using TurboID (May et al., 2020). Our functionally active BirA-PRMT6 and BirA expressing MCF7 and MDA-MB-231 cells are therefore verified in their application in all experiments throughout this project.

4.3 Combined SILAC BioID AP/MS approaches identify BirA-PRMT6 protein interactors.

Elucidating large-scale protein-protein networks is valuable for under-researched disease states involving PRMT6. For this purpose, the PRMT6 interactome can be elucidated with MS techniques incorporating BioID for proximal indirect interactions and stable or transient direct protein interaction detection. MaxQuant software was used for further data analysis after LC-MS/MS protein identification of BirA-PRMT6 interactors. Two reciprocal MS experiments were completed for each cell line to account for the null effect of SILAC labelling. In experiment 1, Arg10Lys8 (heavy) and Arg0Lys0 (light) were used for the experimental and control groups while SILAC labelling was flipped in the second experiment (Figure 6).

BioID followed by mass spectrometry analysis identified candidate PRMT6 interactor, ADAR1. BirA-PRMT6 enrichment levels of ADAR1 from the mass spectrometry analysis are variable for both cell lines but the reproducibility of ADAR1 enrichment for BirA-PRMT6 expressing MCF7 cells supports ADAR1 as a candidate PRMT6 interactor. The lack of reproducibility in MDA-MB-231 cells suggests a possible cell type-specific interaction reflecting the relevance of the ADAR1 interactor in the differences for SG regulation observed in

bortezomib treated MCF7 and MDA-MB-231 cells. A related study concerning bortezomib resistant and sensitive cells established a cell type-specific interaction dependent on bortezomib that mediates the apoptotic pathway. Bortezomib was demonstrated to downregulate the phosphatase inhibitor CIP2A resulting in the phosphatase PP2A downregulation of p-AKT and thus leading to apoptosis in bortezomib sensitive MDA-MB-231 cells. CIP2A was not downregulated in MCF7 bortezomib resistant cells resulting in the inhibition of phosphatase PP2A and the apoptotic pathway (Tseng et al., 2012). Similarly, the differences in the cell type-specific response to bortezomib treatment assessed by SG formation between MCF7 and MDA-MB-231 breast cancer cells (A. J. Morettin, 2015) may emerge from different cell-specific PRMT6 protein interactions involving ADAR1.

Biotinylation is a rare modification in mammalian cells that endogenously occurs on proteins that bind biotin directly. This modification occurs on only four protein species called carboxylases (Roux et al., 2012). Due to their biotinylation, carboxylases such as propionyl-CoA subunits (PCCA and PCCB), pyruvate carboxylase (PC), acetyl-CoA (ACACA), and methylcrotonyl-CoA (MCCC1 and MCCC2) appear abundant in all BioID pulldowns and represent background contaminants (Roux et al., 2018; Sears et al., 2019). Carboxylase background proteins are beneficial in MS analysis data normalization to separate candidate interactors enriched more than 2-fold above the background threshold compared to BirA control samples (Gaudreau-Lapierre et al., 2023; Sears et al., 2019). These guidelines were followed for our MS analysis to reveal potential interactors if that protein's ratio was enriched more than 2-fold above the background ratio threshold. The protein ratio is the protein detected in the BirA-PRMT6 sample over the protein detected in the BirA control sample. Detection of unique unquantified proteins in the BirA-PRMT6 samples means the proteins identified were absent in

the BirA sample (SD Table 1) and are not compared to the background ratio. These proteins are of interest due to their identification being isolated to the BirA-PRMT6 sample. We determined that the majority of unique unquantified proteins tended to have minimal peptide spectral counts around 1-3 indicating trivial protein abundance found in the sample (Vogel & Marcotte, 2009). Therefore, these specific proteins were not selected for further investigation and to validate as a PRMT6 protein interactor.

Contaminants can be described as proteins that non-specifically bind to the affinity matrix, such as nonspecific binding to the streptavidin-sepharose beads we used in affinity purification to isolate biotinylated protein. The sepharose bead proteome includes a list of proteins from dataset screens of non-specifically binding sepharose beads. The sepharose bead proteome includes ADAR1, albeit identification occurred in only 11% of datasets pooled from 27 independent SILAC pull-down experiments using whole lysate (Trinkle-Mulcahy et al., 2008). We also detected ADAR1 p110 protein in the BirA-only control group which can be attributed to background contaminants that have an affinity to the biotin ligase or streptavidin-sepharose beads used for affinity purification. Background contaminants are proteins that may be nonspecific to the protein of interest and can be further assessed based on a web-accessible contaminant repository resource for negative controls (Mellacheruvu et al., 2013). ADAR1 does appear as a contaminant identified in the repository, although, a considerable proportion of the BirA-only control experiments using an agarose affinity support in the database identified zero to minimal peptide spectral counts of ADAR1. The minimal detection of ADAR1 p110 as a background contaminant based on the proteomic database supports our MS and WB analysis following BioID. To further support ADAR1 as a candidate PRMT6 interactor and not a contaminant, our MS analysis identified the putative ADAR1 interactor enriched to a similar

extent as ILF2 and ILF3 known PRMT6 interactors. It is important to verify that the MS experiment was successful by identifying previously discovered PRMT6 interactors like ILF2 and ILF3 alongside novel candidate interactors. ADAR1 has not been previously identified as a PRMT6 interactor in MCF7 or MDA-MB-231 cells which prompts further validation by BioID and IP methods to strengthen our finding.

The ILF2 and ILF3 proteins are known PRMT6 interactors in lymphoblast cells that were previously identified by SILAC-based mass spectrometry (Schneider et al., 2021). ILF2 also contains an N-terminal RGG domain, a feature specified for PRMT6 arginine methylation preference (X. Jiang et al., 2021). However, a study determined ILF2 was not a PRMT6 substrate but instead established a noncatalytic role for PRMT6 in an ILF2 signalling axis to activate tumour-associated macrophages to potentiate lung tumour progression (Avasarala et al., 2020). This corresponds to our analysis identifying ILF2 and ILF3 by BioID AP/MS enriched above the background ratio threshold thus validating our assay. Compared to ILF2 and ILF3 proteins, ADAR1 was similarly enriched in MCF7 cells MS analysis. MDA-MB-231 cells detected ADAR1 also similarly enriched to ILF2 and ILF3 in one replicate but not above the background ratio threshold. The similarity of ILF2 and ILF3 enrichment levels compared to ADAR1 indicates higher confidence for ADAR1 identified as a PRMT6 candidate interactor.

Intriguingly, ILF2 and ILF3 have previously been detected as ADAR1 interacting proteins, along with other proteins containing a DZF domain (domain associated with zinc fingers) that promotes protein dimerization and RNA binding (Freund et al., 2020). Another study specified the ILF3 and ADAR1 interaction was localized to the cytoplasm and the interaction occurred in an RNA-dependent manner (Guan et al., 2008; Nie et al., 2005). Furthermore, ILF3 was characterized as a negative regulator of RNA editing. Freund and

colleagues utilized BioID for the identification of transiently interacting site-specific regulators of ADAR1 (Freund et al., 2020). The potential ADAR1 and PRMT6 interaction may form a complex or a signalling pathway with their shared ILF2 and ILF3 known interactors that impact RNA editing and transcriptional regulation. The transient nature of interacting site-specific RNA regulators suggests that our methods may find proteins with similar roles identified with our BirA-PRMT6 BioID cells. Another DZF domain protein, ZFR (zinc finger RNA binding protein) appeared in the proteins identified from the MS analysis for MCF7 and MDA-MB-231 cells for each replicate but was not consistently enriched above the background ratio threshold. PRMT6 has been previously demonstrated to methylate the splicing factors RDA288 and hnRNP D, thus identifying PRMT6 as an RNA processing regulator altering gene expression through its substrates (Harrison et al., 2010). Dysregulation of PRMT6 can influence RNA processing by modifying Syk gene alternative splicing through the promotion of the pro-survival Syk isoform associated in breast cancer tissue (Harrison et al., 2010; Prinos et al., 2011). Our identification of these other potential PRMT6 interactors (ILF2, ILF3, ADAR1 and ZFR) capable of RNA binding proposes a novel RNA regulatory role for PRMT6 through these protein interactions.

PRMT6 and its potential interactor, ADAR1 both share the same known interactors ILF2 and ILF3. Along with the RNA regulatory role of ILF3 and ILF2 through RNA binding, both proteins are also implicated in SG regulation. SG disassembly was augmented with increased ILF2 expression rendering the cell vulnerable to arsenite stress (Shiina & Nakayama, 2014). ILF3 was revealed to be a component of SGs that after ILF3 knockdown resulted in the disassembly of polyinosinic:polycytidylic acid (poly I:C) induced SGs. Interestingly, SGs induced with sodium arsenite did not display decreased SG formation after ILF3 KD indicating ILF3's role in SG formation requires the poly I:C activated PKR (Wen et al., 2014). Similarly,

SG formation is also regulated by PRMT6 and ADAR1 as previously mentioned. PRMT6 depletion impeded bortezomib-induced SG formation (A. J. Morettin, 2015). Conversely, ADAR1 depletion increased IFN-induced SG formation revealing an ADAR1 mechanism inhibiting translation and repressing PKR activity (John & Samuel, 2014). Similar to ILF2 and ILF3's RNA regulatory role, ADAR1 additionally inhibits SG formation by modulating dsRNA which is hypothesized to restrict RNA-RNA and RNA-protein interactions required in SG formation (Corbet et al., 2021). Our MS analysis results reveal PRMT6's candidate interactor ADAR1, and that intriguingly both proteins share known ILF2 and ILF3 interactors. Furthermore, each of these proteins are demonstrated in SG regulation albeit through different mechanisms dependent on distinctive SG induction methods. The similar roles shared by these interacting proteins emphasize the potential for their interactions to impact SG regulation.

In summary, consistent ADAR1 enrichment in BirA-PRMT6 MCF7 cells by SILAC-based BioID AP/MS experiments similar to the enrichment of PRMT6 interactors, ILF2 and ILF3, establishes ADAR1 as a convincing candidate PRMT6 interactor. The shared ILF2 and ILF3 interactors between PRMT6 and ADAR1 and each protein's similar role in SG regulation are worth further investigation. Specifically, the similarities are a compelling rationale for ADAR1's implication in the unknown molecular mechanisms involving PRMT6 in bortezomib-induced SG formation.

4.4 ADAR1 is a novel PRMT6 interaction partner candidate.

The ADAR1 protein is capable of being co-expressed as both isoforms p150 or p110. Coupled expression is permitted at the p110 start codon due to leaky ribosome scanning downstream of the p150 isoform start codon (T. Sun et al., 2021). Although the p110 isoform does not require interferons to induce expression compared to the interferon-inducible p150

isoform, the p110 isoform expression can be upregulated following interferon treatment. This upregulation following interferon treatment suggests that the p110 isoform has increased editing frequency at shared p150/p110 RNA editing sites (T. Sun et al., 2021). Our BioID experiment followed by WB analysis found that the ADAR1 p110 isoform is a candidate interactor of PRMT6. Faint bands appear at the expected molecular weight of ADAR1 p150 isoform (150kDa) in our WB analysis. Select cancer cells have been found to constitutively produce interferons and this self-production was uncovered in 46% of breast cancer cases (Cheon et al., 2023). Interferon self-production occurs through activation of the cGAS-STING pathways following endogenous DNA damage from damaged replication forks and oxidative stress associated with cancer progression (Cheon et al., 2021, 2023). As previously noted, the ADAR1 p150 isoform is interferon-inducible and may be induced through breast cancer cell interferon production. Reliable and accurate detection of the ADAR1 interferon-inducible p150 isoform as a PRMT6 interaction partner cannot be determined due to the indeterminate presence of interferon under the tested conditions. Investigating the PRMT6 and ADAR1 p150 isoform interaction after interferon treatment is noteworthy for future investigations. In future projects incorporating interferon treatment, we would expect an additional layer of complexity by introducing a stress response signalling protein (IFN) in combination with the stress-inducing drug, bortezomib that both induce SG formation. Combined treatment of bortezomib and IFN-α was found to have a synergistic pro-apoptotic effect in melanoma and renal cancer cells through the extrinsic apoptosis pathway after 48 hours (Lesinski et al., 2008) thus potentially causing undesired effects in our study. Interestingly, 16 hour bortezomib treatment also induces high levels of type-1 interferon and initiates an immunogenic stress response in myeloma cells (Gulla et al., 2021; Zitvogel & Kroemer, 2021). Bortezomib interferon induction or interferon treatment

and subsequent ADAR1 p150 interferon-induced expression would require further examination to assess drug concentration, treatment exposure and protein quantification before investigating an ADAR1 p150 and PRMT6 potential interaction.

BioID of the BirA-PRMT6 and ADAR1 p110 interaction is consistent with MS data through peptide sequencing that correctly corresponds to the ADAR1 protein. For all replicates, the ADAR1 peptide sequences matched the Uniprot ADAR1 sequence following Met 296 start codon, corresponding to ADAR1 p110 translation initiation (SD Figure 10). However, MS analysis of peptide sequences did not match any of the first 295 amino acids specific only to the ADAR1 p150 isoform. This suggests that PRMT6 interaction could be specific to either isoform.

Our BioID and WB analysis of ADAR1 p110 also displayed similar detection between the MCF7 and MDA-MB-231 cell lines suggesting the interaction is not cell type-specific as previously speculated from the lack of ADAR1 detection in the MS analysis MDA-MB-231 replicate. However, our group previously observed the cell type-specific response to the same treatment regarding SG formation; PRMT6 mediates bortezomib-induced SG formation in MCF7 but not in MDA-MB-231 cells that are unable to produce bortezomib-induced SGs (A. J. Morettin, 2015). This is in agreement with other studies revealing cell type-specific PRMT6 function by TSP-1 regulation as seen in U2OS human osteosarcoma cells. In these conditions, PRMT6 is known to repress TSP-1 resulting in increased cell migration and invasion (Michaud-Levesque & Richard, 2009). In contrast, PRMT6 in PC3 and MCF7 cells upregulated TSP-1 inhibiting the same effects (N. H. Kim et al., 2013). The opposing PRMT6 regulatory functions could arise from diverging PRMT6 cellular pathways that are cell type-specific. Similarly, PRMT6 and ADAR1 p110 potentially interact in both MCF7 and MDA-MB-231 cell lines but

we speculate their protein function or interaction itself may be altered following bortezomib treatment pointing towards opposing and possibly distinct mechanisms of action.

Biotinylation of the fusion protein itself indicates a functional fusion protein (Roux et al., 2012). Our BirA-PRMT6 proximity-dependent labelling method was verified by the detection of our positive control, biotinylated fusion protein, BirA-PRMT6. Our positive control increases the validity of our BioID method to detect ADAR1 p110 as a potential interactor. We also blotted for DDX3 to attempt another method of validation but DDX3 was not detected by WB analysis in BirA-PRMT6 cells above BirA-only negative control cells (SD Figure 4). DDX3 was therefore not used as a BioID positive control continuing forward. DDX3 was previously confirmed as a PRMT6 interactor and substrate but required either DDX3 or PRMT6 overexpression for their detection via co-IP (A. J. Morettin, 2015). Difficulty detecting endogenous DDX3 *in vivo* may be attributed to a limited quantity of the total cellular DDX3 interacting with PRMT6 or low DDX3 expression in general. The DEAD-box proteins including DDX3, are a background contaminant for sepharose beads (Trinkle-Mulcahy et al., 2008) which may promote higher DDX3 detection in our BirA control group distributed throughout the cytoplasm and nucleus. DDX3 is also predominantly cytoplasmic but shuttles between the cytoplasm and nucleus (van der Pol et al., 2021) potentially resulting in less DDX3 available in the nucleus to interact with PRMT6. This factor would then limit the BirA-PRMT6 biotinylation of the DDX3 interactor.

4.5 BirA-PRMT6 Biotinylated ADAR1 p110 is nuclear.

PRMT6 and ADAR1 p110 predominantly localize in the nucleus suggesting this is where their interaction mainly occurs. The nuclear colocalization of BirA-PRMT6 and endogenous PRMT6 and ADAR1 by ICC in MCF7 and MDA-MB-231 further supports this. BirA-PRMT6 biotinylated proteins are also localized to the nucleus, similar to ADAR1, indicating PRMT6

interactors are predominantly nuclear in nature. Cellular fractionation demonstrates that along with ADAR1 p110, biotinylated ADAR1 p110 is also localized in the nuclear fraction. Due to the nuclear localization of the endogenous and biotinylated protein, our methods incorporated stringent lysis reagents and sonication methods to ensure nuclear compartment lysis but increase the likeliness of protein-protein dissociation. BioID benefits the identification of these novel weak or transient PRMT6-protein interactions. BioID combined with cellular fractionation further identifies the cytoplasmic or nuclear localization of both strong and weak interactions not demonstrated in our previous experiments. The absence of biotinylated ADAR1 p110 in the cytoplasmic fraction further indicates that the PRMT6-ADAR1 interaction is not cytoplasmic, and additionally, the biotinylated ADAR1 p110 is not shuttled to the cytoplasm after PRMT6 interaction. This is in agreement with the lack of the nuclear export domain in the truncated Zα domain of ADAR1 p110 (T. Sun et al., 2021).

A large portion of our positive control, biotinylated BirA-PRMT6, was detected in the cytoplasmic fraction. This could be attributed to the higher levels of recently translated BirA-PRMT6 being translated from ribosomes in the cytoplasm following doxycycline induction. We reason that in transfected cells PRMT6 is still predominantly nuclear observed by fluorescence microscopy (Figure 13). Our evidence for biotinylated BirA-PRMT6 in the nuclear fraction suggests BirA-PRMT6 can be imported into the nucleus along with endogenous PRMT6 but cytoplasmic BirA-PRMT6 accumulation occurs due to saturation of the nuclear import mechanism as seen with models of overexpression (Bai et al., 2017).

Overexpression of the BirA-PRMT6 fusion protein may contribute to cytoplasmic accumulation but the benefit of cellular fractionation following BioID further confirms candidate PRMT6 interactors identified are relevant to nuclear BirA-PRMT6. The presence of biotinylated

ADAR1 p110 in the nucleus suggests that in the MS experiment, the candidate ADAR1 and PRMT6 interaction was also nuclear. That being said, BioID is a proximity-based assay blind to interaction strength and abundance and does not guarantee a bona fide protein interaction with its fusion protein (Roux et al., 2012). Whilst BioID was used to screen for candidate PRMT6 interactors, identification of the potential PRMT6 and ADAR1 p110 interaction remains to be further validated.

4.6 ADAR1 p110 is an endogenous PRMT6 interactor.

To test if the ADAR1 p110 interaction with endogenous PRMT6 is proximate or physical in MCF7 cells, a co-IP was used. It is presumed that PRMT6 interacts with ADAR1 p110 in MDA-MB-231 cells but the low PRMT6 protein expression makes validation under the co-IP tested conditions inconclusive (Figure 14, SD 8). However, the detection of the co-immunoprecipitated ADAR1 p110 in MCF7 cells validated its physical interaction with PRMT6. The reciprocal immunoprecipitation with ADAR1 was unable to also co-immunoprecipitate PRMT6. Difficulty with immunoprecipitation and detection of ADAR1 enzyme interactors may result from the occupation of the targeted epitope of ADAR1 p110 with its other substrates.

Previously our BioID experiment with BirA-PRMT6 biotinylation labelling of ADAR1 p110 suggested an interaction of at least 10nm either through proximal or physical interaction due to the labelling radius of the BirA biotin ligase (Sears et al., 2019). A co-IP of PRMT6 and ADAR1 p110 further revealed that ADAR1 p110 is a physical interactor of endogenous PRMT6. There is potential for this interaction to exist in a multi-protein complex or require protein binding intermediates. Complete identification of protein complexes and inference of protein binding intermediates from co-immunoprecipitation data remains a challenge due to mechanical and chemical stresses during incubation and washes likely disturbing some of the physiological

interactions. However, co-complex relations are increasingly investigated with algorithms to identify bait proteins that regularly co-associate with the same prey proteins from co-immunoprecipitation data (Geva & Sharan, 2011). Examination of previously discovered PRMT6 and ADAR1 protein interactions revealed shared ILF2 and ILF3 interactors (Freund et al., 2020; Schneider et al., 2021) proposing a potential protein complex or interconnected cellular pathway.

4.7 The PRMT6 and ADAR1 p110 interaction is not altered by chemotherapeutic treatment.

Evidence for ADAR1 context-dependent regulation of SG was observed in IFN-inducible SGs for both ADAR1 deficient cells or ADAR1 sufficient viral infected cells (John & Samuel, 2014). In addition, cells treated with sodium arsenite or hydrogen peroxide demonstrated SG composition to be stress-dependent, with distinct protein interactomes essential in SG formation (Markmiller et al., 2018). Consequently, interferon, sodium arsenite, and hydrogen peroxide-induced SGs may alter protein dynamics differently than the bortezomib-induced SGs relevant to the rationale of this thesis. Due to both PRMT6 and ADAR1's involvement in SG formation, it is pertinent to investigate if the ADAR1 p110 and PRMT6 interaction is also impacted by bortezomib-induced stress. Our results showed that the PRMT6 and ADAR1 p110 interaction is not stress-sensitive. There was not a significant increase or decrease in the PRMT6 and ADAR1 p110 interaction following 4 h bortezomib treatment. Our results determining there was no significant change in the BirA-PRMT6 and ADAR1 p110 interaction after bortezomib treatment supports the idea that ADAR1 p110 localization presumably does not change upon cellular stress. Further research on ADAR1 localization upon oxidative and interferon-induced stress conditions found ADAR1 p150 to localize to the cytoplasm but ADAR1 p110 to remain in the

nucleus (Ng et al., 2013). We speculate that ADAR1 p110 continues to localize to the nucleus upon bortezomib treatment and will interact with PRMT6 in the nucleus similar to our finding of nuclear biotinylated ADAR1 p110 under non-stress conditions. However, further research is required to investigate the potential impact of bortezomib treatment on ADAR1 p110 localization due to bortezomib's influence on multiple cellular functions.

Bortezomib did not alter the physical ADAR1 p110 and PRMT6 interaction but it is conceivable that unidentified molecular mechanisms involving PRMT6 and ADAR1 p110 and larger signalling pathways are at play in bortezomib-induced SGs. Additional regulation that does not occur at the ADAR1 protein level includes ADAR1 mRNA overexpression and subsequent aberrant hyperediting of the multiple myeloma cell transcriptome to mediate bortezomib resistance and poor prognosis. Alternatively, ADAR1 protein expression can be altered but subsequent protein interactions may remain the same. This was observed in the RPMI-8226 P100V bortezomib resistant multiple myeloma cell line that displayed increased ADAR1 p110 and p150 protein expression compared to WT RPMI-8226 cells (Teoh et al., 2018). Similarly, PRMT6 expression was induced in HeLa cells upon bortezomib treatment and PRMT6 depletion decreased cell viability after bortezomib treatment in MCF7 cells (A. J. Morettin, 2015). Overexpression of ADAR1 was found to confer bortezomib resistance, much like PRMT6 in MCF7 cells (Teoh et al., 2018). Both proteins have opposing regulation of SG formation. Depletion of ADAR1 in U2OS cells induced SGs triggered by sodium arsenite (Corbet et al., 2021) but depletion of PRMT6 in MCF7 cells reduces bortezomib-induced SG (A. J. Morettin, 2015). While these results were observed in different cell lines, the comparable involvement in cell viability to bortezomib treatment and mediating SG formation points towards a common mechanism that could potentially be conserved across cancer types. Another relevant

role for ADAR1 was found in the stress response. ADAR1 p110 was demonstrated in a stress response mechanism to suppress apoptosis which is a cellular advantage that promotes drug resistance. This mechanism occurs by UV irradiation and heat shock stress-activated ADAR1 p110 nuclear export following its phosphorylation (Sakurai et al., 2017). Nuclear export of ADAR1 p110 resulted in its anti-apoptotic gene transcript protection from Staufen1-mediated mRNA decay (Sakurai et al., 2017). ADAR1 p110 cytoplasmic relocalization is UV irradiation and heat shock stress-dependent but has not been specifically assessed with bortezomib-induced stress.

As mentioned previously, both PRMT6 and ADAR1 p110 proteins regulate downstream cellular functions. Our unidentified molecular mechanism involving the PRMT6 and ADAR1 p110 interaction could also incorporate additional avenues of downstream cellular regulation independent from protein expression, such as RNA modification and enzymatic activity. This includes ADAR1-based RNA editing which has context-dependent regulation patterns contingent on diverse sequences and structural features that vary across RNA substrates (Liu et al., 2021). In addition to ADAR1 enzymatic activity, PRMT6 exhibits stress-dependent regulation through its enzymatic activity. Chemotherapeutic sorafenib stress-induced hepatocellular carcinoma cells only exhibited autophagic vacuoles with a PRMT6 methyltransferase inactive mutant (Che et al., 2021). The catalytically active PRMT6 is therefore functionally important in autophagy regulation conferring chemotherapeutic resistance. Che and colleagues further revealed that PRMT6 arginine methylation of the BAG5 protein is critical for autophagy regulation to decrease cell death upon sorafenib treatment (Che et al., 2021). This evidence for PRMT6 methylation activity required in the stress response and chemoresistance suggests PRMT6

methylation of the potential substrate ADAR1 p110 could be a potential regulatory mechanism to confer bortezomib resistance through SG formation.

4.8 ADAR1 (1-176) is not methylated by PRMT6 *in vitro*.

PRMT6 preferentially methylates an arginine in a glycine-arginine-rich (GAR) motif of proteins (Lakowski & Frankel, 2008). The human ADAR1 protein sequence exhibits potential GAR domains that would be plausible for PRMT6 arginine methylation (SD Figure 10). An immunoaffinity enrichment and MS analysis of protein methylation identified the ADAR1 Arg26 ADMA site and Arg91, 95, 114 MMA sites in HCT116 colorectal carcinoma cells (Guo et al., 2014). Arginine methylation has been identified in ADAR1, but not yet specified for MCF7 or MDA-MB-231 cells. A methylation assay incorporating ^{3}H labelling is a technique to identify methylation on a specific substrate by an enzyme like PRMT6. To identify if ADAR1 is a PRMT6 substrate we included recombinant purified proteins for PRMT6 and ADAR1 in our methylation reaction *in vitro*. The obtainability of recombinant ADAR1 protein for *in vitro* methylation assays was limited due to either the full-length recombinant ADAR1 protein being unavailable for purchase or the challenge of purifying large proteins (Zhao et al., 2016) such as the 110 kDa ADAR1 protein. Alternatively, a recombinant ADAR1 protein (1-176aa) was used to assess for PRMT6 methylation. Although the ADAR1 (1-176aa) sequence is absent in the 295aa truncated N-terminus of the ADAR1 p110 isoform, the relevant ADAR1 p150 isoform has not been eliminated as a potential PRMT6 interactor and substrate since ADAR1 p150 requires IFN-induction to be properly assessed in the previous experiments. Furthermore, two RGR motifs are present in the ADAR1 (1-176aa) sequence along with four RG motifs that are potential recognition sites of PRMT6 on account of a glycine immediately following an arginine (Hamey et al., 2021). Along with favourable methylation motifs, ADAR1 (1-176aa) is an ADAR1 p150

specific sequence and a worthy candidate for a PRMT6 methylation assay. In addition, it could narrow methylation to a particular area of the ADAR1 p150 sequence if methylation occurs on an arginine present in the first 176 amino acids.

We determined ADAR1 (1-176aa), the N-terminus of ADAR1 p150, is not methylated by PRMT6 *in vitro*, though PRMT6 displayed significant methylation of its known substrates, DDX3 (402-662aa) and histones. Evidence of methylation is required to be increased significantly compared to PRMT6 automethylation to dictate methylation is occurring on the potential substrate and not PRMT6 itself. Conversely, ADAR1 (1-176aa) displayed a significant decrease compared to PRMT6 automethylation background levels. The decrease in PRMT6 automethylation detected in the PRMT6 and ADAR1 (1-176aa) reaction may be attributed to ADAR1 (1-176aa) presence in the reaction reducing the chance for one PRMT6 monomer to dimerize with another PRMT6 monomer. Dimerization of PRMT6 is thought to aid in automethylation, so inhibition of a PRMT6 homodimer would decrease its automethylation (Singhroy et al., 2013), thus reflecting the decreased methylation observed in our ADAR1 (1-176aa)/PRMT6 reaction. The presence of ADAR1 could also impede PRMT6 methyltransferase activity by blocking or altering the catalytic site, reminiscent of the MS049 methyltransferase inhibitor causing PRMT6 conformational changes to inhibit enzymatic activity (Z. Chen et al., 2022). Another reason for the decrease in PRMT6 automethylation with the ADAR1 (1-176aa) protein present may also be attributed to an inhibitory protein binding mechanism comparable to that of another methyltransferase, MLL1. A lysine methyltransferase MLL1, undergoes automethylation like PRMT6. MLL1 automethylation is inhibited when the unmethylated histone substrate binds MLL1 inhibiting closure of its SET domain active site required for

automethylation (Patel et al., 2014). Patel and colleagues' research supports our reasoning that a specific protein bound to PRMT6, like ADAR1, may result in automethylation inhibition.

Our methylation assay results determine that ADAR1 (1-176aa) is not a substrate, but it is plausible that our *in vitro* methylation reaction is absent of critical scaffolding proteins that are required to facilitate PRMT6 methylation of ADAR1 (1-176aa). PRMT6 and ADAR1 p110 were found to physically interact in our previous IP results, but this interaction could be dependent on these scaffolding proteins to bring binding partners together to stably interact (Garbett & Bretscher, 2014). It is also conceivable that a full-length ADAR1 p110 protein is required to properly bind the PRMT6 substrate binding pocket and initiate methyltransferase activity due to conformational selection mechanisms. This mechanism has been observed in other enzymes to require enzyme flexibility and conformational adjustment to properly bind a substrate (Stank et al., 2016). Our results do not demonstrate ADAR1 (1-176) to be a PRMT6 substrate subject to *in vitro* conditions but we cannot eliminate ADAR1 p110 or ADAR1 p150 as potential substrates.

Limited access to full-length ADAR1 p110 recombinant protein restricted our investigation in determining if ADAR1 p110 is a PRMT6 substrate. It is plausible that PRMT6 methylates ADAR1 p110 during their physical interaction. PRMT6 methylation increases TOP3B localization to SGs in the cytoplasm in response to oxidative stress (Huang et al., 2018). This PRMT6 methylation function promoting cytoplasmic localization is similar to ADAR1 p110 translocation to the cytoplasm upon stress induction (Sakurai et al., 2017). Given that PRMT6 already has a role in cytoplasmic protein relocalization upon stress induction, PRMT6 might also take part in ADAR1 p110 cytoplasmic translocation upon stress induction prompted by ADAR1 methylation. Further research is required to determine if PRMT6 methylates ADAR1 p110 and if this regulation is involved in the stress response in reaction to bortezomib treatment.

Conclusion

This study investigated the PRMT6 interactome to identify novel protein interactors that have previously been associated with the stress response. We have established ADAR1 p110 as a novel PRMT6 interactor in the nucleus (Figure 17). An unknown chemoresistance mechanism involving PRMT6 mediation of SG formation led us to explore the PRMT6 and ADAR1 p110 interaction in the context of stress. The PRMT6 and ADAR1 p110 interaction is not impacted by bortezomib treatment suggesting other unidentified molecular mechanisms involving PRMT6 or this novel interaction may contribute to regulation of the stress response. Furthermore, PRMT6 does not regulate the ADAR1 p150 isoform through N-terminal arginine methylation, however, further elucidation of PRMT6 regulation through ADAR1 p110 methylation is required.

The results presented in this study identified ADAR1 p110 as a PRMT6 interactor. We propose that further investigation of PRMT6 regulation of the ADAR1 p110 interaction regarding bortezomib-induced SG formation and non-stress conditions would be beneficial.

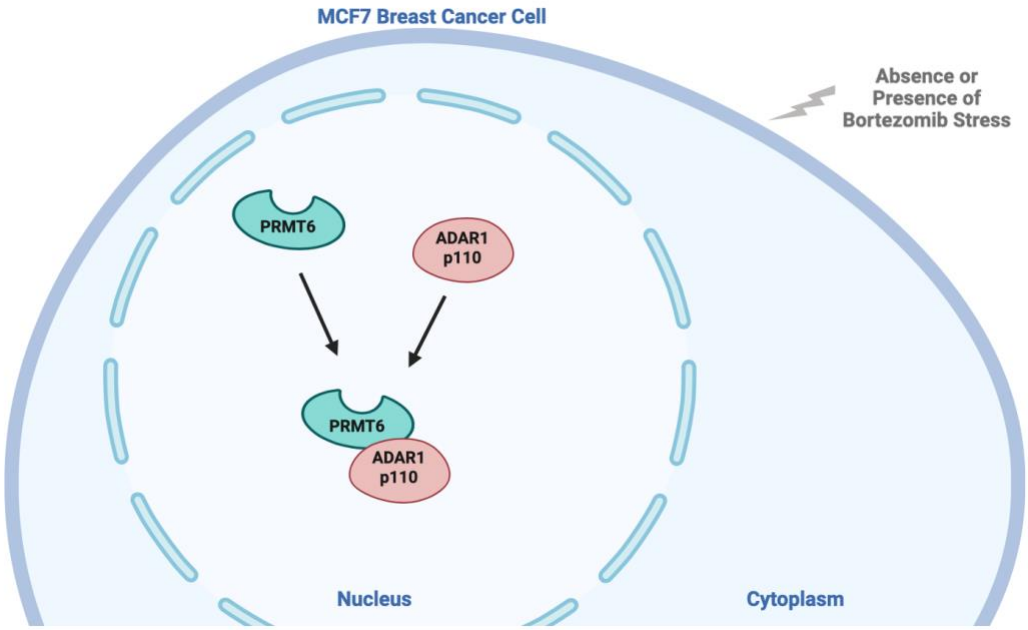

Figure 17: Graphical Abstract of PRMT6 and ADAR1 p110 interaction.

PRMT6 interacts with ADAR1 p110 in the nucleus of MCF7 breast cancer cells. The physical interaction persists in non-stress conditions and with the addition of bortezomib stress. Created with BioRender.com.

Future Directions

Molecular functions involving PRMT6 are regulated by its interactome in breast cancer cells. Identifying novel PRMT6 interactors involved in the stress response is crucial to elucidating these molecular mechanisms involving PRMT6 regulation of chemoresistance. We identified the novel PRMT6 interactor, ADAR1 p110 previously demonstrated in other studies to regulate SG formation. This interaction has the potential to provide insight into the unknown PRMT6 mechanism also regulating SG formation and promoting chemoresistance. To study this, we would characterize ADAR1 p110 function in SG formation by performing siRNA ADAR1 p110 KD and assess bortezomib-induced SG formation with ICC compared to WT cells. A double ADAR1 p110 and PRMT6 KD would further reveal how the two interacting proteins are

interconnected in the SG regulation pathway in MCF7 cells. If we observe changes in SG formation by utilizing KDs this would reveal if the PRMT6 and ADAR1 p110 physical interaction is required for SG formation. We would next need to assess if any of these changes are dependent on PRMT6 methyltransferase activity and where PRMT6 methylates ADAR1 p110. First, an ADAR1 p110 IP using WT or PRMT6 KD would be coupled to mass spectrometry with a comparative analysis to identify arginine residues methylated in WT cells and absent in PRMT6 KD cells. The arginine residue(s) would then be investigated by site-directed mutagenesis by mutating arginine residues to lysine and tryptophan residues. The mutated constructs would be assessed in functional rescue experiments using an *in vivo* methylation assay of ADAR1 p110 siRNA KD cells with either overexpression of WT ADAR1 p110 or arginine point mutated ADAR1 p110 constructs. If an ADAR1 p110 arginine residue is identified to be methylated by PRMT6 we will observe WT ADAR1 p110 to rescue methylation levels in KD ADAR1 cells but mutant ADAR1 p110 will not.

Next, this same rescue experiment will be used to investigate this specific PTM during the stress response by treating cells with bortezomib. This will reveal if PRMT6 methyltransferase activity of ADAR1 p110 is necessary for a particular ADAR1 p110 function in the stress response. Specifically, we could measure if there is a change in bortezomib-induced SG formation using ICC. Previous research demonstrated that PRMT6 is necessary for bortezomib induced SG formation in MCF7 cells (A. J. Morettin, 2015) and interestingly, ADAR1 has an inhibitory effect on IFN-SG formation in HeLa cells (John & Samuel, 2014). If the rescue experiment with the ADAR1 p110 mutant construct results in decreased SG formation, and WT ADAR1 p110 overexpression results in increased SG formation, we could then determine that in WT cells PRMT6 methyltransferase activity imparts a repressive effect on

ADAR1, halting ADAR1's ability to impede SG formation. Thus, PRMT6 methylation of ADAR1 results in SG formation (Figure 18).

IFN addition to cell media promotes expression in the IFN-inducible ADAR1 p150 and constitutively expressed ADAR1 p110 isoforms (T. Sun et al., 2021). The ADAR1 p110 and ADAR1 p150 interaction with PRMT6 would be investigated with IFN treatment to induce expression before BioID and immunoprecipitation is performed. We would then test if PRMT6 interacts with both ADAR1 isoforms. Next, the potential PRMT6 and ADAR1 p150 and p110 interactions would be investigated in the context of bortezomib stress and if those interactions are impacted by treatment. ADAR1 was previously investigated in IFN-induced SGs (Ng et al., 2013) but not bortezomib-induced SG, so additional research could provide insight into IFN-inducible ADAR1 isoforms and PRMT6's involvement in the bortezomib-induced stress response.

In summary, analysis of the PRMT6 and ADAR1 interaction or PRMT6 methylation of ADAR1 with or without bortezomib-induced SG formation is important in uncovering how PRMT6 mechanistically contributes to breast cancer prognosis and bortezomib resistance. PRMT6 and ADAR1 could provide potential new targets to improve existing therapeutics in breast cancers exhibiting chemoresistance.

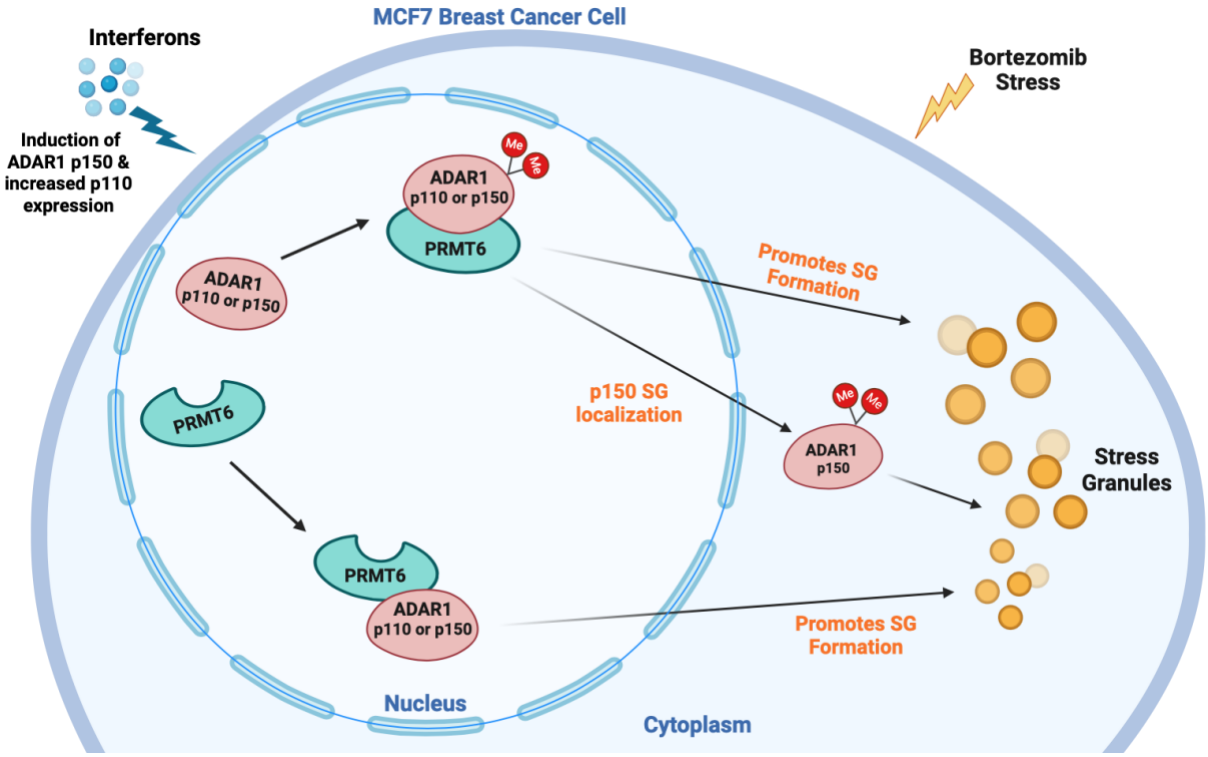

Figure 18: Proposed molecular mechanisms of PRMT6 and ADAR1 interaction based on future directions.

Interferon treatment will induce ADAR1 p150 expression and increase p110 protein expression. ADAR1 either interacts with PRMT6 or interacts and becomes methylated by PRMT6 to promote SG formation under bortezomib stress conditions. PRMT6's potential methylation of ADAR1 or ADAR1 interaction imparts a repressive effect on ADAR1, halting ADAR1's ability to impede SG formation. The ADAR1 p150 protein potentially localizes to SGs after PRMT6 interaction of PRMT6 methylation of p150. Created with BioRender.com.

Appendix A: Supplementary Data

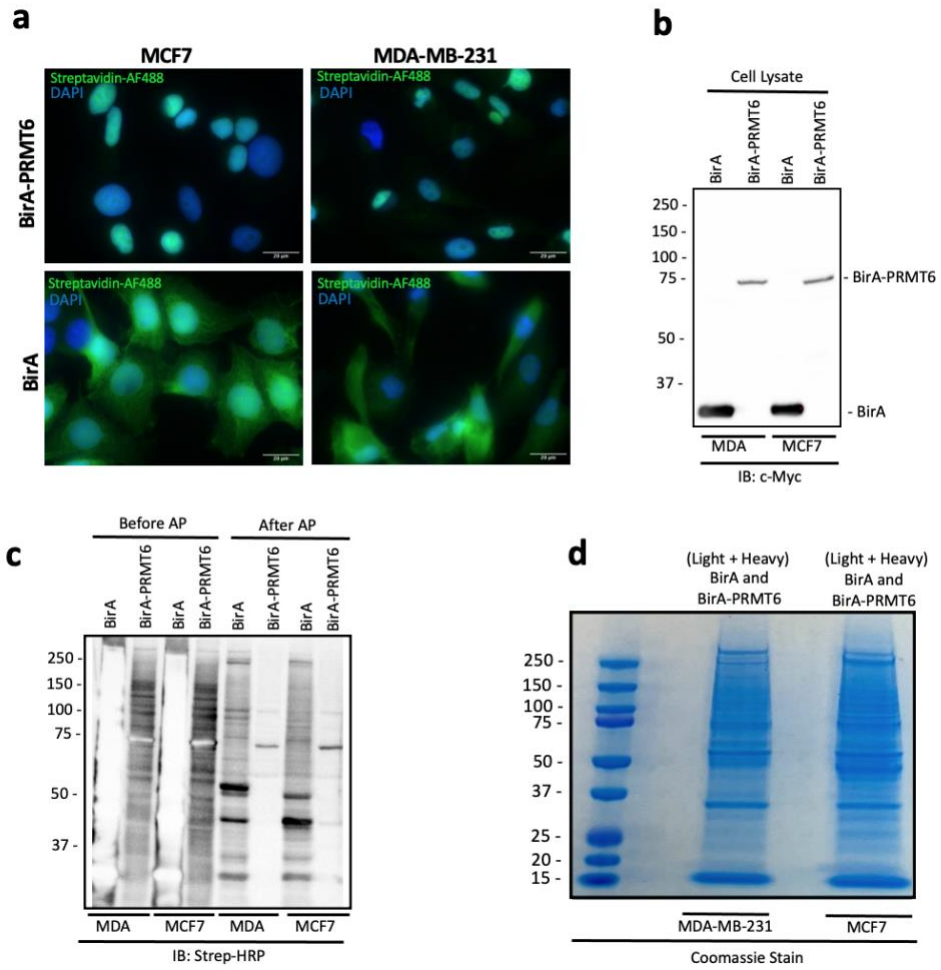

SD Figure 1: Controls and validation of active BioID cells for BioID AP/MS.

Replicate of Figure 7 MS experiment 2 with SILAC labelling flipped. **(a)** ICC of MDA-MB-231 and MCF7s grown in SILAC media after 0.5 µg/mL doxycycline for a 48 h induction of BirA-PRMT6 and BirA, and 50 µM biotin. MCF7 and MDA-MB-231 cells were blotted with streptavidin-AlexaFluor 488 and DAPI. Magnification 63X, scale bars represent 20 µm. Images are representative of each cell line and construct. **(b)** WB analysis of apparent 77 kDa ligase-bait fusion protein, BirA-PRMT6 and 35 kDa BirA-induced expression with an anti-c-Myc antibody **(c)** WB analysis of whole-cell lysate with streptavidin-HRP conjugate before and after AP. **(d)** Coomassie stain of AP product prior to tryptic digestion and MS analysis.

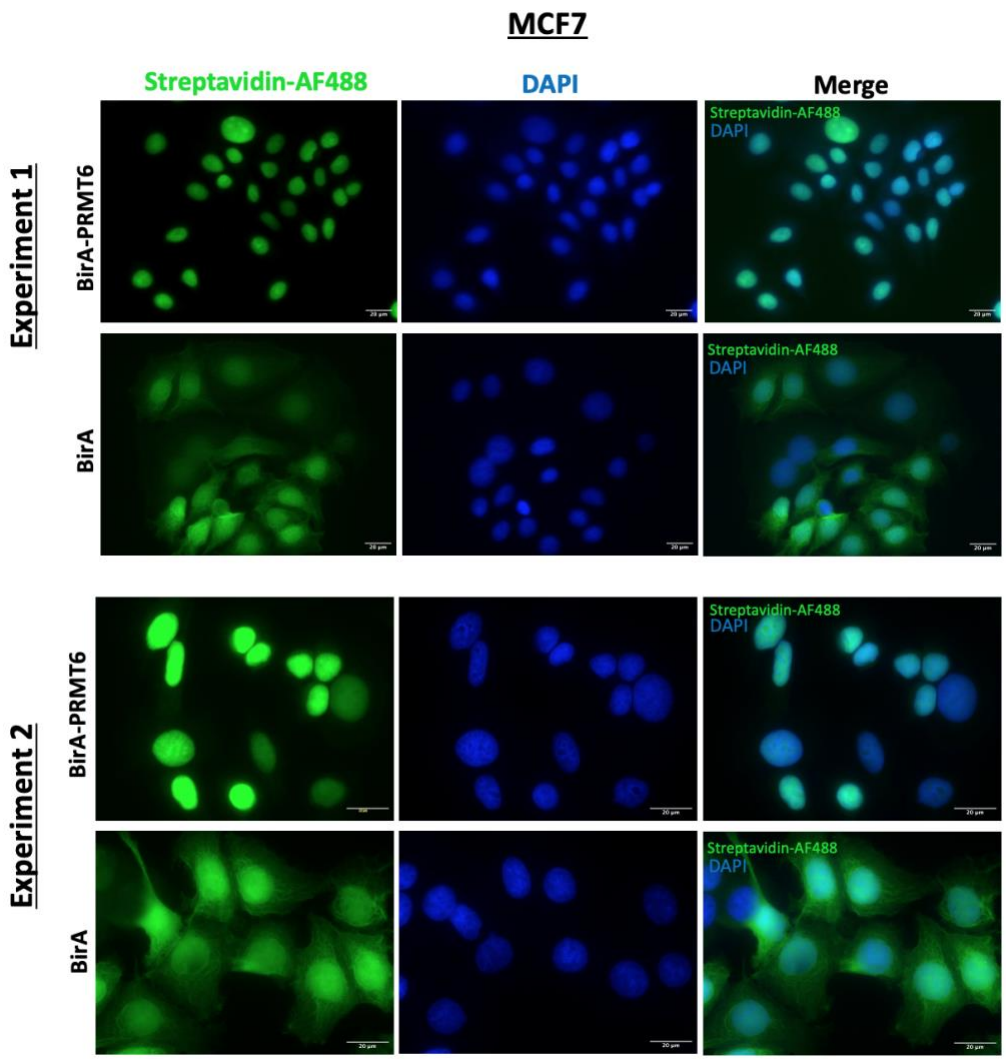
MCF7
Streptavidin-AF488
DAPI
Merge
Experiment 1
BirA-PRMT6
BirA
Experiment 2
BirA-PRMT6
BirA
Streptavidin-AF488
DAPI

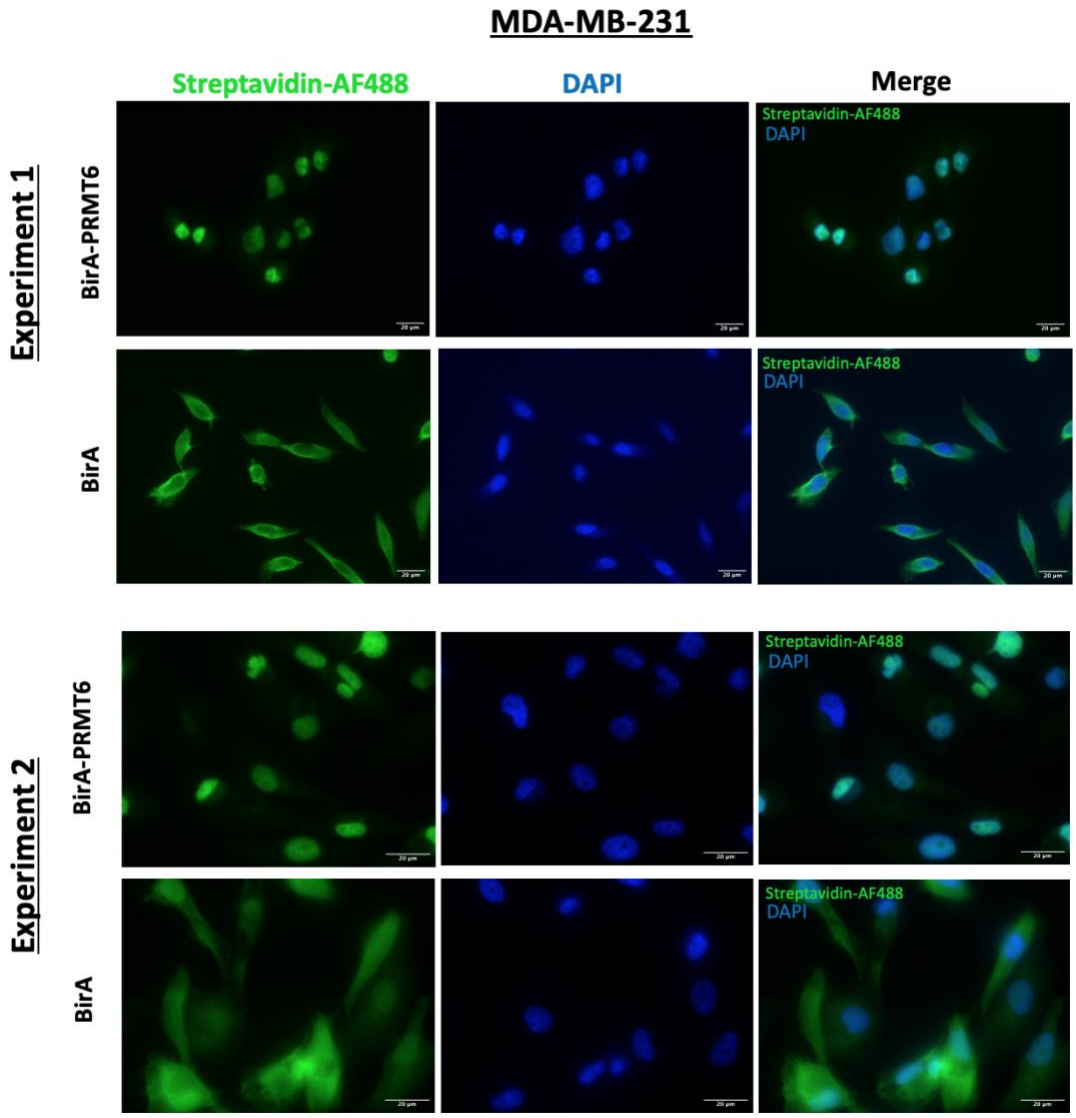

SD Figure 2: Biotinylated protein localization in MDA-MB-231 and MCF7 induced cells by immunocytochemistry.

ICC of Figure 7 cells grown in SILAC media with the addition of 0.5ug/mL doxycycline for a 48 h induction of BirA-PRMT6 and BirA, and 50µM biotin. MCF7 and MDA-MB-231 cells were paraformaldehyde fixed and blotted with Streptavidin-AlexaFluor 488 (green; biotinylated proteins) and DAPI (blue; DNA stain). Magnification 40X for experiment 1 and 63X for experiment 2. Scale bars correspond to 20 µm. Images are representative of each cell line and construct.

SD Table 1: Unique unquantified peptides identified in BirA-PRMT6 BioID/MS replicate experiments done in MDA-MB-231 and MCF7 cells.

MCF7		MDA-MB-231	
UniProt ID	Gene	UniProt ID	Gene
Experiment 1			
Q96G75	RMND5B	Q9Y2K5	R3HDM2
Q96J02	ITCH	Q7Z4K8	TRIM46
Q9HAU5	UPF2	Q9GZZ9	UBA5
Q5VZ89	DENND4C	Q13285	NR5A1
Q8TD17	ZNF398	Q99424	ACOX2
		Q96J02	ITCH
		P11177	PDHB
		Q8IY67	RAVER1
		Q01081	U2AF1

MCF7		MDA-MB-231	
UniProt ID	Gene	UniProt ID	Gene
Experiment 2			
Q96LA8	PRMT6	Q96LA8	PRMT6
Q86UQ4	ABCA13	Q86UQ4	ABCA13
Q86U42	PABPN1	O75843	AP1G2
P61626	LYZ	P36269	GGT5
Q5TCZ1	SH3PXD2A	P35326	SPRR2A
Q9NY47	CACNA2D2	Q5T749	KPRP
Q16678	CYP1B1	Q96DA0	ZG16B
Q96DA0	ZG16B	P04259	KRT6B
Q9UHF7	TRPS1	P12273	PIP

P81605	DCD	Q86YR6	POTED
Q13547	HDAC1	Q9H2K8	TAOK3
P45973	CBX5	Q16678	CYP1B1
Q5T749	KPRP	Q9Y5U5	TNFRSF18
Q14137	BOP1	O60704	TPST2
P10412	HIST1H1E	Q9Y577	TRIM17
P35326	SPRR2A	O95243	MBD4
Q8IUC1	KRTAP11-1	Q9NQH7	XPNPEP3
Q8WVB6	CHTF18	Q15526	SURF1
O14925	TIMM23	Q9Y5V3	MAGED1
O76021	RSL1D1	Q02413	DSG1
Q01469	FABP5	Q8N139	ABCA6
Q15758	SLC1A5	O00522	KRIT1
Q96GX5	MASTL	Q5TAP6	UTP14C
O14579	COPE	O75489	NDUFS3
Q8NFC6	BOD1L1	D6REC4	CFAP99
P42285	SKIV2L2	A1L0T0	ILVBL
		P11177	PDHB
		Q6P597	KLC3
		P12004	PCNA
		Q5T750	XP32
		P14923	JUP
		Q86WZ0	HEATR4
		O75182	SIN3B
		O76031	CLPX
		Q9H7Z3	NRDE2

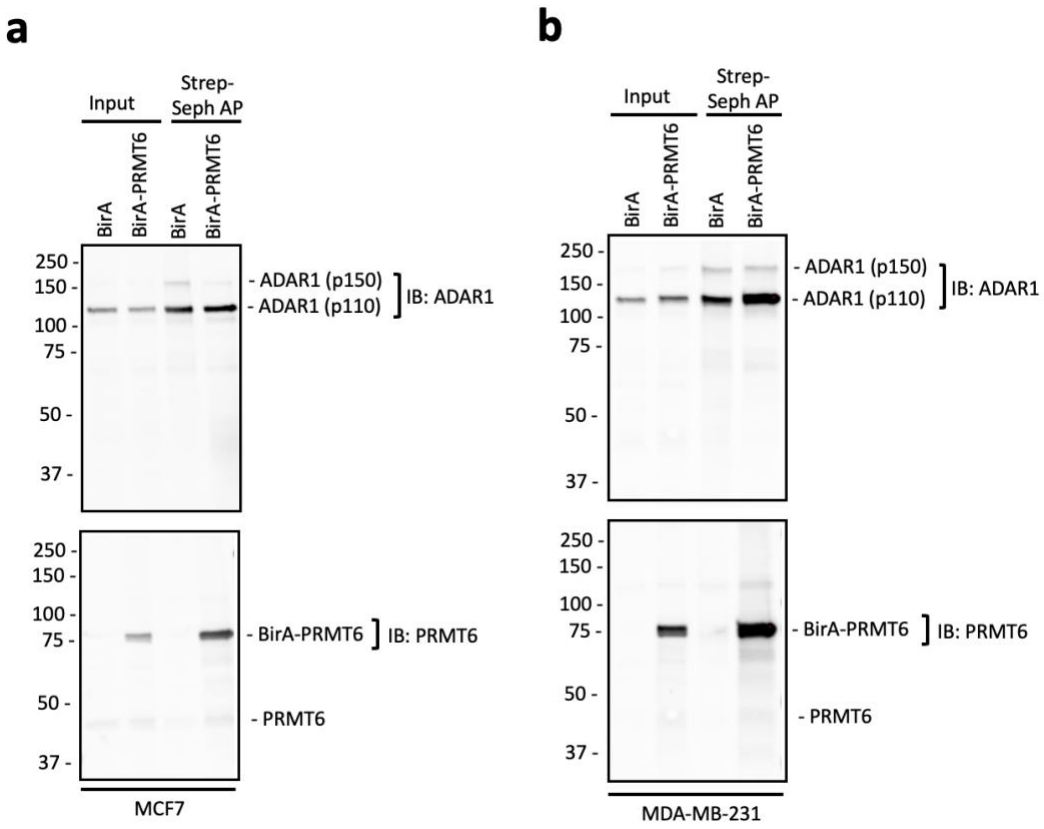

SD Figure 3: Confirmation of candidate PRMT6 interaction partner ADAR1 p110 using BioID.

(a, b) Full WB analysis of Figure 11 blots. Streptavidin-sepharose pull-down of biotinylated ADAR1 p110 and BirA-PRMT6 were detected using anti-ADAR1 and -PRMT6 antibodies, respectively.

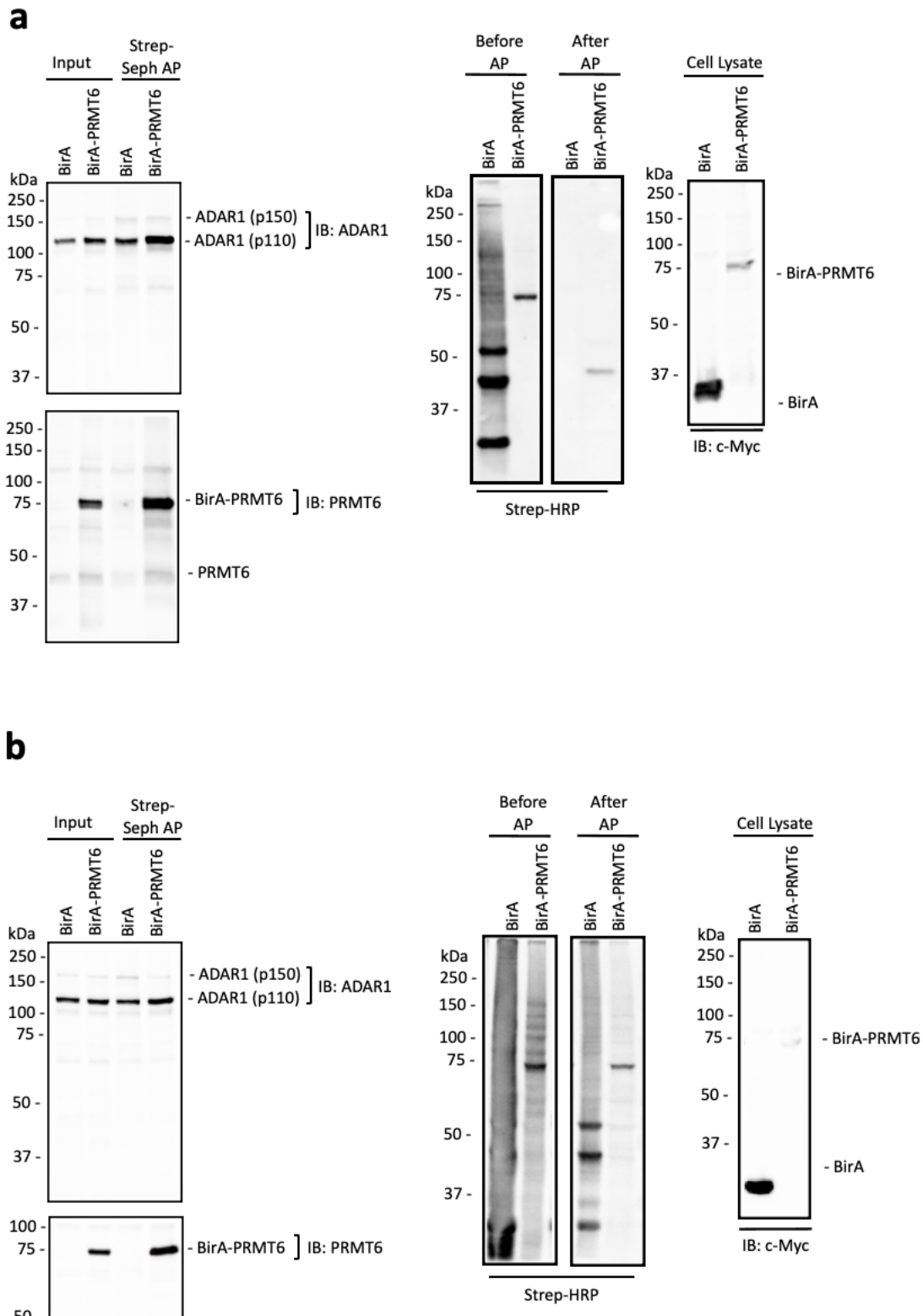
a
Input
Strep-Seph AP
BirA
BirA-PRMT6
kDa
250
150
100
75
50
37
- ADAR1 (p150)
- ADAR1 (p110)
IB: ADAR1
- BirA-PRMT6
IB: PRMT6
- PRMT6
Before AP
After AP
Strep-HRP
Cell Lysate
- BirA-PRMT6
- BirA
IB: c-Myc
b

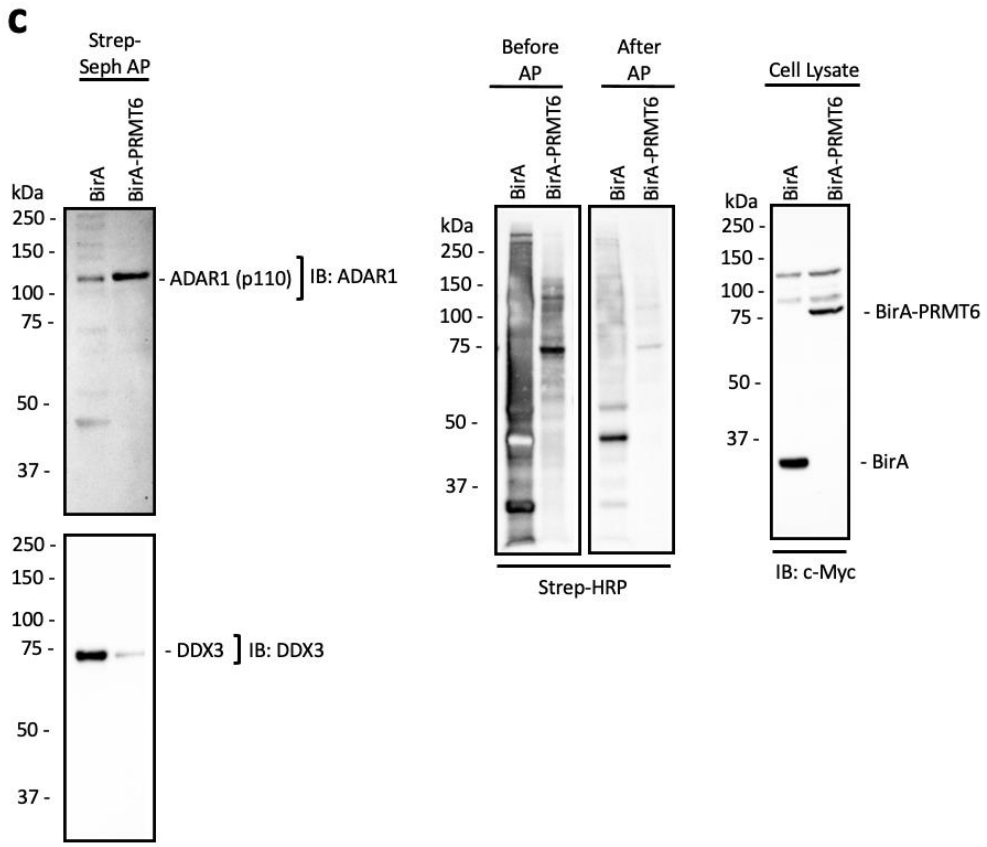

SD Figure 4: Replicate MCF7 blots for confirmation of candidate PRMT6 interaction partner ADAR1 p110 using BioID.

(a-c) Full WB analysis of MCF7 replicates for Figure 11 blots. Streptavidin-sepharose pull-down of biotinylated ADAR1 p110 and BirA-PRMT6 were detected using anti-ADAR1 and -PRMT6 antibodies, respectively. Inputs are 3%. Each replicate has WB analysis of cell lysate displaying apparent 77 kDa ligase-bait fusion protein, BirA-PRMT6 and 35 kDa BirA-induced expression with an anti-c-Myc antibody to detect the N-terminal Myc tag on both biotin-ligases. Western blot analysis of whole-cell lysate confirmed biotinylated protein with streptavidin-HRP conjugate before AP and biotinylated protein depletion after AP.

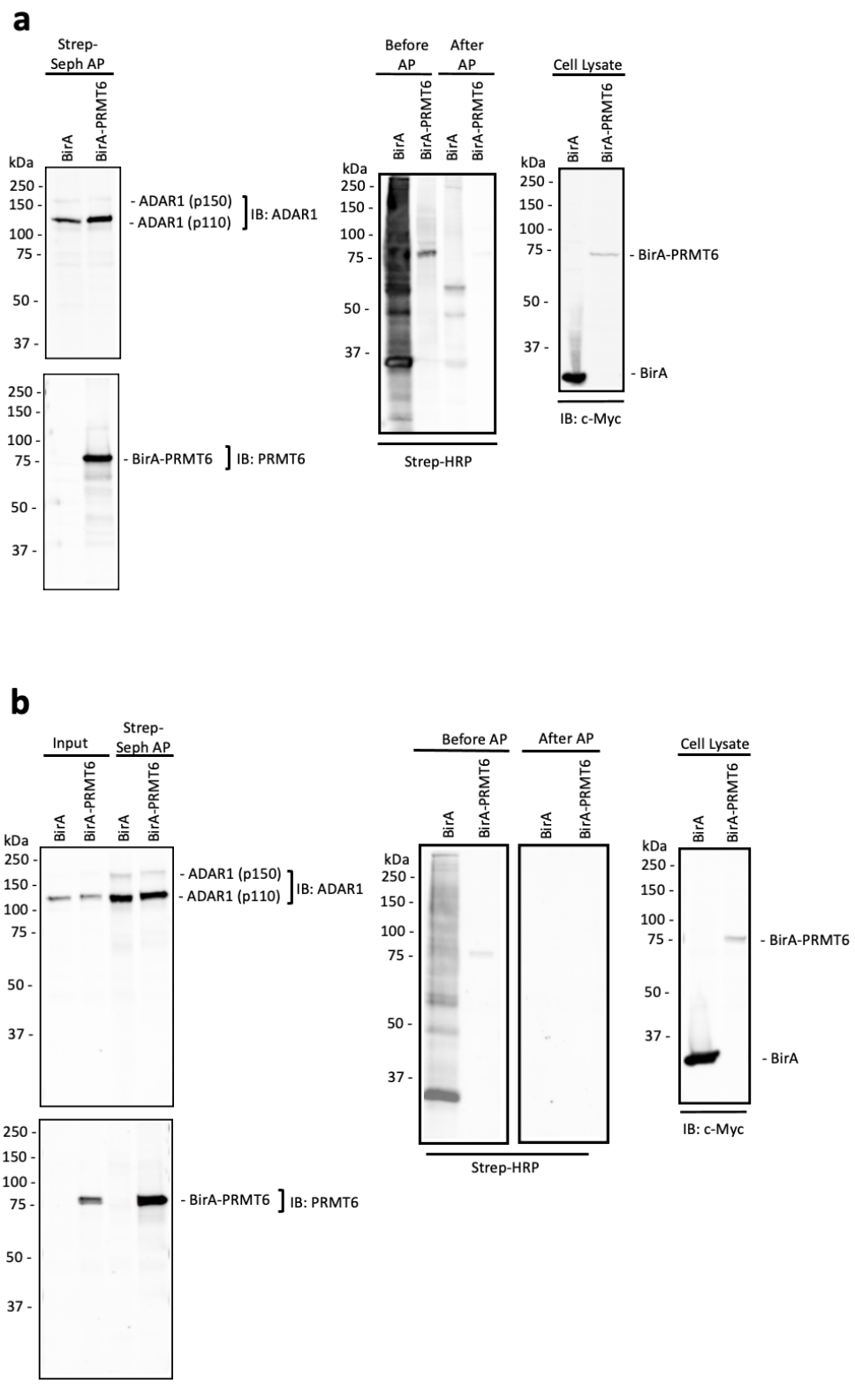
a
Strep-Seph AP
BirA
BirA-PRMT6
kDa
250 -
150 -
100 -
75 -
50 -
37 -
- ADAR1 (p150)
- ADAR1 (p110)
IB: ADAR1
- BirA-PRMT6
IB: PRMT6
Before AP
After AP
Strep-HRP
Cell Lysate
- BirA-PRMT6
- BirA
IB: c-Myc
b
Input
Strep-Seph AP
Before AP
After AP
Cell Lysate
- ADAR1 (p150)
- ADAR1 (p110)
IB: ADAR1
- BirA-PRMT6
IB: PRMT6
Strep-HRP
- BirA
IB: c-Myc

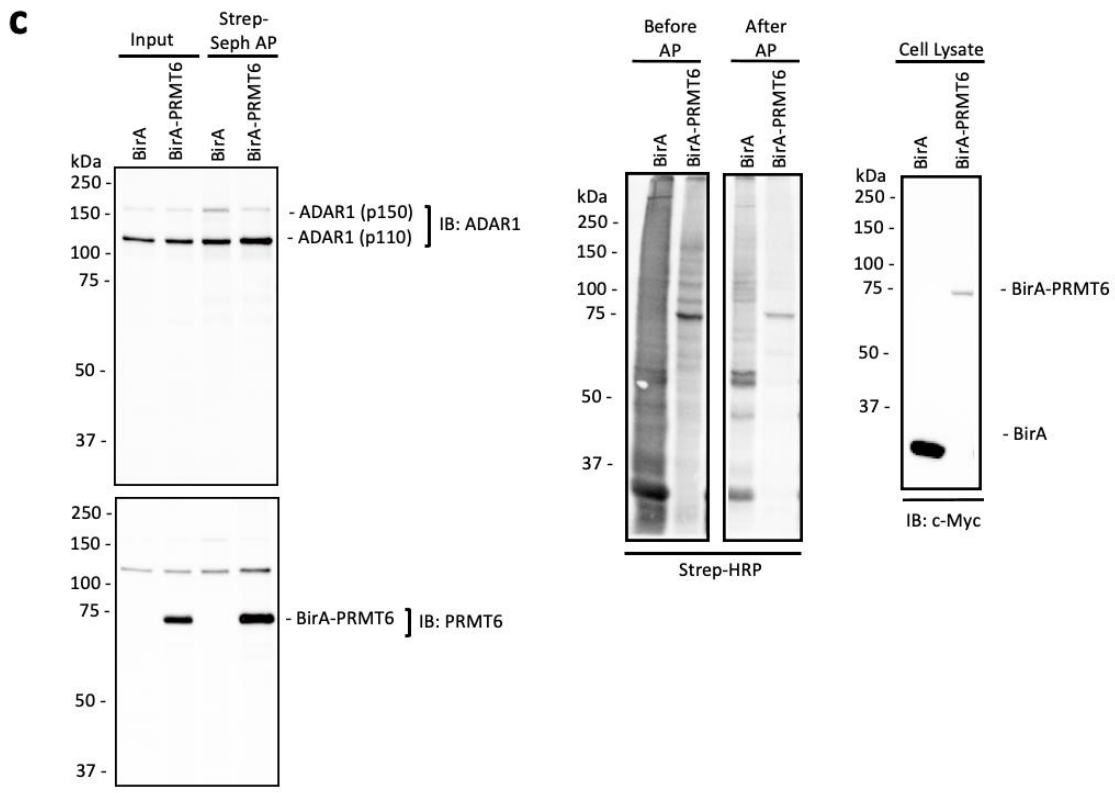

SD Figure 5: Replicate MDA-MB-231 blots for confirmation of candidate PRMT6 interaction partner ADAR1 p110 using BioID.

(a-c) Full WB analysis of MDA-MB-231 replicates for Figure 11 blots. Streptavidin-sepharose pull-down of biotinylated ADAR1 p110 and BirA-PRMT6 were detected using anti-ADAR1 and -PRMT6 antibodies, respectively. Inputs are 3%. Each replicate has WB analysis of cell lysate displaying apparent 77 kDa ligase-bait fusion protein, BirA-PRMT6 and 35 kDa BirA-induced expression with an anti-c-Myc antibody to detect the N-terminal Myc tag on both biotin-ligases. Western blot analysis of whole-cell lysate confirmed biotinylated protein with streptavidin-HRP conjugate before AP and biotinylated protein depletion after AP.

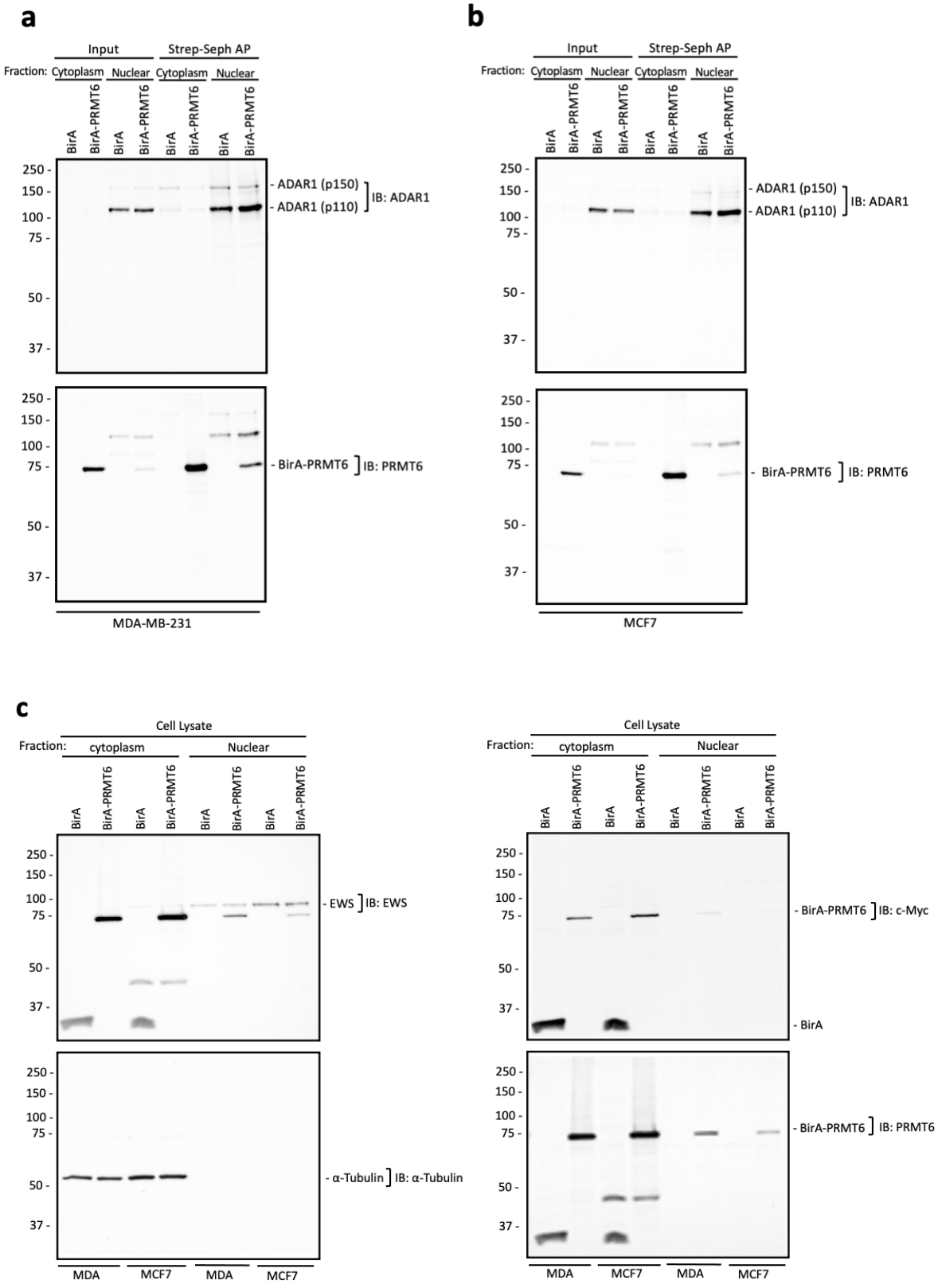
a
Input
Strep-Seph AP
Fraction: Cytoplasm Nuclear Cytoplasm Nuclear
BirA
BirA-PRMT6
250 -
150 -
100 -
75 -
50 -
37 -
- ADAR1 (p150)
- ADAR1 (p110)
IB: ADAR1
- BirA-PRMT6
IB: PRMT6
MDA-MB-231
b
MCF7
c
Cell Lysate
Fraction: cytoplasm Nuclear
- EWS
IB: EWS
- α-Tubulin
IB: α-Tubulin
- BirA-PRMT6
IB: c-Myc
- BirA
MDA
MCF7

SD Figure 6: Cellular fractionation with BioID reveals PRMT6 and ADAR1 interaction is nuclear.

(a,b) Full blots of Figure 12 WB analysis of MDA-MB-231 and MCF7 cells and their cytoplasmic and nuclear fractions for AP of biotinylated ADAR1 (p110) by BirA-PRMT6 vs BirA detected using anti-ADAR1 and -PRMT6 antibodies. (c) WB analysis of full blots for Figure 12 to confirm fractionation of cytoplasm and nucleus with anti- α-Tubulin and -EWS, respectively. BirA-PRMT6 and BirA expression were confirmed with anti -c-Myc and -PRMT6 antibodies.

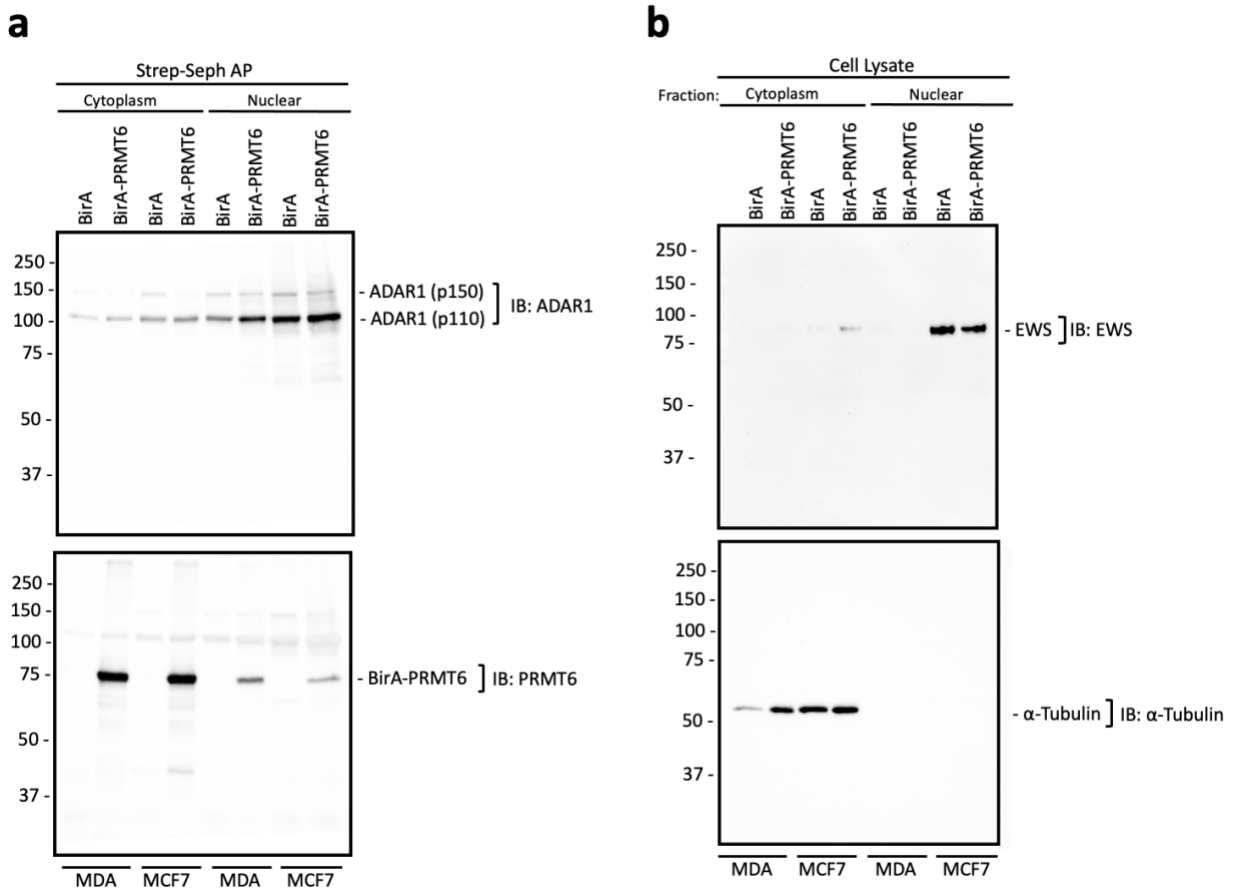

SD Figure 7: Cellular fractionation with BioID reveals PRMT6-ADAR1 interaction is nuclear.

(a,b) Replicate for BioID/AP experiment Figure 12 with cytoplasmic and nuclear fractions. **(a)** Western blot analysis of MDA-MB-231 and MCF7 cells and their cytoplasmic and nuclear fractions for AP of biotinylated ADAR1 (p110) by BirA-PRMT6 vs BirA detected using anti-ADAR1 and -PRMT6 antibodies. **(b)** Western blot analysis to confirm fractionation of cytoplasm and nucleus with anti- α-Tubulin and -EWS, respectively.

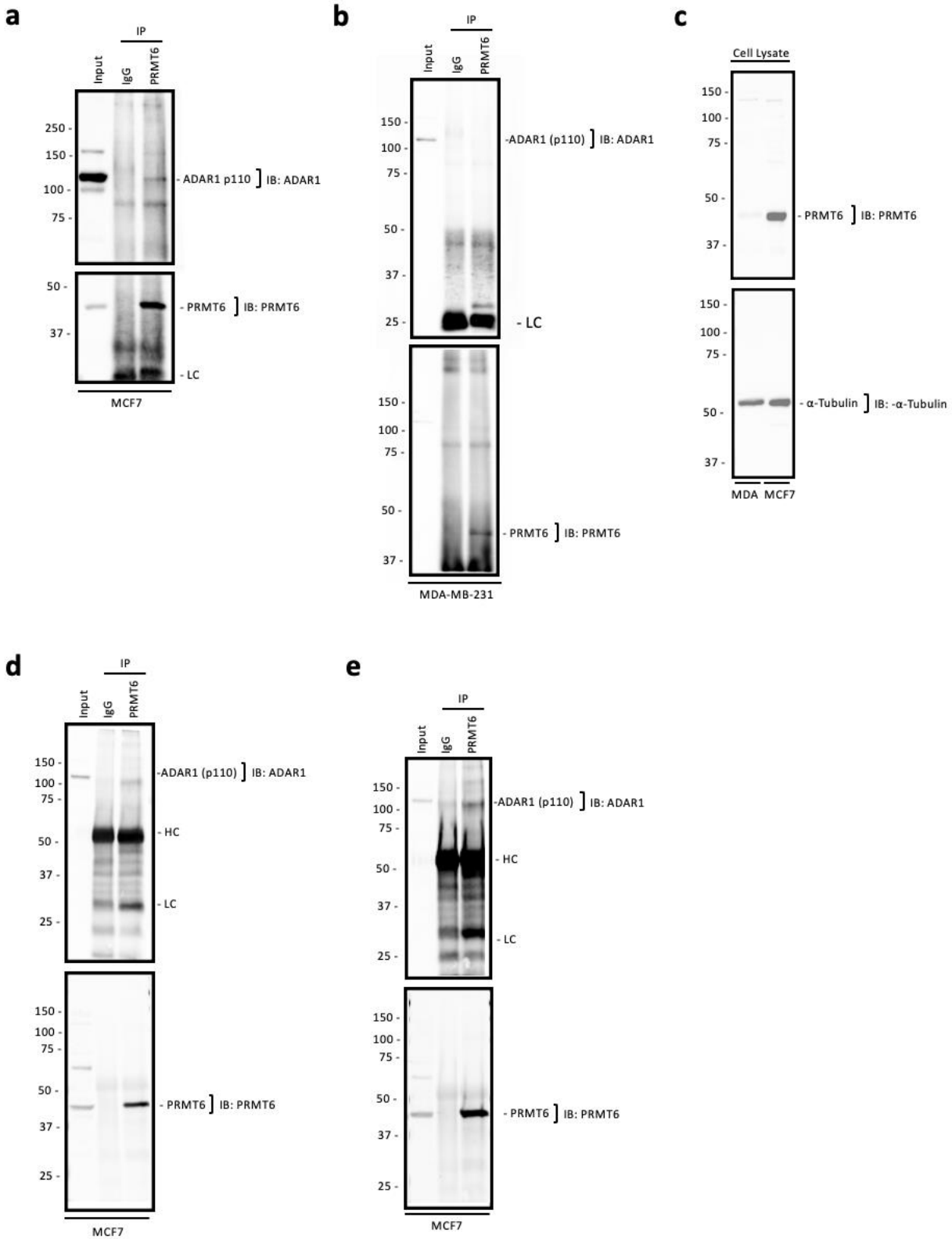
a
IP
Input
IgG
PRMT6
250
150
100
75
50
37
- ADAR1 p110] IB: ADAR1
- PRMT6] IB: PRMT6
- LC
MCF7
b
IP
Input
IgG
PRMT6
150
100
75
50
37
25
-ADAR1 (p110)] IB: ADAR1
- LC
- PRMT6] IB: PRMT6
MDA-MB-231
c
Cell Lysate
150
100
75
50
37
- PRMT6] IB: PRMT6
- α-Tubulin] IB: -α-Tubulin
MDA
MCF7
d
IP
Input
IgG
PRMT6
-ADAR1 (p110)] IB: ADAR1
- HC
- LC
- PRMT6] IB: PRMT6
MCF7
e
IP
Input
IgG
PRMT6
-ADAR1 (p110)] IB: ADAR1
- HC
- LC
- PRMT6] IB: PRMT6
MCF7

SD Figure 8: Validation of endogenous PRMT6-ADAR1 (p110) interaction in MCF7 cells.

Full WB analysis provided for Figure 14 blots and MCF7 IP replicates. **(a,b,d,e)** Co-IP was performed with PRMT6 antibody and A/G beads with total protein extracts from WT MCF7 or MDA-MB-231 cells and 1% input. ADAR1 p110 was detected with anti-ADAR1 antibody and endogenous PRMT6 with anti-PRMT6 antibody. **(c)** WB analysis of cell lysate using anti-PRMT6 antibody displays a difference in PRMT6 expression levels between MDA-MB-231 and MCF7 cell lines. HC and LC denotes heavy and light chain, respectively.

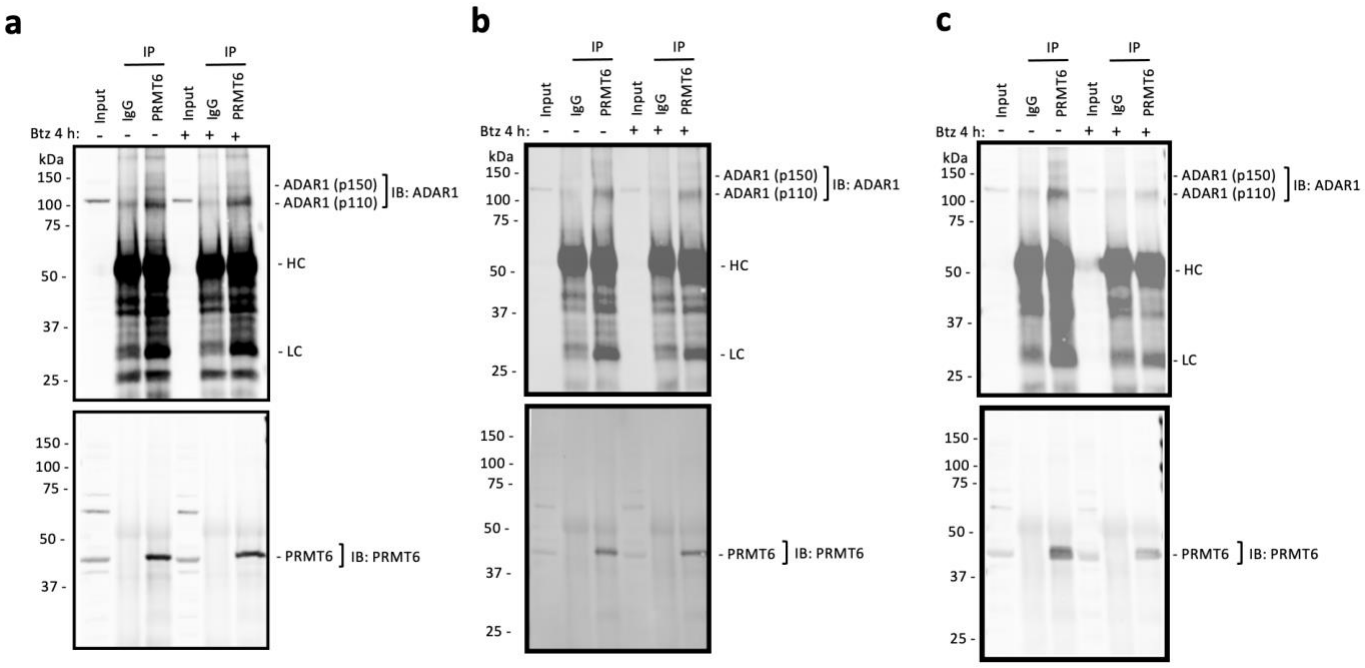

SD Figure 9: The PRMT6 and ADAR1 p110 interaction does not change upon bortezomib treatment in MCF7 cells.

Full blot **(a)** and replicates for Figure 15 co-IP **(c,b)** MCF7 WT cells were treated with 10 μM of bortezomib (btz) or DMSO control for 4 h. Co-IP was performed with PRMT6 antibody and A/G beads with total protein extracts from WT MCF7 and MDA-MB-231 cells and 5% Input. Western blot analysis identified co-IP of ADAR1 p110 with anti-ADAR1 antibody and endogenous PRMT6 with anti-PRMT6 antibody in MCF7 cells. HC and LC denotes heavy and light chain, respectively.

MNPRQGYSLSGYYTHPFQGYEHRQLRYQQPGPGSSPSSFLLKQIEFLKGQLPEAPVIGKQTPSLPPSLPGLRPRF
PVLLASSTRGRQVDIRGVPRGVHLRSQGLQRGFQHPSPRGRSLPQRGVDCLSSHFQELSIYQDQEQRILKFLEEL
GEGKATTAHDLSGKLGTPKKEINRVLYSLAKKGKLQKEAGTPPLWKIAVSTQAWNQHSGVVRPDGHSQGAPN
SDPSLEPEDRNSTSVSEDLLEPFIAVSAQAWNQHSGVVRPDSHSQGSPNSDPGLEPEDSNSTSALEDPLEFLDM
AEIKEKICDYLFNVSDSSALNLAKNIGLTKARDINAVLIDMERQGDVYRQGTTPPIWHLTDKKRERMQIKRNTNS
VPETAPAAIPETKRNAEFLTCNIPTSNASNNMVTTEKVENGQEPVIKLENRQEARPEPARLKPPVHYNGPSKAG
YVDFENGQWATDDIPDDLNSIRAAPGEFRAIMEMPSFYSHGLPRCSPYKKLTECQLKNPISGLLEYAQFASQTCE
FNMIEQSGPPHEPRFKFQVVINGREFPPAEAGSKKVAKQDAAMKAMTILLEEAKAKDSGKSEESSHYSTEKESE
KTAESQTPTPSATSFFSGKSPVTTLLECMHKLGNSCEFRLLSKEGPAHEPKFQYCVAVGAQTFPSVSAPSKKVAK
QMAAEEAMKALHGEATNSMASDNQPEGMISESLDNLESMMPNKVRKIGELVRYLNTNPVGGLLEYARSHGF
AAEFKLVDQSGPPHEPKFVYQAKVGGRWFPAVCAHSKKQGKQEAADAALRVLIGENEKAERMGFTEVTPVTG
ASLRRTMLLLSRSPEAQPKTLPLTGSTFHDQIAMLSHRCFNTLTNSFQPSLLGRKILAAIIMKKDSEDMGVVVSLG
TGNRCVKGDSLSLKGETVNDCHAEIISRRGFIRFLYSELMKYNSQTAKDSIFEPAKGGEKLQIKKTVSFHLYISTAP
CGDGALFDKSCSDRAMESTESRHYPVFENPKQGKLRTKVENGEGTIPVESSDIVPTWDGIRLGERLRTMSCSDK
ILRWNVLGLQGALLTHFLQPIYLKSVTLGYLFSQGHLTRAICCRVTRDGSAFEDGLRHPFIVNHPKVGRVSIYDSK
RQSGKTKETSVNWCLADGYDLEILDGTRGTVDGPRNELSRVSKKNIFLLFKKLCSFRYRRDLLRLSYGEAKKAAR
DYETAKNYFKKGLKDMGYGNWISKPQEEKNFYLCPV

SD Figure 10: Human ADAR1 protein sequence.

P55265 Uniprot ID for ADAR1 sequence that is 1226 amino acids in length. Yellow highlighted Met 1 is where ADAR1 p150 isoform is initiated for translation. Underlined Met 1 to Lys 176 is the GST-ADAR1 (1-176aa) recombinant protein sequence (MyBioSource). Yellow highlighted Met 296 is where ADAR1 p110 isoform is initiated for translation. Underlined red text is the ADAR1 peptide sequence identified from MS experiment 1 in MDA-MB-231 cells. Underlined blue text is the ADAR1 peptide sequence identified from MS experiment 1 in MCF7 cells. Underlined green text is the ADAR1 Peptide sequence for MS experiment 2 in MDA-MB-231 and MCF7 cells.

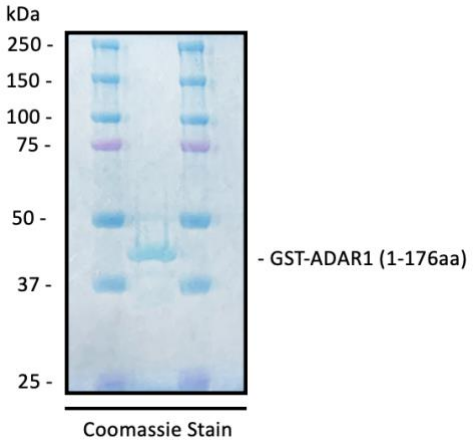

SD Figure 11: Validation of GST-ADAR1 (1-176aa) recombinant purified protein in the sample.

(a) Coomassie stain of 2mg of purified recombinant GST-ADAR1 (1-176aa) protein by SDS-PAGE. GST-ADAR1 (1-176aa) protein was used in methylation assay reactions for Figure 16.

Appendix B: PRMT6 SG formation through eIF4e regulation

Along with my thesis project, I have been working on experiments for the Côté Laboratory's PRMT6/eIF4E project including sucrose density gradient fractionation experiments with assistance from Andréanne Didillon (Appendix B Figure 1).

Background

Stress granule formation can be induced by bortezomib and sodium arsenite and becomes impeded with a PRMT6 knockdown (A. J. Morettin, 2015). SG formation is regulated by eukaryotic translation initiation factors with regulation further categorized as an eIF2α-dependent and -independent mechanism (F. Wang et al., 2020). The eIF4E protein binds the 5'mRNA cap forming a complex with eIF4G and eIF4A to initiate translation through recruitment of ribosomes (Amorim et al., 2018).

PRMT6 involvement in SG formation functions through eIF4E regulation (an eIF2α-independent mechanism) for SG formation (Figure 3). Specifically, PRMT6 was found to mediate SG formation through eIF4E regulation, ultimately promoting bortezomib resistance (A. J. Morettin, 2015). We are currently investigating if PRMT6 regulation of eIF4E affects global translation activity by examining the polyribosomal profiles with PRMT6 knockdown cells and a sucrose density gradient fractionation assay.

Methods

Sucrose Gradient Assay for Polyribosome Profiling

HeLa pTRIPZ scramble and HeLa pTRIPZ shPRMT6 cells were seeded at 10^6 cells/ 10 cm plate and treated with 0.5µg/ml doxycycline to induce shRNA. After 72 h, plates were washed 3 x with 1X PBS and scrapped in lysis buffer (20mM Tris-HCl pH 7.4, 150mM NaCl, 1.25mM $MgCl_2$, 1% NP-40, 1 mM DTT, 8 U/mL RNase out, Roche complete protease inhibitor cocktail). Cells were passed through a syringe (1CC 28 1/2G) and lysed for 15 min on ice before centrifugation at 12000rpm for 20 min at 4^{o}C. 20OD of material was onto a 15-55% sucrose gradient and spun at 37 000rpm at 4^{o}C for 2.5 h using the L90 ultracentrifuge and SW41 Ti rotor (Beckman). Fractions were collected using the Foxy R1 Fraction Collector (Brandel) and UA-6 Absorbance Detector (ISCO) to create polyribosome profiles.

Results

A sucrose density gradient fractionation experiment was used to investigate the polyribosomal profile for PRMT6 knockdown changes affecting translation. PRMT6 protein levels in pTRIPZ HeLa shPRMT6 doxycycline-inducible cells were verified by WB analysis (Appendix B Figure 1c). After ultracentrifugation, sample fractions were collected and RNA content was read by an absorbance detector (A254 nm) to create polysome profiles.

Translation activity is assessed by the polysome profiles by measuring the ratio of surface area under the polysomes peak (blue filled curve) over the monosomes indicated by the 80S peak (purple filled curve) (Appendix B Figure 1a). There does appear to be a trend for the induced PRMT6 KD polyribosomal profile displaying an increase in the monosome (80S) peak and a

decrease of the polysomes peak (Appendix B Figure 1b) represented by a smaller polysome/monosome ratio (Appendix B Figure 1d). This would suggest a decrease in translation activity upon PRMT6 KD. Although there is a decrease in ratio, no significant differences in the polysomes/monosomes ratio observed in polyribosomal profiles upon PRMT6 KD was found. This indicates there was no significant decrease in translation activity with PRMT6 KD (Appendix B Figure 1d). Similar uninduced shPRMT6 and induced shPRMT6 ratios are a potential characteristic of a leaky expression system. Tetracycline is naturally present in cell media FBS and can increase basal expression of the inducible system. Doxycycline used for induction of the expression system is a synthetic derivative of tetracycline. This may contribute to not seeing a significant difference between shPRMT6 uninduced shPRMT6 and induced shPRMT6 ratios.

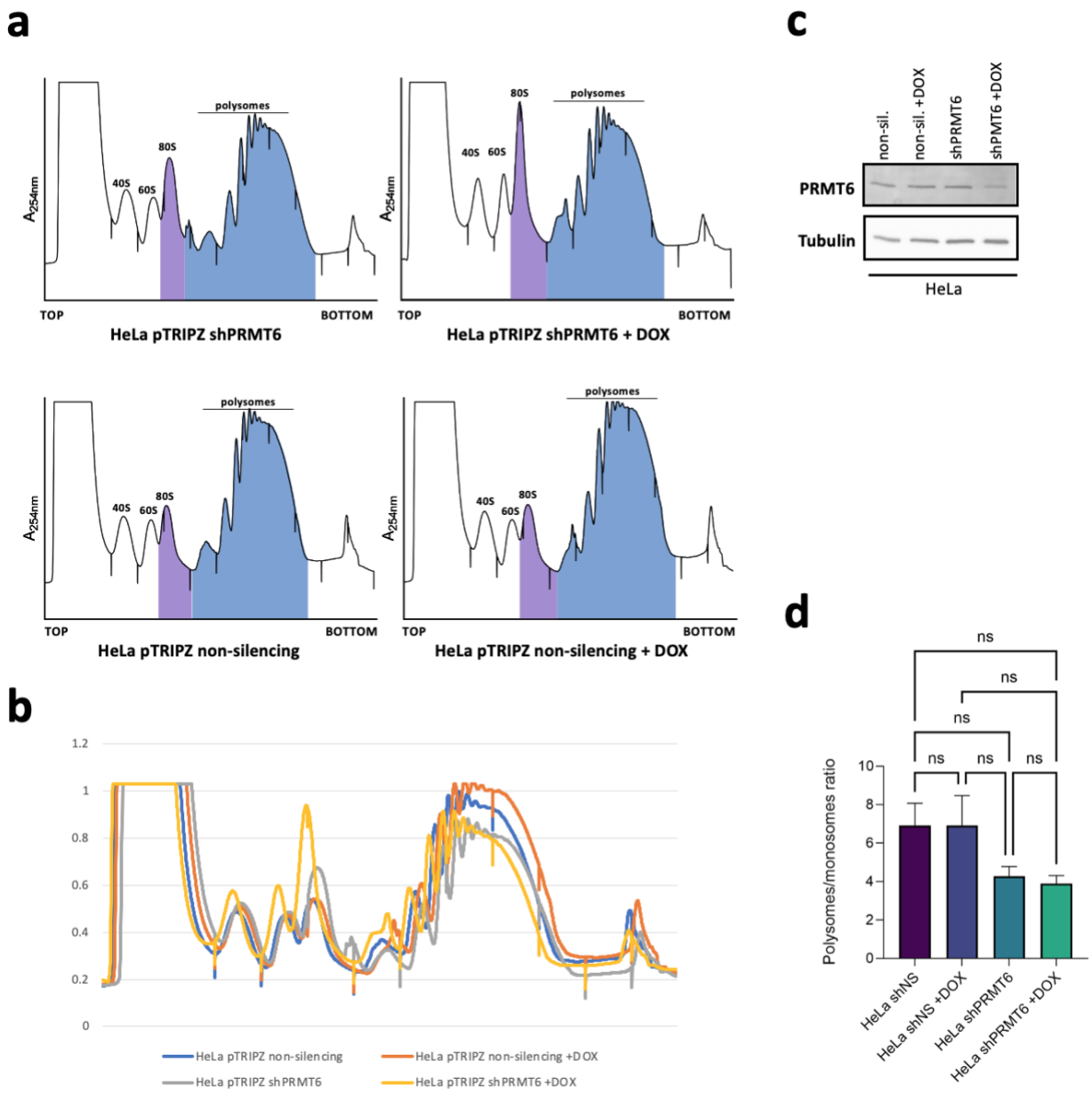

Appendix B Figure 1: Polyribosomal profiling in HeLa pTRIPZ shPRMT6.

HeLa pTRIPZ non-silencing or shPRMT6 with the addition of 0.5 µg/mL doxycycline for 72 h to induce shRNA. **(a, b)** HeLa PRMT6 knockdown did not seem to affect translation visualized with separate and overlapping polyribosomal profiling compared to HeLa control cells. The relative absorbance of RNA was read at 254 nm. **(c)** PRMT6 knockdown (~70%) was confirmed in the HeLa pTRIPZ shPRMT6 + Dox cells compared to controls**. (d)** The mean quantification of polysomes/monosomes ratio N=4, (ns) not significant p>0.05, One-way ANOVA with post-hoc Tukey test.

References

Adams, J., & Kauffman, M. (2004). Development of the Proteasome Inhibitor Velcade™ (Bortezomib). *Cancer Investigation*, *22*(2), 304–311. https://doi.org/10.1081/CNV-120030218

Almeida-Rios, D., Graça, I., Vieira, F. Q., Ramalho-Carvalho, J., Pereira-Silva, E., Martins, A. T., Oliveira, J., Gonçalves, C. S., Costa, B. M., Henrique, R., & Jerónimo, C. (2016). Histone methyltransferase PRMT6 plays an oncogenic role of in prostate cancer. *Oncotarget*, *7*(33), 53018–53028. https://doi.org/10.18632/oncotarget.10061

Amorim, I. S., Lach, G., & Gkogkas, C. G. (2018). The Role of the Eukaryotic Translation Initiation Factor 4E (eIF4E) in Neuropsychiatric Disorders. *Frontiers in Genetics*, *9*, 561. https://doi.org/10.3389/fgene.2018.00561

Anderson, P., Kedersha, N., & Ivanov, P. (2015). Stress granules, P-bodies and cancer. *Biochimica et Biophysica Acta (BBA) - Gene Regulatory Mechanisms*, *1849*(7), 861–870. https://doi.org/10.1016/j.bbagrm.2014.11.009

Ashley, C. N., Broni, E., & Miller, W. A. (2024). ADAR Family Proteins: A Structural Review. *Current Issues in Molecular Biology*, *46*(5), 3919–3945. https://doi.org/10.3390/cimb46050243

Avasarala, S., Wu, P.-Y., Khan, S. Q., Yanlin, S., Van Scoyk, M., Bao, J., Di Lorenzo, A., David, O., Bedford, M. T., Gupta, V., Winn, R. A., & Bikkavilli, R. K. (2020). PRMT6 Promotes Lung Tumor Progression via the Alternate Activation of Tumor-Associated Macrophages. *Molecular Cancer Research*, *18*(1), 166–178. https://doi.org/10.1158/1541-7786.MCR-19-0204

Bai, H., Lester, G. M. S., Petishnok, L. C., & Dean, D. A. (2017). Cytoplasmic transport and nuclear import of plasmid DNA. *Bioscience Reports*, *37*(6), BSR20160616. https://doi.org/10.1042/BSR20160616

Baldwin, R. M., Bejide, M., Trinkle-Mulcahy, L., & Côté, J. (2015). Identification of the PRMT1v1 and PRMT1v2 specific interactomes by quantitative mass spectrometry in breast cancer cells. *PROTEOMICS*, *15*(13), 2187–2197. https://doi.org/10.1002/pmic.201400209

Baldwin, R. M., Haghandish, N., Daneshmand, M., Amin, S., Paris, G., Falls, T. J., Bell, J. C., Islam, S., & Côté, J. (2014). Protein arginine methyltransferase 7 promotes breast cancer cell invasion through the induction of MMP9 expression. *Oncotarget*, *6*(5), 3013–3032. https://www.ncbi.nlm.nih.gov/pmc/articles/PMC4413634/

Baldwin, R. M., Morettin, A., Paris, G., Goulet, I., & Côté, J. (2012). Alternatively spliced protein arginine methyltransferase 1 isoform PRMT1v2 promotes the survival and invasiveness of breast cancer cells. *Cell Cycle*, *11*(24), 4597–4612. https://doi.org/10.4161/cc.22871

Baylin, S. B., & Jones, P. A. (2016). Epigenetic Determinants of Cancer. *Cold Spring Harbor Perspectives in Biology*, *8*(9), a019505. https://doi.org/10.1101/cshperspect.a019505

Bedford, M. T., & Clarke, S. G. (2009). Protein Arginine Methylation in Mammals: Who, What, and Why. *Molecular Cell*, *33*(1), 1–13. https://doi.org/10.1016/j.molcel.2008.12.013

Bedford, M. T., & Richard, S. (2005). Arginine Methylation: An Emerging Regulator of Protein Function. *Molecular Cell*, *18*(3), 263–272. https://doi.org/10.1016/j.molcel.2005.04.003

Blanc, R. S., & Richard, S. (2017). Arginine Methylation: The Coming of Age. *Molecular Cell*, *65*(1), 8–24. https://doi.org/10.1016/j.molcel.2016.11.003

Bouchard, C., Sahu, P., Meixner, M., Nötzold, R. R., Rust, M. B., Kremmer, E., Feederle, R., Hart-Smith, G., Finkernagel, F., Bartkuhn, M., Savai Pullamsetti, S., Nist, A., Stiewe, T., Philipsen, S., & Bauer, U.-M. (2018). Genomic Location of PRMT6-Dependent H3R2 Methylation Is Linked to the Transcriptional Outcome of Associated Genes. *Cell Reports*, *24*(12), 3339–3352. https://doi.org/10.1016/j.celrep.2018.08.052

Boulanger, M.-C., Liang, C., Russell, R. S., Lin, R., Bedford, M. T., Wainberg, M. A., & Richard, S. (2005). Methylation of Tat by PRMT6 Regulates Human Immunodeficiency Virus Type 1 Gene Expression. *Journal of Virology*, *79*(1), 124–131. https://doi.org/10.1128/jvi.79.1.124-131.2005

Brobbey, C., Liu, L., Yin, S., & Gan, W. (2022). The Role of Protein Arginine Methyltransferases in DNA Damage Response. *International Journal of Molecular Sciences*, *23*(17), Article 17. https://doi.org/10.3390/ijms23179780

Brown, T., Nguyen, T., Zhou, B., & Zheng, Y. G. (2023). Chemical probes and methods for the study of protein arginine methylation. *RSC Chemical Biology*, *4*(9), 647. https://doi.org/10.1039/d3cb00018d

Campos-Melo, D., Hawley, Z. C. E., Droppelmann, C. A., & Strong, M. J. (2021). The Integral Role of RNA in Stress Granule Formation and Function. *Frontiers in Cell and Developmental Biology*, *9*. https://www.frontiersin.org/articles/10.3389/fcell.2021.621779

Canadian Cancer Society. (2023, November). *Breast cancer statistics*. Canadian Cancer Society. https://cancer.ca/en/cancer-information/cancer-types/breast/statistics

Cao, M.-T., Feng, Y., & Zheng, Y. G. (2023). Protein arginine methyltransferase 6 is a novel substrate of protein arginine methyltransferase 1. *World Journal of Biological Chemistry*, *14*(5), 84–98. https://doi.org/10.4331/wjbc.v14.i5.84

Chan, L. H., Zhou, L., Ng, K. Y., Wong, T. L., Lee, T. K., Sharma, R., Loong, J. H., Ching, Y. P., Yuan, Y.-F., Xie, D., Lo, C. M., Man, K., Artegiani, B., Clevers, H., Yan, H. H., Leung, S. Y., Richard, S., Guan, X.-Y., Huen, M. S. Y., & Ma, S. (2018). PRMT6 Regulates RAS/RAF Binding and MEK/ERK-Mediated Cancer Stemness Activities in Hepatocellular Carcinoma through CRAF Methylation. *Cell Reports*, *25*(3), 690-701.e8. https://doi.org/10.1016/j.celrep.2018.09.053

Chavez, K. J., Garimella, S. V., & Lipkowitz, S. (2010). Triple Negative Breast Cancer Cell Lines: One Tool in the Search for Better Treatment of Triple Negative Breast Cancer. *Breast Disease*, *32*(1–2), 35–48. https://doi.org/10.3233/BD-2010-0307

Che, N., Ng, K.-Y., Wong, T.-L., Tong, M., Kau, P. WF., Chan, L.-H., Lee, T. K., Huen, M. SY., Yun, J.-P., & Ma, S. (2021). PRMT6 deficiency induces autophagy in hostile microenvironments of hepatocellular carcinoma tumors by regulating BAG5-associated HSC70 stability. *Cancer Letters*, *501*, 247–262. https://doi.org/10.1016/j.canlet.2020.11.002

Chen, J.-Q., & Russo, J. (2009). ERα-negative and triple negative breast cancer: Molecular features and potential therapeutic approaches. *Biochimica et Biophysica Acta (BBA) - Reviews on Cancer*, *1796*(2), 162–175. https://doi.org/10.1016/j.bbcan.2009.06.003

Chen, Z., Gan, J., Wei, Z., Zhang, M., Du, Y., Xu, C., & Zhao, H. (2022). The Emerging Role of PRMT6 in Cancer. *Frontiers in Oncology*, *12*. https://www.frontiersin.org/articles/10.3389/fonc.2022.841381

Cheng, D., Gao, G., Lorenzo, A. D., Jayne, S., Hottiger, M. O., Richard, S., & Bedford, M. T. (2020). Genetic evidence for partial redundancy between the arginine methyltransferases CARM1 and PRMT6. *Journal of Biological Chemistry*, *295*(50), 17060–17070. https://doi.org/10.1074/jbc.RA120.014704

Cheon, H., Holvey-Bates, E. G., McGrail, D. J., & Stark, G. R. (2021). PD-L1 sustains chronic, cancer cell–intrinsic responses to type I interferon, enhancing resistance to DNA damage. *Proceedings of the National Academy of Sciences*, *118*(47), e2112258118. https://doi.org/10.1073/pnas.2112258118

Cheon, H., Wang, Y., Wightman, S. M., Jackson, M. W., & Stark, G. R. (2023). How cancer cells make and respond to interferon-I. *Trends in Cancer*, *9*(1), 83–92. https://doi.org/10.1016/j.trecan.2022.09.003

Chiang, D. C., Li, Y., & Ng, S. K. (2021). The Role of the Z-DNA Binding Domain in Innate Immunity and Stress Granules. *Frontiers in Immunology*, *11*. https://www.frontiersin.org/articles/10.3389/fimmu.2020.625504

Chiang, P. K. (1998). Biological Effects of Inhibitors of S-Adenosylhomocysteine Hydrolase. *Pharmacology & Therapeutics*, *77*(2), 115–134. https://doi.org/10.1016/S0163-7258(97)00089-2

Christen, K. E., Davis, R. A., & Kennedy, D. (2019). Psammaplysin F increases the efficacy of bortezomib and sorafenib through regulation of stress granule formation. *The International Journal of Biochemistry & Cell Biology*, *112*, 24–38. https://doi.org/10.1016/j.biocel.2019.04.008

Coley, H. M. (2009). Mechanisms and consequences of chemotherapy resistance in breast cancer. *European Journal of Cancer Supplements*, *7*(1), 3–7. https://doi.org/10.1016/S1359-6349(09)70003-5

Comşa, Ş., Cîmpean, A. M., & Raica, M. (2015). The Story of MCF-7 Breast Cancer Cell Line: 40 years of Experience in Research. *ANTICANCER RESEARCH*.

Cooper, G. M. (2000). The Eukaryotic Cell Cycle. In *The Cell: A Molecular Approach. 2nd edition*. Sinauer Associates. https://www.ncbi.nlm.nih.gov/books/NBK9876/

Corbet, G. A., Burke, J. M., & Parker, R. (2021). ADAR1 limits stress granule formation through both translation-dependent and translation-independent mechanisms. *Journal of Cell Science*, *134*(17), jcs258783. https://doi.org/10.1242/jcs.258783

De Leeuw, F., Zhang, T., Wauquier, C., Huez, G., Kruys, V., & Gueydan, C. (2007). The cold-inducible RNA-binding protein migrates from the nucleus to cytoplasmic stress granules by a methylation-dependent mechanism and acts as a translational repressor. *Experimental Cell Research*, *313*(20), 4130–4144. https://doi.org/10.1016/j.yexcr.2007.09.017

Di Lorenzo, A., & Bedford, M. T. (2011). Histone arginine methylation. *FEBS Letters*, *585*(13), 2024–2031. https://doi.org/10.1016/j.febslet.2010.11.010

Di Lorenzo, A., Yang, Y., Macaluso, M., & Bedford, M. T. (2014). A gain-of-function mouse model identifies PRMT6 as a NF-κB coactivator. *Nucleic Acids Research*, *42*(13), 8297–8309. https://doi.org/10.1093/nar/gku530

Dowhan, D. H., Harrison, M. J., Eriksson, N. A., Bailey, P., Pearen, M. A., Fuller, P. J., Funder, J. W., Simpson, E. R., Leedman, P. J., Tilley, W. D., Brown, M. A., Clarke, C. L., & Muscat, G. E. O. (2012). Protein arginine methyltransferase 6-dependent gene expression and

splicing: Association with breast cancer outcomes. *Endocrine-Related Cancer*, *19*(4), 509–526. https://doi.org/10.1530/ERC-12-0100

El-Andaloussi, N., Valovka, T., Toueille, M., Steinacher, R., Focke, F., Gehrig, P., Covic, M., Hassa, P. O., Schär, P., Hübscher, U., & Hottiger, M. O. (2006). Arginine Methylation Regulates DNA Polymerase β. *Molecular Cell*, *22*(1), 51–62. https://doi.org/10.1016/j.molcel.2006.02.013

Feng, J., Dang, Y., Zhang, W., Zhao, X., Zhang, C., Hou, Z., Jin, Y., McNutt, M. A., Marks, A. R., & Yin, Y. (2019). PTEN arginine methylation by PRMT6 suppresses PI3K–AKT signaling and modulates pre-mRNA splicing. *Proceedings of the National Academy of Sciences*, *116*(14), 6868–6877. https://doi.org/10.1073/pnas.1811028116

Ferreira de Freitas, R., Eram, M. S., Szewczyk, M. M., Steuber, H., Smil, D., Wu, H., Li, F., Senisterra, G., Dong, A., Brown, P. J., Hitchcock, M., Moosmayer, D., Stegmann, C. M., Egner, U., Arrowsmith, C., Barsyte-Lovejoy, D., Vedadi, M., & Schapira, M. (2016). Discovery of a Potent Class I Protein Arginine Methyltransferase Fragment Inhibitor. *Journal of Medicinal Chemistry*, *59*(3), 1176–1183. https://doi.org/10.1021/acs.jmedchem.5b01772

Fournier, M.-J., Coudert, L., Mellaoui, S., Adjibade, P., Gareau, C., Côté, M.-F., Sonenberg, N., Gaudreault, R. C., & Mazroui, R. (2013). Inactivation of the mTORC1-Eukaryotic Translation Initiation Factor 4E Pathway Alters Stress Granule Formation. *Molecular and Cellular Biology*, *33*(11), 2285–2301. https://doi.org/10.1128/MCB.01517-12

Fournier, M.-J., Gareau, C., & Mazroui, R. (2010). The chemotherapeutic agent bortezomib induces the formation of stress granules. *Cancer Cell International*, *10*(1), 12. https://doi.org/10.1186/1475-2867-10-12

Frankel, A. (2012). Inconvenient Truths for PRMT6 Kinetic Studies. *Journal of Biological Chemistry*, *287*(12), 9512. https://doi.org/10.1074/jbc.L111.333609

Frankel, A., & Brown, J. I. (2019). Evaluation of kinetic data: What the numbers tell us about PRMTs. *Biochimica et Biophysica Acta (BBA) - Proteins and Proteomics*, *1867*(3), 306–316. https://doi.org/10.1016/j.bbapap.2018.10.010

Frankel, A., Yadav, N., Lee, J., Branscombe, T. L., Clarke, S., & Bedford, M. T. (2002). The Novel Human Protein Arginine N-Methyltransferase PRMT6 Is a Nuclear Enzyme Displaying Unique Substrate Specificity *. *Journal of Biological Chemistry*, *277*(5), 3537–3543. https://doi.org/10.1074/jbc.M108786200

Freund, E. C., Sapiro, A. L., Li, Q., Linder, S., Moresco, J. J., Yates, J. R., & Li, J. B. (2020). Unbiased Identification of trans Regulators of ADAR and A-to-I RNA Editing. *Cell Reports*, *31*(7), 107656. https://doi.org/10.1016/j.celrep.2020.107656

Fulcher, A. J., Sivakumaran, H., Jin, H., Rawle, D. J., Harrich, D., & Jans, D. A. (2016). The protein arginine methyltransferase PRMT6 inhibits HIV-1 Tat nucleolar retention. *Biochimica et Biophysica Acta (BBA) - Molecular Cell Research*, *1863*(2), 254–262. https://doi.org/10.1016/j.bbamcr.2015.11.019

Fumagalli, D., Gacquer, D., Rothé, F., Lefort, A., Libert, F., Brown, D., Kheddoumi, N., Shlien, A., Konopka, T., Salgado, R., Larsimont, D., Polyak, K., Willard-Gallo, K., Desmedt, C., Piccart, M., Abramowicz, M., Campbell, P. J., Sotiriou, C., & Detours, V. (2015). Principles Governing A-to-I RNA Editing in the Breast Cancer Transcriptome. *Cell Reports*, *13*(2), 277–289. https://doi.org/10.1016/j.celrep.2015.09.032

Garbett, D., & Bretscher, A. (2014). The surprising dynamics of scaffolding proteins. *Molecular Biology of the Cell*, *25*(16), 2315–2319. https://doi.org/10.1091/mbc.E14-04-0878

Gaudreau-Lapierre, A., Klonisch, T., Nicolas, H., Thanasupawat, T., Trinkle-Mulcahy, L., & Hombach-Klonisch, S. (2023). Nuclear High Mobility Group A2 (HMGA2) Interactome Revealed by Biotin Proximity Labeling. *International Journal of Molecular Sciences*, *24*(4), Article 4. https://doi.org/10.3390/ijms24044246

Geva, G., & Sharan, R. (2011). Identification of protein complexes from co-immunoprecipitation data. *Bioinformatics*, *27*(1), 111–117. https://doi.org/10.1093/bioinformatics/btq652

Gong, S., Maegawa, S., Yang, Y., Gopalakrishnan, V., Zheng, G., & Cheng, D. (2021). Licochalcone A is a natural selective inhibitor of arginine methyltransferase 6. *Biochemical Journal*, *478*(2), 389–406. https://doi.org/10.1042/BCJ20200411

Guan, D., Altan-Bonnet, N., Parrott, A. M., Arrigo, C. J., Li, Q., Khaleduzzaman, M., Li, H., Lee, C.-G., Pe'ery, T., & Mathews, M. B. (2008). Nuclear Factor 45 (NF45) Is a Regulatory Subunit of Complexes with NF90/110 Involved in Mitotic Control. *Molecular and Cellular Biology*, *28*(14), 4629–4641. https://doi.org/10.1128/MCB.00120-08

Guccione, E., & Richard, S. (2019). The regulation, functions and clinical relevance of arginine methylation. *Nature Reviews Molecular Cell Biology*, *20*(10), 642–657. https://doi.org/10.1038/s41580-019-0155-x

Gulla, A., Morelli, E., Samur, M. K., Botta, C., Hideshima, T., Bianchi, G., Fulciniti, M., Malvestiti, S., Prabhala, R. H., Talluri, S., Wen, K., Tai, Y.-T., Richardson, P. G., Chauhan, D., Sewastianik, T., Carrasco, R. D., Munshi, N. C., & Anderson, K. C. (2021). Bortezomib Induces Anti–Multiple Myeloma Immune Response Mediated by cGAS/STING Pathway Activation. *Blood Cancer Discovery*, *2*(5), 468–483. https://doi.org/10.1158/2643-3230.BCD-21-0047

Guo, A., Gu, H., Zhou, J., Mulhern, D., Wang, Y., Lee, K. A., Yang, V., Aguiar, M., Kornhauser, J., Jia, X., Ren, J., Beausoleil, S. A., Silva, J. C., Vemulapalli, V., Bedford, M. T., & Comb, M. J. (2014). Immunoaffinity enrichment and mass spectrometry analysis of protein methylation. *Molecular & Cellular Proteomics: MCP*, *13*(1), 372–387. https://doi.org/10.1074/mcp.O113.027870

Gupta, S., Kadumuri, R. V., Singh, A. K., Chavali, S., & Dhayalan, A. (2021). Structure, Activity and Function of the Protein Arginine Methyltransferase 6. *Life*, *11*(9), 951. https://doi.org/10.3390/life11090951

Guzikowski, A. R., Chen, Y. S., & Zid, B. M. (2019). Stress-induced mRNP granules: Form and function of processing bodies and stress granules. *WIREs RNA*, *10*(3), e1524. https://doi.org/10.1002/wrna.1524

Hamey, J. J., Rakow, S., Bouchard, C., Senst, J. M., Kolb, P., Bauer, U.-M., Wilkins, M. R., & Hart-Smith, G. (2021). Systematic investigation of PRMT6 substrate recognition reveals broad specificity with a preference for an RG motif or basic and bulky residues. *The FEBS Journal*, *288*(19), 5668–5691. https://doi.org/10.1111/febs.15837

Harrison, M. J., Tang, Y. H., & Dowhan, D. H. (2010). Protein arginine methyltransferase 6 regulates multiple aspects of gene expression. *Nucleic Acids Research*, *38*(7), 2201–2216. https://doi.org/10.1093/nar/gkp1203

Herglotz, J., Kuvardina, O. N., Kolodziej, S., Kumar, A., Hussong, H., Grez, M., & Lausen, J. (2013). Histone arginine methylation keeps RUNX1 target genes in an intermediate state. *Oncogene*, *32*(20), Article 20. https://doi.org/10.1038/onc.2012.274

Herrmann, F., Pably, P., Eckerich, C., Bedford, M. T., & Fackelmayer, F. O. (2009). Human protein arginine methyltransferases in vivo – distinct properties of eight canonical

members of the PRMT family. *Journal of Cell Science*, *122*(5), 667–677. https://doi.org/10.1242/jcs.039933

Hofmann, S., Kedersha, N., Anderson, P., & Ivanov, P. (2021). Molecular mechanisms of stress granule assembly and disassembly. *Biochimica et Biophysica Acta (BBA) - Molecular Cell Research*, *1868*(1), 118876. https://doi.org/10.1016/j.bbamcr.2020.118876

Hofweber, M., Hutten, S., Bourgeois, B., Spreitzer, E., Niedner-Boblenz, A., Schifferer, M., Ruepp, M.-D., Simons, M., Niessing, D., Madl, T., & Dormann, D. (2018). Phase Separation of FUS Is Suppressed by Its Nuclear Import Receptor and Arginine Methylation. *Cell*, *173*(3), 706-719.e13. https://doi.org/10.1016/j.cell.2018.03.004

Hu, H., Qian, K., Ho, M.-C., & Zheng, Y. G. (2016). Small Molecule Inhibitors of Protein Arginine Methyltransferases. *Expert Opinion on Investigational Drugs*, *25*(3), 335–358. https://doi.org/10.1517/13543784.2016.1144747

Hu, M., & Polyak, K. (2008). Molecular characterisation of the tumour microenvironment in breast cancer. *European Journal of Cancer*, *44*(18), 2760–2765. https://doi.org/10.1016/j.ejca.2008.09.038

Hu, T., Hou, W., Xiao, E., & Long, M. (2022). Mechanism and effect of stress granule formation in cancer and its potential roles in breast cancer therapy. *Genes & Diseases*, *9*(3), 659–667. https://doi.org/10.1016/j.gendis.2021.02.005

Huang, L., Wang, Z., Narayanan, N., & Yang, Y. (2018). Arginine methylation of the C-terminus RGG motif promotes TOP3B topoisomerase activity and stress granule localization. *Nucleic Acids Research*, *46*(6), 3061–3074. https://doi.org/10.1093/nar/gky103

Hubers, L., Valderrama-Carvajal, H., Laframboise, J., Timbers, J., Sanchez, G., & Côté, J. (2011). HuD interacts with survival motor neuron protein and can rescue spinal muscular

atrophy-like neuronal defects. *Human Molecular Genetics*, *20*(3), 553–579. https://doi.org/10.1093/hmg/ddq500

Hyllus, D., Stein, C., Schnabel, K., Schiltz, E., Imhof, A., Dou, Y., Hsieh, J., & Bauer, U.-M. (2007). PRMT6-mediated methylation of R2 in histone H3 antagonizes H3 K4 trimethylation. *Genes & Development*, *21*(24), 3369–3380. https://doi.org/10.1101/gad.447007

Jiang, M.-P., Huang, X., Yin, Y.-M., & Tang, J.-H. (2022). The pathological and clinical landscape of refractory metastatic triple negative breast cancer: A narrative review. *Annals of Translational Medicine*, *10*(16), 907. https://doi.org/10.21037/atm-22-3434

Jiang, N., Li, Q.-L., Pan, W., Li, J., Zhang, M.-F., Cao, T., Su, S.-G., & Shen, H. (2020). PRMT6 promotes endometrial cancer via AKT/mTOR signaling and indicates poor prognosis. *The International Journal of Biochemistry & Cell Biology*, *120*, 105681. https://doi.org/10.1016/j.biocel.2019.105681

Jiang, X., Zhang, X., Ren, C., Ruan, Y., Lu, Y., Yuan, L., Li, J., Yan, A., Wang, Y., Luo, P., Hu, C., & Chen, T. (2021). Interleukin-2 enhancer binding factor 2 (ILF2) in pacific white shrimp (*Litopenaeus vannamei*): Alternatively spliced isoforms with different responses in the immune defenses against vibrio infection. *Developmental & Comparative Immunology*, *118*, 103975. https://doi.org/10.1016/j.dci.2020.103975

John, L., & Samuel, C. E. (2014). Induction of stress granules by interferon and down-regulation by the cellular RNA adenosine deaminase ADAR1. *Virology*, *454–455*, 299–310. https://doi.org/10.1016/j.virol.2014.02.025

Kallunki, T., Barisic, M., Jäättelä, M., & Liu, B. (2019). How to Choose the Right Inducible Gene Expression System for Mammalian Studies? *Cells*, *8*(8), 796. https://doi.org/10.3390/cells8080796

Kim, N. H., Kim, S.-N., Seo, D.-W., Han, J.-W., & Kim, Y. K. (2013). PRMT6 overexpression upregulates TSP-1 and downregulates MMPs: Its implication in motility and invasion. *Biochemical and Biophysical Research Communications*, *432*(1), 60–65. https://doi.org/10.1016/j.bbrc.2013.01.085

Kim, S., Kim, N. H., Park, J. E., Hwang, J. W., Myung, N., Hwang, K.-T., Kim, Y. A., Jang, C.-Y., & Kim, Y. K. (2020). PRMT6-mediated H3R2me2a guides Aurora B to chromosome arms for proper chromosome segregation. *Nature Communications*, *11*(1), Article 1. https://doi.org/10.1038/s41467-020-14511-w

Kleinschmidt, M. A., Graaf, P. de, Teeffelen, H. A. A. M. van, & Timmers, H. T. M. (2012). Cell Cycle Regulation by the PRMT6 Arginine Methyltransferase through Repression of Cyclin-Dependent Kinase Inhibitors. *PLOS ONE*, *7*(8), e41446. https://doi.org/10.1371/journal.pone.0041446

Kubitz, L., Bitsch, S., Zhao, X., Schmitt, K., Deweid, L., Roehrig, A., Barazzone, E. C., Valerius, O., Kolmar, H., & Béthune, J. (2022). Engineering of ultraID, a compact and hyperactive enzyme for proximity-dependent biotinylation in living cells. *Communications Biology*, *5*(1), 1–14. https://doi.org/10.1038/s42003-022-03604-5

Kung, C.-P., Cottrell, K. A., Ryu, S., Bramel, E. R., Kladney, R. D., Bao, E. A., Freeman, E. C., Sabloak, T., Maggi Jr., L., & Weber, J. D. (2021). Evaluating the therapeutic potential of ADAR1 inhibition for triple-negative breast cancer. *Oncogene*, *40*(1), Article 1. https://doi.org/10.1038/s41388-020-01515-5

Lakowski, T. M., & Frankel, A. (2008). A Kinetic Study of Human Protein Arginine N-Methyltransferase 6 Reveals a Distributive Mechanism *. *Journal of Biological Chemistry*, *283*(15), 10015–10025. https://doi.org/10.1074/jbc.M710176200

Lee, A. V., Oesterreich, S., & Davidson, N. E. (2015). MCF-7 Cells—Changing the Course of Breast Cancer Research and Care for 45 Years. *JNCI: Journal of the National Cancer Institute*, *107*(7), djv073. https://doi.org/10.1093/jnci/djv073

Lesinski, G. B., Raig, E. T., Guenterberg, K., Brown, L., Go, M. R., Shah, N. N., Lewis, A., Quimper, M., Hade, E., Young, G., Chaudhury, A. R., Ladner, K. J., Guttridge, D. C., Bouchard, P., & Carson, W. E. (2008). Interferon-alpha and bortezomib overcome Bcl-2 and Mcl-1 over-expression in melanoma cells by stimulating the extrinsic pathway of apoptosis. *Cancer Research*, *68*(20), 8351–8360. https://doi.org/10.1158/0008-5472.CAN-08-0426

Leung, E., Kim, J. E., Askarian-Amiri, M., Finlay, G. J., & Baguley, B. C. (2014). Evidence for the Existence of Triple-Negative Variants in the MCF-7 Breast Cancer Cell Population. *BioMed Research International*, *2014*, 836769. https://doi.org/10.1155/2014/836769

Li, T., Zeng, Z., Fan, C., & Xiong, W. (2023). Role of stress granules in tumorigenesis and cancer therapy. *Biochimica et Biophysica Acta (BBA) - Reviews on Cancer*, *1878*(6), 189006. https://doi.org/10.1016/j.bbcan.2023.189006

Liu, X., Sun, T., Shcherbina, A., Li, Q., Jarmoskaite, I., Kappel, K., Ramaswami, G., Das, R., Kundaje, A., & Li, J. B. (2021). Learning cis-regulatory principles of ADAR-based RNA editing from CRISPR-mediated mutagenesis. *Nature Communications*, *12*(1), Article 1. https://doi.org/10.1038/s41467-021-22489-2

Lorton, B. M., & Shechter, D. (2019). Cellular Consequences of Arginine Methylation. *Cellular and Molecular Life Sciences : CMLS*, *76*(15), 2933–2956. https://doi.org/10.1007/s00018-019-03140-2

Mann, M., Zou, Y., Chen, Y., Brann, D., & Vadlamudi, R. (2014). PELP1 oncogenic functions involve alternative splicing via PRMT6. *Molecular Oncology*, *8*(2), 389–400. https://doi.org/10.1016/j.molonc.2013.12.012

Markmiller, S., Soltanieh, S., Server, K. L., Mak, R., Jin, W., Fang, M. Y., Luo, E.-C., Krach, F., Yang, D., Sen, A., Fulzele, A., Wozniak, J. M., Gonzalez, D. J., Kankel, M. W., Gao, F.-B., Bennett, E. J., Lécuyer, E., & Yeo, G. W. (2018). Context-Dependent and Disease-Specific Diversity in Protein Interactions within Stress Granules. *Cell*, *172*(3), 590-604.e13. https://doi.org/10.1016/j.cell.2017.12.032

Mateju, D., Eichenberger, B., Voigt, F., Eglinger, J., Roth, G., & Chao, J. A. (2020). Single-Molecule Imaging Reveals Translation of mRNAs Localized to Stress Granules. *Cell*, *183*(7), 1801-1812.e13. https://doi.org/10.1016/j.cell.2020.11.010

May, D. G., Scott, K. L., Campos, A. R., & Roux, K. J. (2020). Comparative Application of BioID and TurboID for Protein-Proximity Biotinylation. *Cells*, *9*(5), Article 5. https://doi.org/10.3390/cells9051070

Mayr, C. (2019). What Are 3′ UTRs Doing? *Cold Spring Harbor Perspectives in Biology*, *11*(10), a034728. https://doi.org/10.1101/cshperspect.a034728

Mellacheruvu, D., Wright, Z., Couzens, A. L., Lambert, J.-P., St-Denis, N. A., Li, T., Miteva, Y. V., Hauri, S., Sardiu, M. E., Low, T. Y., Halim, V. A., Bagshaw, R. D., Hubner, N. C., al-Hakim, A., Bouchard, A., Faubert, D., Fermin, D., Dunham, W. H., Goudreault, M., … Nesvizhskii, A. I. (2013). The CRAPome: A contaminant repository for affinity

purification–mass spectrometry data. *Nature Methods*, *10*(8), Article 8. https://doi.org/10.1038/nmeth.2557

Michaud-Levesque, J., & Richard, S. (2009). Thrombospondin-1 Is a Transcriptional Repression Target of PRMT6 *. *Journal of Biological Chemistry*, *284*(32), 21338–21346. https://doi.org/10.1074/jbc.M109.005322

Migazzi, A., Scaramuzzino, C., Anderson, E. N., Tripathy, D., Hernández, I. H., Grant, R. A., Roccuzzo, M., Tosatto, L., Virlogeux, A., Zuccato, C., Caricasole, A., Ratovitski, T., Ross, C. A., Pandey, U. B., Lucas, J. J., Saudou, F., Pennuto, M., & Basso, M. (2021). Huntingtin-mediated axonal transport requires arginine methylation by PRMT6. *Cell Reports*, *35*(2), 108980. https://doi.org/10.1016/j.celrep.2021.108980

Milani, M., Rzymski, T., Mellor, H. R., Pike, L., Bottini, A., Generali, D., & Harris, A. L. (2009). The Role of ATF4 Stabilization and Autophagy in Resistance of Breast Cancer Cells Treated with Bortezomib. *Cancer Research*, *69*(10), 4415–4423. https://doi.org/10.1158/0008-5472.CAN-08-2839

Morettin, A., Bourassa, J., Mahadevan, K., Trinkle-Mulcahy, L., & Cote, J. (2020). Using affinity purification coupled with stable isotope labeling by amino acids in cell culture quantitative mass spectrometry to identify novel interactors/substrates of protein arginine methyltransferases. *Methods*, *175*, 44–52. https://doi.org/10.1016/j.ymeth.2019.11.015

Morettin, A. J. (2015). *Investigating the Role of Protein Arginine Methyltransferases in Breast Cancer Etiology* [Thesis, Université d'Ottawa / University of Ottawa]. https://doi.org/10.20381/ruor-2679

Nakakido, M., Deng, Z., Suzuki, T., Dohmae, N., Nakamura, Y., & Hamamoto, R. (2015). PRMT6 increases cytoplasmic localization of p21CDKN1A in cancer cells through

arginine methylation and makes more resistant to cytotoxic agents. *Oncotarget*, *6*(31), 30957–30967. https://www.ncbi.nlm.nih.gov/pmc/articles/PMC4741580/

Ng, S. K., Weissbach, R., Ronson, G. E., & Scadden, A. D. J. (2013). Proteins that contain a functional Z-DNA-binding domain localize to cytoplasmic stress granules. *Nucleic Acids Research*, *41*(21), 9786–9799. https://doi.org/10.1093/nar/gkt750

Nie, Y., Ding, L., Kao, P. N., Braun, R., & Yang, J.-H. (2005). ADAR1 Interacts with NF90 through Double-Stranded RNA and Regulates NF90-Mediated Gene Expression Independently of RNA Editing. *Molecular and Cellular Biology*, *25*(16), 6956–6963. https://doi.org/10.1128/MCB.25.16.6956-6963.2005

Obianyo, O., & Thompson, P. R. (2012). Kinetic Mechanism of Protein Arginine Methyltransferase 6 (PRMT6) *. *Journal of Biological Chemistry*, *287*(8), 6062–6071. https://doi.org/10.1074/jbc.M111.333609

Okuno, K., Akiyama, Y., Shimada, S., Nakagawa, M., Tanioka, T., Inokuchi, M., Yamaoka, S., Kojima, K., & Tanaka, S. (2019). Asymmetric dimethylation at histone H3 arginine 2 by PRMT6 in gastric cancer progression. *Carcinogenesis*, *40*(1), 15–26. https://doi.org/10.1093/carcin/bgy147

Patel, A., Vought, V. E., Swatkoski, S., Viggiano, S., Howard, B., Dharmarajan, V., Monteith, K. E., Kupakuwana, G., Namitz, K. E., Shinsky, S. A., Cotter, R. J., & Cosgrove, M. S. (2014). Automethylation Activities within the Mixed Lineage Leukemia-1 (MLL1) Core Complex Reveal Evidence Supporting a “Two-active Site” Model for Multiple Histone H3 Lysine 4 Methylation *. *Journal of Biological Chemistry*, *289*(2), 868–884. https://doi.org/10.1074/jbc.M113.501064

Paz-Yaacov, N., Bazak, L., Buchumenski, I., Porath, H. T., Danan-Gotthold, M., Knisbacher, B. A., Eisenberg, E., & Levanon, E. Y. (2015). Elevated RNA Editing Activity Is a Major Contributor to Transcriptomic Diversity in Tumors. *Cell Reports*, *13*(2), 267–276. https://doi.org/10.1016/j.celrep.2015.08.080

Peng, X., Xu, X., Wang, Y., Hawke, D. H., Yu, S., Han, L., Zhou, Z., Mojumdar, K., Jeong, K. J., Labrie, M., Tsang, Y. H., Zhang, M., Lu, Y., Hwu, P., Scott, K. L., Liang, H., & Mills, G. B. (2018). A-to-I RNA Editing Contributes to Proteomic Diversity in Cancer. *Cancer Cell*, *33*(5), 817-828.e7. https://doi.org/10.1016/j.ccell.2018.03.026

Phalke, S., Mzoughi, S., Bezzi, M., Jennifer, N., Mok, W. C., Low, D. H. P., Thike, A. A., Kuznetsov, V. A., Tan, P. H., Voorhoeve, P. M., & Guccione, E. (2012). P53-Independent regulation of p21Waf1/Cip1 expression and senescence by PRMT6. *Nucleic Acids Research*, *40*(19), 9534–9542. https://doi.org/10.1093/nar/gks858

Poulard, C., Corbo, L., & Romancer, M. L. (2016). Protein arginine methylation/demethylation and cancer. *Oncotarget*, *7*(41), 67532–67550. https://doi.org/10.18632/oncotarget.11376

Prinos, P., Garneau, D., Lucier, J.-F., Gendron, D., Couture, S., Boivin, M., Brosseau, J.-P., Lapointe, E., Thibault, P., Durand, M., Tremblay, K., Gervais-Bird, J., Nwilati, H., Klinck, R., Chabot, B., Perreault, J.-P., Wellinger, R. J., & Elela, S. A. (2011). Alternative splicing of SYK regulates mitosis and cell survival. *Nature Structural & Molecular Biology*, *18*(6), 673–679. https://doi.org/10.1038/nsmb.2040

Qian, K., Hu, H., Xu, H., & Zheng, Y. G. (2018). Detection of PRMT1 inhibitors with stopped flow fluorescence. *Signal Transduction and Targeted Therapy*, *3*(1), Article 1. https://doi.org/10.1038/s41392-018-0009-6

Quan, X., Yue, W., Luo, Y., Cao, J., Wang, H., Wang, Y., & Lu, Z. (2015). The protein arginine methyltransferase PRMT5 regulates Aβ-induced toxicity in human cells and Caenorhabditis elegans models of Alzheimer's disease. *Journal of Neurochemistry*, *134*(5), 969–977. https://doi.org/10.1111/jnc.13191

Raveendran, V. V., Al-Haffar, K., Kunhi, M., Belhaj, K., Al-Habeeb, W., Al-Buraiki, J., Eyjolsson, A., & Poizat, C. (2020). Protein arginine methyltransferase 6 mediates cardiac hypertrophy by differential regulation of histone H3 arginine methylation. *Heliyon*, *6*(5). https://doi.org/10.1016/j.heliyon.2020.e03864

Roheel, A., Khan, A., Anwar, F., Akbar, Z., Akhtar, M. F., Imran Khan, M., Sohail, M. F., & Ahmad, R. (2023). Global epidemiology of breast cancer based on risk factors: A systematic review. *Frontiers in Oncology*, *13*. https://www.frontiersin.org/articles/10.3389/fonc.2023.1240098

Roux, K. J., Kim, D. I., Burke, B., & May, D. G. (2018). BioID: A Screen for Protein-Protein Interactions. *Current Protocols in Protein Science*, *91*, 19.23.1-19.23.15. https://doi.org/10.1002/cpps.51

Roux, K. J., Kim, D. I., Raida, M., & Burke, B. (2012). A promiscuous biotin ligase fusion protein identifies proximal and interacting proteins in mammalian cells. *The Journal of Cell Biology*, *196*(6), 801–810. https://doi.org/10.1083/jcb.201112098

Sagredo, E. A., Blanco, A., Sagredo, A. I., Pérez, P., Sepúlveda-Hermosilla, G., Morales, F., Müller, B., Verdugo, R., Marcelain, K., Harismendy, O., & Armisén, R. (2018). ADAR1-mediated RNA-editing of 3′UTRs in breast cancer. *Biological Research*, *51*, 36. https://doi.org/10.1186/s40659-018-0185-4

Sakurai, M., Shiromoto, Y., Ota, H., Song, C., Kossenkov, A. V., Wickramasinghe, J., Showe, L. C., Skordalakes, E., Tang, H.-Y., Speicher, D. W., & Nishikura, K. (2017). ADAR1 controls apoptosis of stressed cells by inhibiting Staufen1-mediated mRNA decay. *Nature Structural & Molecular Biology*, *24*(6), Article 6. https://doi.org/10.1038/nsmb.3403

Samuel, S. F., Barry, A., Greenman, J., & Beltran-Alvarez, P. (2021). Arginine methylation: The promise of a 'silver bullet' for brain tumours? *Amino Acids*, *53*(4), 489–506. https://doi.org/10.1007/s00726-020-02937-x

Sardo, A. L., Altamura, S., Pegoraro, S., Maurizio, E., Sgarra, R., & Manfioletti, G. (2013). Identification and Characterization of New Molecular Partners for the Protein Arginine Methyltransferase 6 (PRMT6). *PLoS ONE*, *8*(1). https://doi.org/10.1371/journal.pone.0053750

Sayegh, J., Webb, K., Cheng, D., Bedford, M. T., & Clarke, S. G. (2007). Regulation of Protein Arginine Methyltransferase 8 (PRMT8) Activity by Its N-terminal Domain *. *Journal of Biological Chemistry*, *282*(50), 36444–36453. https://doi.org/10.1074/jbc.M704650200

Scaramuzzino, C., Casci, I., Parodi, S., Lievens, P. M. J., Polanco, M. J., Milioto, C., Chivet, M., Monaghan, J., Mishra, A., Badders, N., Aggarwal, T., Grunseich, C., Sambataro, F., Basso, M., Fackelmayer, F. O., Taylor, J. P., Pandey, U. B., & Pennuto, M. (2015). Protein Arginine Methyltransferase 6 Enhances Polyglutamine-Expanded Androgen Receptor Function and Toxicity in Spinal and Bulbar Muscular Atrophy. *Neuron*, *85*(1), 88–100. https://doi.org/10.1016/j.neuron.2014.12.031

Schneider, L., Herkt, S., Wang, L., Feld, C., Wesely, J., Kuvardina, O. N., Meyer, A., Oellerich, T., Häupl, B., Seifried, E., Bonig, H., & Lausen, J. (2021). PRMT6 activates cyclin D1

expression in conjunction with the transcription factor LEF1. *Oncogenesis*, *10*(5), 42. https://doi.org/10.1038/s41389-021-00332-z

Sears, R. M., May, D. G., & Roux, K. J. (2019). BioID as a Tool for Protein-Proximity Labeling in Living Cells. *Methods in Molecular Biology (Clifton, N.J.)*, *2012*, 299–313. https://doi.org/10.1007/978-1-4939-9546-2_15

Shen, Y., Li, F., Szewczyk, M. M., Halabelian, L., Park, K., Chau, I., Dong, A., Zeng, H., Chen, H., Meng, F., Barsyte-Lovejoy, D., Arrowsmith, C. H., Brown, P. J., Liu, J., Vedadi, M., & Jin, J. (2020). Discovery of a First-in-Class Protein Arginine Methyltransferase 6 (PRMT6) Covalent Inhibitor. *Journal of Medicinal Chemistry*, *63*(10), 5477–5487. https://doi.org/10.1021/acs.jmedchem.0c00406

Shiina, N., & Nakayama, K. (2014). RNA Granule Assembly and Disassembly Modulated by Nuclear Factor Associated with Double-stranded RNA 2 and Nuclear Factor 45 *. *Journal of Biological Chemistry*, *289*(30), 21163–21180. https://doi.org/10.1074/jbc.M114.556365

Siegel, R. L., Miller, K. D., Wagle, N. S., & Jemal, A. (2023). Cancer statistics, 2023. *CA: A Cancer Journal for Clinicians*, *73*(1), 17–48. https://doi.org/10.3322/caac.21763

Singhroy, D. N., Mesplède, T., Sabbah, A., Quashie, P. K., Falgueyret, J.-P., & Wainberg, M. A. (2013). Automethylation of protein arginine methyltransferase 6 (PRMT6) regulates its stability and its anti-HIV-1 activity. *Retrovirology*, *10*, 73. https://doi.org/10.1186/1742-4690-10-73

Stank, A., Kokh, D. B., Fuller, J. C., & Wade, R. C. (2016). Protein Binding Pocket Dynamics. *Accounts of Chemical Research*, *49*(5), 809–815. https://doi.org/10.1021/acs.accounts.5b00516

Stein, C., Riedl, S., Rüthnick, D., Nötzold, R. R., & Bauer, U.-M. (2012). The arginine methyltransferase PRMT6 regulates cell proliferation and senescence through transcriptional repression of tumor suppressor genes. *Nucleic Acids Research*, *40*(19), 9522–9533. https://doi.org/10.1093/nar/gks767

Sun, T., Yu, Y., Wu, X., Acevedo, A., Luo, J.-D., Wang, J., Schneider, W. M., Hurwitz, B., Rosenberg, B. R., Chung, H., & Rice, C. M. (2021). Decoupling expression and editing preferences of ADAR1 p150 and p110 isoforms. *Proceedings of the National Academy of Sciences*, *118*(12), e2021757118. https://doi.org/10.1073/pnas.2021757118

Sun, Y., Chung, H. H., Woo, A. R. E., & Lin, V. C.-L. (2014). Protein arginine methyltransferase 6 enhances ligand-dependent and -independent activity of estrogen receptor α via distinct mechanisms. *Biochimica et Biophysica Acta (BBA) - Molecular Cell Research*, *1843*(9), 2067–2078. https://doi.org/10.1016/j.bbamcr.2014.04.008

Sutanto, F., Konstantinidou, M., & Dömling, A. (2020). Covalent inhibitors: A rational approach to drug discovery. *RSC Medicinal Chemistry*, *11*(8), 876–884. https://doi.org/10.1039/d0md00154f

Tadesse, H., Deschênes-Furry, J., Boisvenue, S., & Côté, J. (2008). KH-type splicing regulatory protein interacts with survival motor neuron protein and is misregulated in spinal muscular atrophy. *Human Molecular Genetics*, *17*(4), 506–524. https://doi.org/10.1093/hmg/ddm327

Teoh, P. J., An, O., Chung, T.-H., Chooi, J. Y., Toh, S. H. M., Fan, S., Wang, W., Koh, B. T. H., Fullwood, M. J., Ooi, M. G., de Mel, S., Soekojo, C. Y., Chen, L., Ng, S. B., Yang, H., & Chng, W. J. (2018). Aberrant hyperediting of the myeloma transcriptome by ADAR1

confers oncogenicity and is a marker of poor prognosis. *Blood*, *132*(12), 1304–1317. https://doi.org/10.1182/blood-2018-02-832576

Thandapani, P., O'Connor, T. R., Bailey, T. L., & Richard, S. (2013). Defining the RGG/RG Motif. *Molecular Cell*, *50*(5), 613–623. https://doi.org/10.1016/j.molcel.2013.05.021

Tradewell, M. L., Yu, Z., Tibshirani, M., Boulanger, M.-C., Durham, H. D., & Richard, S. (2012). Arginine methylation by PRMT1 regulates nuclear-cytoplasmic localization and toxicity of FUS/TLS harbouring ALS-linked mutations. *Human Molecular Genetics*, *21*(1), 136–149. https://doi.org/10.1093/hmg/ddr448

Trinkle-Mulcahy, L. (2019). Recent advances in proximity-based labeling methods for interactome mapping. *F1000Research*, *8*, F1000 Faculty Rev-135. https://doi.org/10.12688/f1000research.16903.1

Trinkle-Mulcahy, L., Boulon, S., Lam, Y. W., Urcia, R., Boisvert, F.-M., Vandermoere, F., Morrice, N. A., Swift, S., Rothbauer, U., Leonhardt, H., & Lamond, A. (2008). Identifying specific protein interaction partners using quantitative mass spectrometry and bead proteomes. *Journal of Cell Biology*, *183*(2), 223–239. https://doi.org/10.1083/jcb.200805092

Tseng, L.-M., Liu, C.-Y., Chang, K.-C., Chu, P.-Y., Shiau, C.-W., & Chen, K.-F. (2012). CIP2A is a target of bortezomib in human triple negative breast cancer cells. *Breast Cancer Research : BCR*, *14*(2), R68. https://doi.org/10.1186/bcr3175

van der Pol, C. C., Moelans, C. B., Manson, Q. F., Batenburg, M. C. T., van der Wall, E., Borel Rinkes, I., Verkooijen, L., Raman, V., & van Diest, P. J. (2021). Cytoplasmic DDX3 as prognosticator in male breast cancer. *Virchows Archiv*, *479*(4), 647–655. https://doi.org/10.1007/s00428-021-03107-4

Varnaitė, R., & MacNeill, S. A. (2016). Meet the neighbors: Mapping local protein interactomes by proximity-dependent labeling with BioID. *PROTEOMICS*, *16*(19), 2503–2518. https://doi.org/10.1002/pmic.201600123

Veland, N., Hardikar, S., Zhong, Y., Gayatri, S., Dan, J., Strahl, B. D., Rothbart, S. B., Bedford, M. T., & Chen, T. (2017). The arginine methyltransferase PRMT6 regulates DNA methylation and contributes to global DNA hypomethylation in cancer. *Cell Reports*, *21*(12), 3390–3397. https://doi.org/10.1016/j.celrep.2017.11.082

Vogel, C., & Marcotte, E. M. (2009). Absolute abundance for the masses. *Nature Biotechnology*, *27*(9), 825–826. https://doi.org/10.1038/nbt0909-825

Wagner, K.-U. (2022). Know thy cells: Commonly used triple-negative human breast cancer cell lines carry mutations in RAS and effectors. *Breast Cancer Research*, *24*(1), 44. https://doi.org/10.1186/s13058-022-01538-8

Wang, F., Li, J., Fan, S., Jin, Z., & Huang, C. (2020). Targeting stress granules: A novel therapeutic strategy for human diseases. *Pharmacological Research*, *161*, 105143. https://doi.org/10.1016/j.phrs.2020.105143

Wang, J., Xiao, Z., Li, P., Wu, C., Li, Y., Wang, Q., Chen, Y., Zhou, H., Li, Z., Wang, Z., Lan, Q., & Wang, Y. (2023). PRMT6-CDC20 facilitates glioblastoma progression via the degradation of CDKN1B. *Oncogene*, *42*(14), 1088–1100. https://doi.org/10.1038/s41388-023-02624-7

Wang, N., Ma, T., & Yu, B. (2023). Targeting epigenetic regulators to overcome drug resistance in cancers. *Signal Transduction and Targeted Therapy*, *8*(1), Article 1. https://doi.org/10.1038/s41392-023-01341-7

Wang, X., Huang, Y., Zhao, J., Zhang, Y., Lu, J., & Huang, B. (2012). Suppression of PRMT6-mediated arginine methylation of p16 protein potentiates its ability to arrest A549 cell proliferation. *The International Journal of Biochemistry & Cell Biology*, *44*(12), 2333–2341. https://doi.org/10.1016/j.biocel.2012.09.015

Wei, H., Mundade, R., Lange, K. C., & Lu, T. (2014). Protein arginine methylation of non-histone proteins and its role in diseases. *Cell Cycle (Georgetown, Tex.)*, *13*(1), 32–41. https://doi.org/10.4161/cc.27353

Wei, H.-H., Fan, X.-J., Hu, Y., Tian, X.-X., Guo, M., Mao, M.-W., Fang, Z.-Y., Wu, P., Gao, S.-X., Peng, C., Yang, Y., & Wang, Z. (2021). A systematic survey of PRMT interactomes reveals the key roles of arginine methylation in the global control of RNA splicing and translation. *Science Bulletin*, *66*(13), 1342–1357. https://doi.org/10.1016/j.scib.2021.01.004

Welsh, J. (2013). Chapter 40—Animal Models for Studying Prevention and Treatment of Breast Cancer. In P. M. Conn (Ed.), *Animal Models for the Study of Human Disease* (pp. 997–1018). Academic Press. https://doi.org/10.1016/B978-0-12-415894-8.00040-3

Wen, X., Huang, X., Mok, B. W.-Y., Chen, Y., Zheng, M., Lau, S.-Y., Wang, P., Song, W., Jin, D.-Y., Yuen, K.-Y., & Chen, H. (2014). NF90 Exerts Antiviral Activity through Regulation of PKR Phosphorylation and Stress Granules in Infected Cells. *The Journal of Immunology*, *192*(8), 3753–3764. https://doi.org/10.4049/jimmunol.1302813

Winter, D. L., Hart-Smith, G., & Wilkins, M. R. (2018). Characterization of Protein Methyltransferases Rkm1, Rkm4, Efm4, Efm7, Set5 and Hmt1 Reveals Extensive Post-Translational Modification. *Journal of Molecular Biology*, *430*(1), 102–118. https://doi.org/10.1016/j.jmb.2017.11.009

Wu, H., Zheng, W., Eram, M. S., Vhuiyan, M., Dong, A., Zeng, H., He, H., Brown, P., Frankel, A., Vedadi, M., Luo, M., & Min, J. (2016). Structural basis of arginine asymmetrical dimethylation by PRMT6. *Biochemical Journal*, *473*(19), 3049–3063. https://doi.org/10.1042/BCJ20160537

Yang, T., Huang, W., Ma, T., Yin, X., Zhang, J., Huo, M., Hu, T., Gao, T., Liu, W., Zhang, D., Yu, H., Teng, X., Zhang, M., Qin, H., Yang, Y., Yuan, B., & Wang, Y. (2023). The PRMT6/PARP1/CRL4B Complex Regulates the Circadian Clock and Promotes Breast Tumorigenesis. *Advanced Science*, *10*(14), 2202737. https://doi.org/10.1002/advs.202202737

Yang, Y., & Bedford, M. T. (2013). Protein arginine methyltransferases and cancer. *Nature Reviews Cancer*, *13*(1), Article 1. https://doi.org/10.1038/nrc3409

Yao, R., Jiang, H., Ma, Y., Wang, L., Wang, L., Du, J., Hou, P., Gao, Y., Zhao, L., Wang, G., Zhang, Y., Liu, D.-X., Huang, B., & Lu, J. (2014). PRMT7 Induces Epithelial-to-Mesenchymal Transition and Promotes Metastasis in Breast Cancer. *Cancer Research*, *74*(19), 5656–5667. https://doi.org/10.1158/0008-5472.CAN-14-0800

Yoshimatsu, M., Toyokawa, G., Hayami, S., Unoki, M., Tsunoda, T., Field, H. I., Kelly, J. D., Neal, D. E., Maehara, Y., Ponder, B. A. J., Nakamura, Y., & Hamamoto, R. (2011). Dysregulation of PRMT1 and PRMT6, Type I arginine methyltransferases, is involved in various types of human cancers. *International Journal of Cancer*, *128*(3), 562–573. https://doi.org/10.1002/ijc.25366

Zhang, H., Han, C., Li, T., Li, N., & Cao, X. (2019). The methyltransferase PRMT6 attenuates antiviral innate immunity by blocking TBK1–IRF3 signaling. *Cellular & Molecular Immunology*, *16*(10), Article 10. https://doi.org/10.1038/s41423-018-0057-4

Zhao, Q., Xu, W., Xing, L., & Lin, Z. (2016). Recombinant production of medium- to large-sized peptides in Escherichia coli using a cleavable self-aggregating tag. *Microbial Cell Factories*, *15*(1), 136. https://doi.org/10.1186/s12934-016-0534-3

Zhu, Y., Xia, T., Chen, D.-Q., Xiong, X., Shi, L., Zuo, Y., Xiao, H., & Liu, L. (2024). Promising role of protein arginine methyltransferases in overcoming anti-cancer drug resistance. *Drug Resistance Updates*, *72*, 101016. https://doi.org/10.1016/j.drup.2023.101016

Zitvogel, L., & Kroemer, G. (2021). Bortezomib Induces Immunogenic Cell Death in Multiple Myeloma. *Blood Cancer Discovery*, *2*(5), 405–407. https://doi.org/10.1158/2643-3230.BCD-21-0059